Heliyon 10 (2024) e25274

Contents lists available at ScienceDirect

Heliyon

journal homepage: www.cell.com/heliyon

Research article

Analytical solutions for macroscopic elastic moduli and thermal expansion coefficient of composite materials containing coated fillers oriented randomly based on the double inclusion method

Hiroyuki Ono

Division of Mechanical Engineering, Kyoto Institute of Technology, 1 Matsugasaki, Sakyo-ku, Kyoto City, Kyoto, Japan

ARTICLE INFO

Keywords:
Micromechanics
Double inclusion method
Self-consistent method
Mori-Tanaka theorem
Macroscopic elastic moduli
Macroscopic thermal expansion coefficient

ABSTRACT

In this study, micromechanical analysis will be performed to derive explicit solutions of the macroscopic elastic moduli and thermal expansion coefficient for composite materials, where spheroidal-coated fillers are oriented randomly in the material. This analysis is carried out by combining the double inclusion method with the self-consistent method or the Mori-Tanaka theorem. Furthermore, using these solutions, explicit solutions of the macroscopic elastic moduli and thermal expansion coefficient are also derived for composite materials containing various types of coated fillers with different physical properties and shapes. To verify the validity of the obtained solutions, the results of the analytical solutions are compared with the experimental ones for a composite material in which carbon nanotube (CNT) fillers with Al_4C_3 interfacial layer are randomly oriented in an Al matrix. The analytical results show good quantitative agreement with the experimental ones. Additionally, the analytical results are compared with the approximate numerical results using the finite element method for the macroscopic thermal expansion coefficient, and find good agreement within a certain range of the volume fraction and the interfacial layer thickness of the CNT fillers. Furthermore, the changes in the macroscopic Young's modulus and the thermal expansion coefficient are investigated by continuously changing the aspect ratio of the CNT filler. The results show that to exhibit high elastic modulus and low thermal expansion in CNT/Al composites, the CNT fillers should have a shape closer to being spherical or flattened rather than fibrous. Moreover, design guidelines are proposed for the shape of the CNT fillers and interfacial layer thickness for a given volume fraction of the CNT fillers. In conclusion, the validity of the proposed analytical solutions is verified and demonstrated their usefulness for practical materials.

1. Introduction

In recent years, there has been an increasing demand for multifunctional composite materials in various industries such as aerospace and space. These materials are designed to possess multiple excellent characteristics within a single material. For instance, lightweight, high-strength, and high-rigidity panel materials are needed in vehicles to improve fuel efficiency, while materials with low thermal expansion and high thermal conductivity are sought after for downsizing terminal devices. To create such materials, two methods are commonly considered: incorporating fillers with different physical properties into the matrix, and forming a coating

E-mail address: hono@kit.ac.jp.

https://doi.org/10.1016/j.heliyon.2024.e25274
Received 3 August 2023; Received in revised form 5 January 2024; Accepted 23 January 2024

Available online 27 January 2024

layer on the surface of the fillers. The latter method offers improved adhesion between the matrix and fillers, as well as additional properties resulting from the dual nested structure composed of the fillers and the interface layer. The coating technology applied to carbon fibers and carbon nanotubes (CNT) has been developed in recent years, and their applications are rapidly expanding.

The type of coating applied to these fillers varies depending on whether they are impregnated into a resin matrix or a metal matrix [1] [2]. For instance, composite materials have been developed by impregnating short carbon fibers coated with graphene oxide (GO) into a polyethersulfone matrix. The coating of GO has been reported to improve not only the tensile elastic modulus but also the tensile strength of the composite material [3]. Carbon fillers coated with a metal such as nickel and copper, as well as a ceramic such as SiC and Al_2O_3, have been investigated to improve wettability with Al matrices [4]. Furthermore, in a CNT/Al, a layer of aluminum carbide (Al_4C_3) is formed at the interface between CNT fillers and the Al matrix. It has been reported that this interface layer simultaneously increases the elastic modulus of the material and reduces the thermal expansion coefficient of the material [5] [6]. Establishing analytical methods to determine the macroscopic mechanical, thermal, and electromagnetic properties of composite materials containing such coated fillers is significant in material development.

For normal fillers without a coating layer, which are single-phase inhomogeneous inclusions, systematic analytical methods combining Eshelby's equivalent inclusion method and the Mori-Tanaka homogenization theory have been comprehensively compiled by Mura [7]. Coated fillers, characterized by a dual structure with regions possessing different physical properties from the matrix, are referred to as double inhomogeneous inclusions. An analytical method for such materials is the double inclusion method developed by Nemat-Nasser and Hori, which extends Eshelby's solution [8]. Araki et al. utilized this method to derive the stress field within a composite material containing unidirectionally aligned thin-coated fibers, and examined the validity of the solution by comparing it with the solution proposed by Mikata et al. [9] [10]. In recent years, the author has been employing the double inclusion method and the Mori-Tanaka theorem to derive the macroscopic elastic moduli and thermal expansion coefficients of composite materials containing coated fillers [11] [12]. In these analyses, for the case where spheroidal-shaped coated fillers are unidirectionally oriented, the accuracy of the solutions was validated by comparing them with the solution of upper and lower bounds obtained by Hashin et al. [13] [14] [15] and Qiu's theoretical solutions [16] for various combinations of material properties of constituents. Furthermore, using the same approach, the thermal and electromagnetic properties of composites with anisotropic coated fillers oriented unidirectionally were also analyzed [17]. Thus, the effectiveness of the double inclusion method has been sufficiently demonstrated for cases where coated fillers are oriented unidirectionally. However, in cases where the shape of the fillers is other than long fibrous, it is rare for the filler to orient unidirectionally in the matrix.

When incorporating fillers into a resin matrix, an intermediate material called SMC (Sheet Molding Compound) or BMC (Bulk Molding Compound) is typically prepared by mixing the fillers with the resin matrix. These intermediate materials are then placed in molds and subjected to pressure and heat to manufacture the components. On the other hand, when impregnating fillers into a metal matrix, they are mixed with metal powders and formed using a combination of ball milling and hot pressing methods [5]. In the above two molding methods, the fillers are generally distributed randomly in the material. The solutions of the macroscopic physical properties considering such distributions of fillers are important in engineering. Tandon and Weng analyzed the macroscopic elastic moduli of materials containing non-coated spheroidal fillers randomly oriented in two-dimensional or three-dimensional by using Eshelby's equivalent inclusion method and the Mori-Tanaka theorem [18]. We utilized two homogenization theories, the Mori-Tanaka theorem and the self-consistent method [19], in addition to geometrical factors defined by the author's research group, to explicitly derive solutions for the macroscopic elastic moduli, thermal expansion coefficients, and electromagnetic properties of materials where ellipsoidal fillers are oriented randomly in the matrix. By comparing the analytical results with experimental ones, the validity of the obtained solutions is carefully examined [20] [21].

Wenxiang et al. analyzed the macroscopic elastic constants of a composite material containing spheroidal particles with an interfacial layer using the double inclusion method and the Mori-Tanaka theorem. They avoided complicated calculations of the orientation distribution of particles by using an approximation that replaces spheroidal particles with equivalent spherical ones [22]. Weiqi et al. analyzed the macroscopic elastic constants, thermal expansion coefficients, and thermal conductivity of cementitious composites in which bulk paste contains air-pores, water-pores, and spheroidal aggregates surrounded by an interfacial transition zone [23]. This analysis used the self-consistent method to homogenize the double region consisting of the interfacial transition zone and the spheroidal aggregate, and replaced it with a single phase with isotropic physical properties. After this homogenization, they used Christensen's method to determine the macroscopic elastic constants of the material. Christensen's method is an approximate method that uses the macroscopic elastic constants when the inclusions are oriented unidirectionally to estimate those when the inclusions are oriented randomly in three-dimensional [24]. This method has the disadvantage that interactions of inclusions with different orientations are not considered. By using the double inclusion method and Christensen's method, the elastic constants and hydraulic transport properties of composite materials containing coated fillers were analyzed [25] [26] [27]. These analyses do not deal with a direct model of the three-dimensional random orientation state of the coated fillers, but rather use a two-step procedure. Therefore, the solutions for macroscopic physical properties obtained are not explicit but formal.

Considering this situation, the present study aims to derive explicit solutions for the macroscopic elastic moduli and thermal expansion coefficient of materials with spheroidal-coated fillers oriented randomly in the matrix. This will be achieved by combining the double inclusion method with either the self-consistent method or the Mori-Tanaka theorem. This analysis is performed such that the stress and strain fields in the constituents hold consistency with the macroscopic stress and strain fields of the whole material. Therefore, there are no approximations other than those inherent in the double inclusion method and homogenization theories, and exact solutions can be obtained. For later comparison, how to derive solutions for macroscopic physical properties using Christensen's method is also shown. Furthermore, obtained solutions are extended to the case where various types of coated fillers with different physical properties and shapes coexist in the material. In this analysis, both the filler and the interface layer are modeled as coaxial

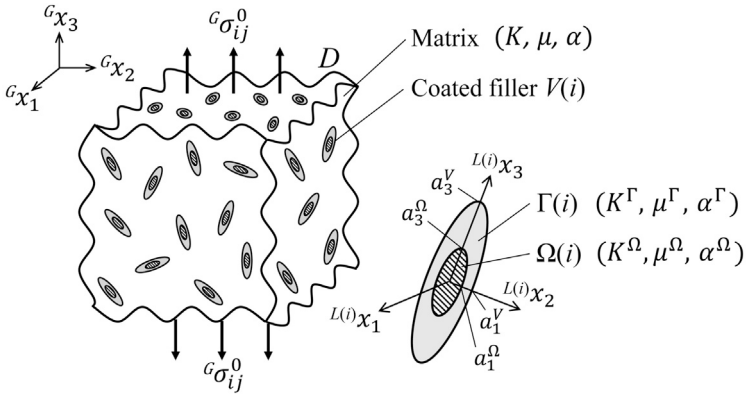

Fig. 1. Composite material containing many spheroidal-coated fillers oriented randomly.

spheroids. Their shapes do not have to be similar to each other, and their aspect ratios are assumed to be different. While the shape of the coated fillers is limited to a spheroidal shape, this analytical solution can be widely applied to carbon fibers and chopped-strand glass fibers, making its applicability extensive. In addition, due to its ability to handle various types of coated fillers, this analytical solution is expected to be valuable in the design of multifunctional composite materials. To validate the obtained solutions, the macroscopic elastic moduli and thermal expansion coefficient of the composite material will be calculated where CNT fillers with an Al_4C_3 interfacial layer are randomly oriented in the Al matrix. The analytical results will be compared both with experimental results and numerically calculated results obtained by the finite element method. Furthermore, the influence of filler shape, volume fraction, and coating layer thickness on the macroscopic elastic moduli and thermal expansion coefficient of the material will be investigated. This will provide design guidelines for CNT/Al composites and evaluate the practical applicability of the analytical solutions to real materials.

2. Analysis of macroscopic elastic moduli and thermal expansion coefficient for composite materials containing coated fillers oriented randomly

2.1. Self-consistent method

2.1.1. Analytical model

Fig. 1 shows a composite material containing coated fillers oriented randomly in the matrix. The coated fillers have the same shape and physical properties, but differ only in orientation. Therefore, the coated fillers are classified by (i) according to the difference in orientation, and there are n kinds of orientations. Let $V(i)$ be the region of the (i)-th coated filler, and D be the region of the whole material. Also, as shown in the lower right of the figure, the region inside the coated filler $V(i)$ is $\Omega(i)$, and the region surrounding $\Omega(i)$ is $\Gamma(i)$. We assume complete bonding at the interfaces between the matrix and the $\Gamma(i)$ regions, as well as between the $\Gamma(i)$ and $\Omega(i)$ regions. Let f_V represent the volume fraction of all coated fillers within the whole material region D, and denote the volume fraction of the (i)-th coated filler as $f_{V(i)}$. It follows that $f_V = \sum_{i=1}^{n} f_{V(i)}$. Let f be the volume fraction of the region $\Omega(i)$ occupied in the region $V(i)$.

The shapes of $\Omega(i)$ and $V(i)$ are coaxial spheroids, but need not be similar. We take a local coordinate system ${}^{L(i)}x_i$ along the orientation of these principal semi-axes, and define the ${}^{L(i)}x_3$ axis as the rotational symmetry axis of the spheroid. Furthermore, we denote the lengths of the minor axes of $\Omega(i)$ and $V(i)$ as a_1^Ω and a_1^V, and the lengths of the major axes as a_3^Ω and a_3^V. Using these axial lengths, we express the aspect ratios of $\Omega(i)$ and $V(i)$ as $\omega_3^\Omega = a_3^\Omega/a_1^\Omega$ and $\omega_3^V = a_3^V/a_1^V$, respectively. A global coordinate system ${}^{G}x_i$ is taken along the direction of the stress ${}^{G}\sigma_{ij}^0$ acting externally on the material. Throughout this study, we will indicate field quantities related to the global or local coordinate system by adding ^{G} or ${}^{L(i)}$ to the left shoulder of the symbols for field quantities.

The properties of regions $\Omega(i)$ and $\Gamma(i)$ within the coated filler $V(i)$ are assumed to be isotropic. The bulk moduli for these regions are denoted as K^Ω and K^Γ, the shear moduli as μ^Ω and μ^Γ, and the thermal expansion coefficients as α^Ω and α^Γ. Furthermore, the matrix is also considered an isotropic material, with the bulk modulus K, shear modulus μ, and thermal expansion coefficient α. When a temperature change occurs, thermal expansion strains occur inside the material because the thermal expansion coefficients of the coated filler and the matrix are different. As described in subsequent sections, these thermal expansion strains are given as eigenstrains $\varepsilon_{ij}^{p\Omega}$ and $\varepsilon_{ij}^{p\Gamma}$ within the $\Omega(i)$ and $\Gamma(i)$ regions, respectively.

Fig. 2 shows the model where the material surrounding a coated filler $V(i)$, as shown in Fig. 1, is replaced by a material with unknown macroscopic elastic moduli $\overline{K}$, $\overline{\mu}$, and thermal expansion coefficient $\overline{\alpha}$. we should note that due to the three-dimensional random orientation of fillers within the material, the whole material exhibits macroscopic isotropy. Furthermore, as shown in Fig. 3, we transform the external stress ${}^{G}\sigma_{ij}^0$ in Fig. 2 to ${}^{L(i)}\sigma_{ij}^0$ in the local coordinate system ${}^{L(i)}x_i$. Analysis of the model in Fig. 2 requires coordinate transformation for the Eshelby tensor, which appears in the equivalent equations shown later, so we cannot derive smartly the solutions of the equivalent equation. Therefore, in this analysis, the model in Fig. 3 will be utilized as the analytical model.

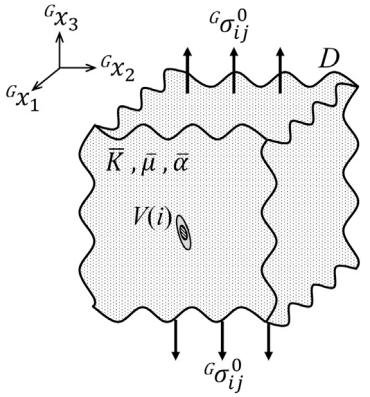

Fig. 2. Model smeared out with unknown macroscopic elastic moduli and thermal expansion coefficient in the global coordinate system.

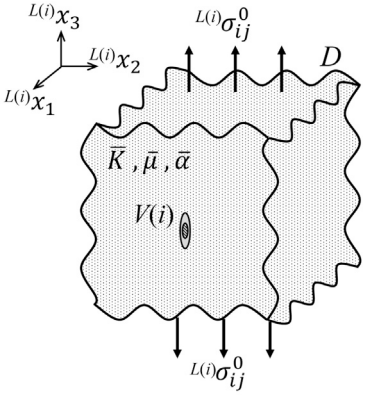

Fig. 3. Model smeared out with unknown macroscopic elastic moduli and thermal expansion coefficient in the local coordinate system.

2.1.2. Equivalent equations and equivalent eigenstrains

In Fig. 3, the elastic moduli of the region $V(i)$ are different from those of the surrounding region $D-V(i)$, then the region $V(i)$ can be treated as a so-called double inhomogeneous inclusion. Thus, we consider equivalent equations for replacing the elastic moduli of the coated filler $V(i)$ with those of surrounding region $D-V(i)$ [8]. By resolving stresses and strains into hydrostatic components and deviatoric ones, equivalent equations for each component in the region $\Omega(i)$ and $\Gamma(i)$ can be expressed as follows, respectively: hydrostatic component:

$$
\begin{aligned}
&{}^{L(i)}\sigma_{ii}^{0} + {}^{L(i)}<\sigma_{ii}^{\infty}>_{\Omega} \\
&= 3K^{\Omega}\left\{ {}^{L(i)}\overline{\varepsilon}_{ii} + (S_{iikl}^{\Omega} - I_{iikl})\,{}^{L(i)}<\varepsilon_{kl}^{**\Omega}>_{\Omega} + (S_{iikl}^{V} - S_{iikl}^{\Omega})\,{}^{L(i)}<\varepsilon_{kl}^{**\Gamma}>_{\Gamma} + {}^{L(i)}<\varepsilon_{ii}^{*\Omega}>_{\Omega} \right\} \\
&= 3\overline{K}\left\{ {}^{L(i)}\overline{\varepsilon}_{ii} + (S_{iikl}^{\Omega} - I_{iikl})\,{}^{L(i)}<\varepsilon_{kl}^{**\Omega}>_{\Omega} + (S_{iikl}^{V} - S_{iikl}^{\Omega})\,{}^{L(i)}<\varepsilon_{kl}^{**\Gamma}>_{\Gamma} \right\} \quad in\ \Omega\,, \qquad (1a) \\
&{}^{L(i)}\sigma_{ii}^{0} + {}^{L(i)}<\sigma_{ii}^{\infty}>_{\Gamma} \\
&= 3K^{\Gamma}\left\{ {}^{L(i)}\overline{\varepsilon}_{ii} + (S_{iikl}^{V} - I_{iikl})\,{}^{L(i)}<\varepsilon_{kl}^{**\Gamma}>_{\Gamma} + \frac{f}{1-f}(S_{iikl}^{V} - S_{iikl}^{\Omega})({}^{L(i)}<\varepsilon_{kl}^{**\Omega}>_{\Omega} - {}^{L(i)}<\varepsilon_{kl}^{**\Gamma}>_{\Gamma}) + {}^{L(i)}<\varepsilon_{ii}^{*\Gamma}>_{\Gamma} \right\} \\
&= 3\overline{K}\left\{ {}^{L(i)}\overline{\varepsilon}_{ii} + (S_{iikl}^{V} - I_{iikl})\,{}^{L(i)}<\varepsilon_{kl}^{**\Gamma}>_{\Gamma} + \frac{f}{1-f}(S_{iikl}^{V} - S_{iikl}^{\Omega})({}^{L(i)}<\varepsilon_{kl}^{**\Omega}>_{\Omega} - {}^{L(i)}<\varepsilon_{kl}^{**\Gamma}>_{\Gamma}) \right\} \quad in\ \Gamma\,, \qquad (1b)
\end{aligned}
$$

deviatoric (or shear) component:

$$
\begin{aligned}
&{}'^{L(i)}\sigma_{ij}^{0} + {}'^{L(i)}<\sigma_{ij}^{\infty}>_{\Omega} \\
&= 2\mu^{\Omega}\left\{ {}'^{L(i)}\overline{\varepsilon}_{ij} + {}'S_{ijkl}^{\Omega}\,{}^{L(i)}<\varepsilon_{kl}^{**\Omega}>_{\Omega} - {}'^{L(i)}<\varepsilon_{ij}^{**\Omega}>_{\Omega} + ({}'S_{ijkl}^{V} - {}'S_{ijkl}^{\Omega})\,{}^{L(i)}<\varepsilon_{kl}^{**\Gamma}>_{\Gamma} + {}'^{L(i)}<\varepsilon_{ij}^{*\Omega}>_{\Omega} \right\} \\
&= 2\overline{\mu}\left\{ {}'^{L(i)}\overline{\varepsilon}_{ij} + {}'S_{ijkl}^{\Omega}\,{}^{L(i)}<\varepsilon_{kl}^{**\Omega}>_{\Omega} - {}'^{L(i)}<\varepsilon_{ij}^{**\Omega}>_{\Omega} + ({}'S_{ijkl}^{V} - {}'S_{ijkl}^{\Omega})\,{}^{L(i)}<\varepsilon_{kl}^{**\Gamma}>_{\Gamma} \right\} \quad in\ \Omega\,, \qquad (2a) \\
&{}'^{L(i)}\sigma_{ij}^{0} + {}'^{L(i)}<\sigma_{ij}^{\infty}>_{\Gamma} \\
&= 2\mu^{\Gamma}\left\{ {}'^{L(i)}\overline{\varepsilon}_{ij} + {}'S_{ijkl}^{V}\,{}^{L(i)}<\varepsilon_{kl}^{**\Gamma}>_{\Gamma} - {}'^{L(i)}<\varepsilon_{ij}^{**\Gamma}>_{\Gamma} + \frac{f}{1-f}({}'S_{ijkl}^{V} - {}'S_{ijkl}^{\Omega})({}^{L(i)}<\varepsilon_{kl}^{**\Omega}>_{\Omega} - {}^{L(i)}<\varepsilon_{kl}^{**\Gamma}>_{\Gamma}) + {}'^{L(i)}<\varepsilon_{ij}^{*\Gamma}>_{\Gamma} \right\}
\end{aligned}
$$

$$= 2\overline{\mu}\left\{ {}'^{L(i)}\overline{\varepsilon}_{ij} + {}'S^{V}_{ijkl}\,{}^{L(i)}\langle \varepsilon^{**\Gamma}_{kl}\rangle_{\Gamma} - {}'^{L(i)}\langle \varepsilon^{**\Gamma}_{ij}\rangle_{\Gamma} + \frac{f}{1-f}({}'S^{V}_{ijkl} - {}'S^{\Omega}_{ijkl})({}^{L(i)}\langle \varepsilon^{**\Omega}_{kl}\rangle_{\Omega} - {}^{L(i)}\langle \varepsilon^{**\Gamma}_{kl}\rangle_{\Gamma}) \right\} \quad in\,\Gamma\,. \tag{2b}$$

The superscript $'$ on the left shoulder of the stresses and strains in Eq. (2) represents the deviatoric component. Eq. (2) becomes equivalent equations for the shear component by removing $'$ attached to the left shoulder of the stresses and strains. $S^{X}_{ijkl}(X=\Omega,\,V)$ in the equations is the Eshelby tensor [7] in the region X. If the shapes of Ω and V are similar and have the same axis of rotational symmetry, then $S^{\Omega}_{ijkl} = S^{V}_{ijkl}$. ${}'S^{X}_{ijkl}(X=\Omega,\,V)$ represents the deviatoric component of the Eshelby tensor, which is given by

$${}'S^{X}_{ijkl} = S^{X}_{ijkl} - \frac{1}{3}S^{X}_{iikl} \qquad ,\quad (X=\Omega,\,V)\,. \tag{3}$$

${}^{L(i)}\langle \sigma^{\infty}_{ij}\rangle_{X}$ $(X=\Omega,\,\Gamma)$ in Eqs. (1) and (2) are the eigenstress in the region X representing the disturbance of internal stresses. Note that $\langle\ \ \rangle_{X}$ represents the volume average over the region X. ${}^{L(i)}\langle \varepsilon^{**X}_{ij}\rangle_{X}$ $(X=\Omega,\,\Gamma)$ is the sum of eigenstrains $\langle \varepsilon^{pX}_{ij}\rangle_{X}$ and unknown equivalent eigenstrains ${}^{L(i)}\langle \varepsilon^{*X}_{ij}\rangle_{X}$ that substitute for the difference in elastic moduli between the coated filler and the matrix, and is given by

$${}^{L(i)}\langle \varepsilon^{**X}_{ij}\rangle_{X} = \langle \varepsilon^{pX}_{ij}\rangle_{X} + {}^{L(i)}\langle \varepsilon^{*X}_{ij}\rangle_{X} \qquad ,\quad (X=\Omega,\,\Gamma)\,. \tag{4}$$

$\langle \varepsilon^{pX}_{ij}\rangle_{X}$ $(X=\Omega,\,\Gamma)$ in Eq. (4) is given as thermal expansion strains, residual strains, or other misfit strains in the region X. Therefore, since it is obvious that $\langle \varepsilon^{pX}_{ij}\rangle_{X}$ is a quantity in the local coordinate system, ${}^{L(i)}$ indicating that it is a quantity in the local coordinate system is not added to the left shoulder of the strain.

The unknown quantity to be obtained is the equivalent eigenstrain ${}^{L(i)}\langle \varepsilon^{*X}_{ij}\rangle_{X}$ $(X=\Omega,\,\Gamma)$. But, to simplify the analysis, we let ${}^{L(i)}\langle \varepsilon^{**X}_{ij}\rangle_{X}$ in Eq. (4) be an unknown quantity to be obtained. ${}^{L(i)}\overline{\varepsilon}_{ij}$ in Eqs. (1) and (2) are the strain induced in the whole material by the applied stress ${}^{L(i)}\sigma^{0}_{ij}$. I_{ijkl} is the identity matrix.

Araki et al. expressed the Eshelby tensor S_{ijkl} in a completely separated form into the Poisson's ratio of the matrix and the geometrical factors which include only the aspect ratio of the filler [28]. The geometrical factors and the Eshelby tensor of the spheroid expressed by using the geometrical factors are given in Appendix A.1. After substituting Eq. (3) into Eqs. (1) and (2), and further substituting the Eshelby tensor, we get the following equations:
hydrostatic component:

$$\begin{aligned} &3(1-\overline{\nu})({}^{L(i)}\overline{\varepsilon}_{ii} - L^{\Omega}_{K}\langle \varepsilon^{p\Omega}_{ii}\rangle_{\Omega}) + L^{\Omega}_{\mathrm{I}}\,{}^{L(i)}\langle \varepsilon^{**\Omega}_{ii}\rangle_{\Omega} \\ &\quad - \frac{3}{2}(1-2\overline{\nu})\alpha^{\Omega}_{3}\,{}'^{L(i)}\langle \varepsilon^{**\Omega}_{33}\rangle_{\Omega} - \frac{3}{2}(1-2\overline{\nu})\Delta\alpha_{3}\,{}'^{L(i)}\langle \varepsilon^{**\Gamma}_{33}\rangle_{\Gamma} = 0 \quad in\,\Omega\,, \end{aligned} \tag{5a}$$

$$\begin{aligned} &3(1-\overline{\nu})({}^{L(i)}\overline{\varepsilon}_{ii} - L^{\Gamma}_{K}\langle \varepsilon^{p\Gamma}_{ii}\rangle_{\Gamma}) + L^{\Gamma}_{\mathrm{I}}\,{}^{L(i)}\langle \varepsilon^{**\Gamma}_{ii}\rangle_{\Gamma} \\ &\quad - \frac{3}{2}(1-2\overline{\nu})\alpha^{V}_{3}\,{}'^{L(i)}\langle \varepsilon^{**\Gamma}_{33}\rangle_{\Gamma} - \frac{3f}{2(1-f)}(1-2\overline{\nu})\Delta\alpha_{3}({}'^{L(i)}\langle \varepsilon^{**\Omega}_{33}\rangle_{\Omega} - {}'^{L(i)}\langle \varepsilon^{**\Gamma}_{33}\rangle_{\Gamma}) = 0 \quad in\,\Gamma\,, \end{aligned} \tag{5b}$$

deviatoric component 11:

$$\begin{aligned} &2(1-\overline{\nu})({}'^{L(i)}\overline{\varepsilon}_{11} - L^{\Omega}_{\mu}\,{}'\langle \varepsilon^{p\Omega}_{11}\rangle_{\Omega}) + L^{\Omega}_{\mathrm{II}}\,{}'^{L(i)}\langle \varepsilon^{**\Omega}_{11}\rangle_{\Omega} - \frac{3}{2}R^{\Omega}_{3}\,{}'^{L(i)}\langle \varepsilon^{**\Omega}_{22}\rangle_{\Omega} + \frac{1}{9}(1+\overline{\nu})\alpha^{\Omega}_{3}\,{}^{L(i)}\langle \varepsilon^{**\Omega}_{ii}\rangle_{\Omega} \\ &\quad + \frac{1}{9}(1+\overline{\nu})\Delta\alpha_{3}\,{}^{L(i)}\langle \varepsilon^{**\Gamma}_{ii}\rangle_{\Gamma} - \frac{3}{2}\left(\Delta R_{3}\,{}'^{L(i)}\langle \varepsilon^{**\Gamma}_{22}\rangle_{\Gamma} - \frac{2}{3}\Delta H_{\mathrm{I}}\,{}'^{L(i)}\langle \varepsilon^{**\Gamma}_{11}\rangle_{\Gamma}\right) = 0 \quad in\,\Omega\,, \end{aligned} \tag{6a}$$

$$\begin{aligned} &2(1-\overline{\nu})({}'^{L(i)}\overline{\varepsilon}_{11} - L^{\Gamma}_{\mu}\,{}'\langle \varepsilon^{p\Gamma}_{11}\rangle_{\Gamma}) + L^{\Gamma}_{\mathrm{II}}\,{}'^{L(i)}\langle \varepsilon^{**\Gamma}_{11}\rangle_{\Gamma} - \frac{3}{2}R^{V}_{3}\,{}'^{L(i)}\langle \varepsilon^{**\Gamma}_{22}\rangle_{\Gamma} + \frac{1}{9}(1+\overline{\nu})\alpha^{V}_{3}\,{}^{L(i)}\langle \varepsilon^{**\Gamma}_{ii}\rangle_{\Gamma} \\ &\quad + \frac{f}{9(1-f)}(1+\overline{\nu})\Delta\alpha_{3}({}^{L(i)}\langle \varepsilon^{**\Omega}_{ii}\rangle_{\Omega} - {}^{L(i)}\langle \varepsilon^{**\Gamma}_{ii}\rangle_{\Gamma}) \\ &\quad - \frac{3f}{2(1-f)}\left\{\Delta R_{3}({}'^{L(i)}\langle \varepsilon^{**\Omega}_{22}\rangle_{\Omega} - {}'^{L(i)}\langle \varepsilon^{**\Gamma}_{22}\rangle_{\Gamma}) - \frac{2}{3}\Delta H_{\mathrm{I}}({}'^{L(i)}\langle \varepsilon^{**\Omega}_{11}\rangle_{\Omega} - {}'^{L(i)}\langle \varepsilon^{**\Gamma}_{11}\rangle_{\Gamma}) = 0 \quad in\,\Gamma\,, \right. \end{aligned} \tag{6b}$$

deviatoric component 33:

$$\begin{aligned} &2(1-\overline{\nu})({}'^{L(i)}\overline{\varepsilon}_{33} - L^{\Omega}_{\mu}\,{}'\langle \varepsilon^{p\Omega}_{33}\rangle_{\Omega}) + \left(L^{\Omega}_{\mathrm{II}} - \frac{3}{2}R^{\Omega}_{3}\right){}'^{L(i)}\langle \varepsilon^{**\Omega}_{33}\rangle_{\Omega} - \frac{2}{9}(1+\overline{\nu})\alpha^{\Omega}_{3}\,{}^{L(i)}\langle \varepsilon^{**\Omega}_{ii}\rangle_{\Omega} \\ &\quad - \frac{2}{9}(1+\overline{\nu})\Delta\alpha_{3}\,{}^{L(i)}\langle \varepsilon^{**\Gamma}_{ii}\rangle_{\Gamma} - \frac{3}{2}\left(\Delta R_{3} - \frac{2}{3}\Delta H_{\mathrm{I}}\right){}'^{L(i)}\langle \varepsilon^{**\Gamma}_{33}\rangle_{\Gamma} = 0 \quad in\,\Omega\,, \end{aligned} \tag{7a}$$

$$\begin{aligned} &2(1-\overline{\nu})({}'^{L(i)}\overline{\varepsilon}_{33} - L^{\Gamma}_{\mu}\,{}'\langle \varepsilon^{p\Gamma}_{33}\rangle_{\Gamma}) + \left(L^{\Gamma}_{\mathrm{II}} - \frac{3}{2}R^{V}_{3}\right){}'^{L(i)}\langle \varepsilon^{**\Gamma}_{33}\rangle_{\Gamma} - \frac{2}{9}(1+\overline{\nu})\alpha^{V}_{3}\,{}^{L(i)}\langle \varepsilon^{**\Gamma}_{ii}\rangle_{\Gamma} \\ &\quad - \frac{2f}{9(1-f)}(1+\overline{\nu})\Delta\alpha_{3}({}^{L(i)}\langle \varepsilon^{**\Omega}_{ii}\rangle_{\Omega} - {}^{L(i)}\langle \varepsilon^{**\Gamma}_{ii}\rangle_{\Gamma}) \\ &\quad - \frac{3f}{2(1-f)}\left(\Delta R_{3} - \frac{2}{3}\Delta H_{\mathrm{I}}\right)({}'^{L(i)}\langle \varepsilon^{**\Omega}_{33}\rangle_{\Omega} - {}'^{L(i)}\langle \varepsilon^{**\Gamma}_{33}\rangle_{\Gamma}) = 0 \quad in\,\Gamma\,, \end{aligned} \tag{7b}$$

shear component 23:

$$2(1-\overline{\nu})({}^{L(i)}\overline{\varepsilon}_{23}-L_{\mu}^{\Omega}<\varepsilon_{23}^{p\Omega}>_{\Omega})+\left\{L_{\mathrm{II}}^{\Omega}-\frac{3}{4}R_{3}^{\Omega}-\frac{1}{2}(5H_{\mathrm{I}}^{\Omega}-2)\right\}{}^{L(i)}<\varepsilon_{23}^{**\Omega}>_{\Omega}-\frac{3}{4}(\Delta R_{3}+2\Delta H_{\mathrm{I}})\,{}^{L(i)}<\varepsilon_{23}^{**\Gamma}>_{\Gamma}=0\quad in\,\Omega\,, \tag{8a}$$

$$2(1-\overline{\nu})({}^{L(i)}\overline{\varepsilon}_{23}-L_{\mu}^{\Gamma}<\varepsilon_{23}^{p\Gamma}>_{\Gamma})+\left\{L_{\mathrm{II}}^{\Gamma}-\frac{3}{4}R_{3}^{V}-\frac{1}{2}(5H_{\mathrm{I}}^{V}-2)\right\}{}^{L(i)}<\varepsilon_{23}^{**\Gamma}>_{\Gamma}$$
$$-\frac{3f}{4(1-f)}(\Delta R_{3}+2\Delta H_{\mathrm{I}})({}^{L(i)}<\varepsilon_{23}^{**\Omega}>_{\Omega}-{}^{L(i)}<\varepsilon_{23}^{**\Gamma}>_{\Gamma})=0\quad in\,\Gamma\,, \tag{8b}$$

shear component 12:

$$2(1-\overline{\nu})({}^{L(i)}\overline{\varepsilon}_{12}-L_{\mu}^{\Omega}<\varepsilon_{12}^{p\Omega}>_{\Omega})+\left(L_{\mathrm{II}}^{\Omega}+\frac{3}{2}R_{3}^{\Omega}\right){}^{L(i)}<\varepsilon_{12}^{**\Omega}>_{\Omega}+\frac{3}{2}\left(\Delta R_{3}+\frac{2}{3}\Delta H_{\mathrm{I}}\right){}^{L(i)}<\varepsilon_{12}^{**\Gamma}>_{\Gamma}=0\quad in\,\Omega\,, \tag{9a}$$

$$2(1-\overline{\nu})({}^{L(i)}\overline{\varepsilon}_{12}-L_{\mu}^{\Gamma}<\varepsilon_{12}^{p\Gamma}>_{\Gamma})+\left(L_{\mathrm{II}}^{\Gamma}+\frac{3}{2}R_{3}^{V}\right){}^{L(i)}<\varepsilon_{12}^{**\Gamma}>_{\Gamma}+\frac{3f}{2(1-f)}\left(\Delta R_{3}+\frac{2}{3}\Delta H_{\mathrm{I}}\right)({}^{L(i)}<\varepsilon_{12}^{**\Omega}>_{\Omega}-{}^{L(i)}<\varepsilon_{12}^{**\Gamma}>_{\Gamma})$$
$$=0\ in\,\Gamma\,. \tag{9b}$$

The equivalent expression for the normal component 22 is obtained by simply replacing the strain subscript $_{11}$ in the equivalent expression for the 11 component in Eq. (6) with $_{22}$. Similarly, the equivalent expression for the shear component 31 is obtained by replacing the strain subscript $_{23}$ in the equivalent expression for the 23 component in Eq. (8) with $_{31}$. Such a formal agreement of equivalent equations can be easily understood from the fact that the spheroid has the x_3 axis as its rotational symmetry axis. Each coefficients in Eqs. (5) to (9) are given as

$$\alpha_{3}^{X}=1-3H_{3}^{X}\quad,\quad R_{3}^{X}=\frac{2}{9}(1-2\overline{\nu})\alpha_{3}^{X}+\frac{1}{6}(1-H_{31}^{X})-(H_{3}^{X}-H_{31}^{X})\quad,\quad(X=\Omega,\,V)\,, \tag{10a}$$

$$H_{\mathrm{I}}^{X}=\frac{1}{4}(1-H_{31}^{X})+\frac{3}{2}(H_{3}^{X}-H_{31}^{X})\quad,\quad(X=\Omega,\,V)\,, \tag{10b}$$

$$\Delta\alpha_{3}=\alpha_{3}^{V}-\alpha_{3}^{\Omega}\quad,\quad\Delta R_{3}=R_{3}^{V}-R_{3}^{\Omega}\quad,\quad\Delta H_{\mathrm{I}}=H_{\mathrm{I}}^{V}-H_{\mathrm{I}}^{\Omega}\,, \tag{10c}$$

$$L_{\mathrm{I}}^{\Omega}=3(1-\overline{\nu})L_{K}^{\Omega}-2(1-2\overline{\nu})\quad,\quad L_{\mathrm{I}}^{\Gamma}=3(1-\overline{\nu})L_{K}^{\Gamma}-2(1-2\overline{\nu})\,, \tag{10d}$$

$$L_{\mathrm{II}}^{\Omega}=2(1-\overline{\nu})L_{\mu}^{\Omega}-\frac{1}{3}(1-2\overline{\nu})+H_{\mathrm{I}}^{\Omega}-1\quad,\quad L_{\mathrm{II}}^{\Gamma}=2(1-\overline{\nu})L_{\mu}^{\Gamma}-\frac{1}{3}(1-2\overline{\nu})+H_{\mathrm{I}}^{V}-1\,, \tag{10e}$$

$$L_{K}^{X}=\frac{K^{X}}{K^{X}-\overline{K}}\quad,\quad L_{\mu}^{X}=\frac{\mu^{X}}{\mu^{X}-\overline{\mu}}\quad,\quad(X=\Omega,\,\Gamma)\,. \tag{10f}$$

H_{3}^{X} and H_{31}^{X} in Eq. (10) are referred to as the geometrical factors [29], which are determined solely by the aspect ratios $\omega_{3}^{X}(X=\Omega,\,V)$ of each region X. Therefore, α_{3}^{X}, R_{3}^{X} and $H_{\mathrm{I}}^{X}(X=\Omega,\,V)$ including the geometrical factors are the coefficients that govern the shape of the region X. $\Delta\alpha_{3}$, ΔR_{3} and ΔH_{I} are the coefficients representing the difference in shape between the Ω and V regions. Coefficients with Δ are used in subsequent analysis, which means coefficients composed of $\Delta\alpha_{3}$, ΔR_{3}, and ΔH_{I}.

We find that the equivalent equations (5) to (9) have the following features.

(1) The equivalent equations for the hydrostatic components include not only the hydrostatic components of strain but also the deviatoric components of strain. The same is true for the equivalent equations for the deviation components. That is, the hydrostatic components and the deviatoric ones of strain couple with each other.

(2) Equivalent equations for the shear components are expressed only by the same component of shear strain. That is, the different components of shear strain do not couple with each other.

(3) Regardless of the type of equivalent equations, the equations for the Ω region include the eigenstrains in the Γ region and vice versa. This is due to the nested structure of the Ω and Γ regions.

(4) If the shapes of the Ω and V regions are similar and coaxial, that is, they have the same aspect ratio, $\Delta\alpha_{3}$ and ΔR_{3} and ΔH_{I} representing the differences in their shapes become zero. As a result, all the coupling terms included in Eqs. (5) to (9) vanish and the equivalent equations reduce to a very simple form. This feature is also indicated by Wenxiang et al. [26] and Pin et al. [25], which used the double inclusion method. The same feature can be also found in the analysis of the macroscopic hydraulic conductivity by Jinyang et al. [27].

From Eqs. (5) to (9), the equivalent eigenstrains in the Ω and Γ regions are given by

$${}^{L(i)}<\varepsilon_{ii}^{**\Omega}>_{\Omega}=-\frac{(1-\overline{\nu})}{A_{3}}\left[3A_{3}^{\Gamma}\left(L_{\mathrm{II}}^{\Omega}-\frac{3}{2}R_{3}^{\Omega}\right)-\frac{f}{2(1-f)}\left\{\frac{9}{2}\left(\Delta R_{3}-\frac{2}{3}\Delta H_{\mathrm{I}}\right)\Delta F_{3}^{\Gamma}+2(1+\overline{\nu})(1-2\overline{\nu})\Delta\alpha_{3}\Delta G_{3}^{\Gamma}\right\}\right]$$
$$\times({}^{L(i)}\overline{\varepsilon}_{ii}-L_{K}^{\Omega}<\varepsilon_{ii}^{p\Omega}>_{\Omega})-\frac{(1-\overline{\nu})(1+\overline{\nu})(1-2\overline{\nu})}{A_{3}}\Delta P_{\mathrm{II}}({}^{L(i)}\overline{\varepsilon}_{ii}-L_{K}^{\Gamma}<\varepsilon_{ii}^{p\Gamma}>_{\Gamma})$$
$$-\frac{3(1-\overline{\nu})(1-2\overline{\nu})}{A_{3}}\left\{A_{3}^{\Gamma}\alpha_{3}^{\Omega}+\frac{f}{2(1-f)}\Delta\alpha_{3}\Delta F_{3}^{\Gamma}\right\}({}'^{L(i)}\overline{\varepsilon}_{33}-L_{\mu}^{\Omega\,\prime}<\varepsilon_{33}^{p\Omega}>_{\Omega})$$
$$-\frac{3(1-\overline{\nu})(1-2\overline{\nu})}{A_{3}}\Delta P_{\mathrm{III}}({}'^{L(i)}\overline{\varepsilon}_{33}-L_{\mu}^{\Gamma\,\prime}<\varepsilon_{33}^{p\Gamma}>_{\Gamma})\quad, \tag{11a}$$

$$
\begin{aligned}
{}^{L(i)}\langle\varepsilon_{ii}^{**\Gamma}\rangle_{\Gamma} = & -\frac{(1-\overline{\nu})}{A_3}\left[3A_3^{\Omega}\left(L_{\mathrm{II}}^{\Gamma}-\frac{3}{2}R_3^{\Gamma}\right)-\frac{f}{2(1-f)}\left\{\frac{9}{2}\left(\Delta R_3-\frac{2}{3}\Delta H_1\right)\Delta F_3^{\Omega}+2(1+\overline{\nu})(1-2\overline{\nu})\Delta\alpha_3\Delta G_3^{\Omega}\right\}\right] \\
& \times({}^{L(i)}\overline{\varepsilon}_{ii}-L_K^{\Gamma}\langle\varepsilon_{ii}^{p\Gamma}\rangle_{\Gamma})-\frac{f(1-\overline{\nu})(1+\overline{\nu})(1-2\overline{\nu})}{(1-f)A_3}\Delta P_{\mathrm{II}}({}^{L(i)}\overline{\varepsilon}_{ii}-L_K^{\Omega}\langle\varepsilon_{ii}^{p\Omega}\rangle_{\Omega}) \\
& -\frac{3(1-\overline{\nu})(1-2\overline{\nu})}{A_3}\left\{A_3^{\Omega}\alpha_3^{\Gamma}+\frac{f}{2(1-f)}\Delta\alpha_3\Delta F_3^{\Omega}\right\}({}'^{L(i)}\overline{\varepsilon}_{33}-L_{\mu}^{\Gamma}{}'\langle\varepsilon_{33}^{p\Gamma}\rangle_{\Gamma}) \\
& -\frac{3f(1-\overline{\nu})(1-2\overline{\nu})}{(1-f)A_3}\Delta P_{\mathrm{IV}}({}'^{L(i)}\overline{\varepsilon}_{33}-L_{\mu}^{\Omega}{}'\langle\varepsilon_{33}^{p\Omega}\rangle_{\Omega}) \quad , \qquad (11b)
\end{aligned}
$$

$$
\begin{aligned}
{}'^{L(i)}\langle\varepsilon_{11}^{**\Omega}\rangle_{\Omega}-{}'^{L(i)}\langle\varepsilon_{22}^{**\Omega}\rangle_{\Omega} = & -\frac{2(1-\overline{\nu})}{A_{12}}\left\langle A_{12}^{\Gamma}\left\{({}'^{L(i)}\overline{\varepsilon}_{11}-{}'^{L(i)}\overline{\varepsilon}_{22})-L_{\mu}^{\Omega}({}'\langle\varepsilon_{11}^{p\Omega}\rangle_{\Omega}-{}'\langle\varepsilon_{22}^{p\Omega}\rangle_{\Omega}\right\}\right. \\
& \left.-\frac{3}{2}\left(\Delta R_3+\frac{2}{3}\Delta H_1\right)\left\{({}'^{L(i)}\overline{\varepsilon}_{11}-{}'^{L(i)}\overline{\varepsilon}_{22})-L_{\mu}^{\Gamma}({}'\langle\varepsilon_{11}^{p\Gamma}\rangle_{\Gamma}-{}'\langle\varepsilon_{22}^{p\Gamma}\rangle_{\Gamma})\right\}\right\rangle \quad , \qquad (12a)
\end{aligned}
$$

$$
\begin{aligned}
{}'^{L(i)}\langle\varepsilon_{11}^{**\Gamma}\rangle_{\Gamma}-{}'^{L(i)}\langle\varepsilon_{22}^{**\Gamma}\rangle_{\Gamma} = & -\frac{2(1-\overline{\nu})}{A_{12}}\left\langle A_{12}^{\Omega}\left\{({}'^{L(i)}\overline{\varepsilon}_{11}-{}'^{L(i)}\overline{\varepsilon}_{22})-L_{\mu}^{\Gamma}({}'\langle\varepsilon_{11}^{p\Gamma}\rangle_{\Gamma}-{}'\langle\varepsilon_{22}^{p\Gamma}\rangle_{\Gamma})\right\}\right. \\
& \left.-\frac{3f}{2(1-f)}\left(\Delta R_3+\frac{2}{3}\Delta H_1\right)\left\{({}'^{L(i)}\overline{\varepsilon}_{11}-{}'^{L(i)}\overline{\varepsilon}_{22})-L_{\mu}^{\Omega}({}'\langle\varepsilon_{11}^{p\Omega}\rangle_{\Omega}-{}'\langle\varepsilon_{22}^{p\Omega}\rangle_{\Omega}\right\}\right\rangle \quad , \qquad (12b)
\end{aligned}
$$

$$
\begin{aligned}
{}'^{L(i)}\langle\varepsilon_{33}^{**\Omega}\rangle_{\Omega} = & -\frac{2(1-\overline{\nu})(1+\overline{\nu})}{3A_3}\left\{A_3^{\Gamma}\alpha_3^{\Omega}+\frac{f}{2(1-f)}\Delta\alpha_3\Delta F_3^{\Gamma}\right\}({}^{L(i)}\overline{\varepsilon}_{ii}-L_K^{\Omega}\langle\varepsilon_{ii}^{p\Omega}\rangle_{\Omega}) \\
& -\frac{2(1-\overline{\nu})}{A_3}\left\{A_3^{\Gamma}L_{\mathrm{I}}^{\Omega}-\frac{f(1+\overline{\nu})(1-2\overline{\nu})}{3(1-f)}L_{\mathrm{I}}^{\Gamma}(\Delta\alpha_3)^2\right\}({}'^{L(i)}\overline{\varepsilon}_{33}-L_{\mu}^{\Omega}{}'\langle\varepsilon_{33}^{p\Omega}\rangle_{\Omega}) \\
& -\frac{2(1-\overline{\nu})(1+\overline{\nu})}{3A_3}\Delta P_{\mathrm{IV}}({}^{L(i)}\overline{\varepsilon}_{ii}-L_K^{\Gamma}\langle\varepsilon_{ii}^{p\Gamma}\rangle_{\Gamma})-\frac{2(1-\overline{\nu})}{A_3}\Delta P_{\mathrm{I}}({}'^{L(i)}\overline{\varepsilon}_{33}-L_{\mu}^{\Gamma}{}'\langle\varepsilon_{33}^{p\Gamma}\rangle_{\Gamma}) \quad , \qquad (13a)
\end{aligned}
$$

$$
\begin{aligned}
{}'^{L(i)}\langle\varepsilon_{33}^{**\Gamma}\rangle_{\Gamma} = & -\frac{2(1-\overline{\nu})(1+\overline{\nu})}{3A_3}\left\{A_3^{\Omega}\alpha_3^{\Gamma}+\frac{f}{2(1-f)}\Delta\alpha_3\Delta F_3^{\Omega}\right\}({}^{L(i)}\overline{\varepsilon}_{ii}-L_K^{\Gamma}\langle\varepsilon_{ii}^{p\Gamma}\rangle_{\Gamma}) \\
& -\frac{2(1-\overline{\nu})}{A_3}\left\{A_3^{\Omega}L_{\mathrm{I}}^{\Gamma}-\frac{f(1+\overline{\nu})(1-2\overline{\nu})}{3(1-f)}L_{\mathrm{I}}^{\Omega}(\Delta\alpha_3)^2\right\}({}'^{L(i)}\overline{\varepsilon}_{33}-L_{\mu}^{\Gamma}{}'\langle\varepsilon_{33}^{p\Gamma}\rangle_{\Gamma}) \\
& -\frac{2f(1-\overline{\nu})(1+\overline{\nu})}{3(1-f)A_3}\Delta P_{\mathrm{III}}({}^{L(i)}\overline{\varepsilon}_{ii}-L_K^{\Omega}\langle\varepsilon_{ii}^{p\Omega}\rangle_{\Omega})-\frac{2f(1-\overline{\nu})}{(1-f)A_3}\Delta P_{\mathrm{I}}({}'^{L(i)}\overline{\varepsilon}_{33}-L_{\mu}^{\Omega}{}'\langle\varepsilon_{33}^{p\Omega}\rangle_{\Omega}) \quad , \qquad (13b)
\end{aligned}
$$

$$
{}^{L(i)}\langle\varepsilon_{23}^{**\Omega}\rangle_{\Omega} = -\frac{2(1-\overline{\nu})}{A_{23}}\left\{A_{23}^{\Gamma}({}^{L(i)}\overline{\varepsilon}_{23}-L_{\mu}^{\Omega}\langle\varepsilon_{23}^{p\Omega}\rangle_{\Omega})+\frac{3}{4}(\Delta R_3+2\Delta H_1)({}^{L(i)}\overline{\varepsilon}_{23}-L_{\mu}^{\Gamma}\langle\varepsilon_{23}^{p\Gamma}\rangle_{\Gamma})\right\} \quad , \qquad (14a)
$$

$$
{}^{L(i)}\langle\varepsilon_{23}^{**\Gamma}\rangle_{\Gamma} = -\frac{2(1-\overline{\nu})}{A_{23}}\left\{A_{23}^{\Omega}({}^{L(i)}\overline{\varepsilon}_{23}-L_{\mu}^{\Gamma}\langle\varepsilon_{23}^{p\Gamma}\rangle_{\Gamma})+\frac{3f}{4(1-f)}(\Delta R_3+2\Delta H_1)({}^{L(i)}\overline{\varepsilon}_{23}-L_{\mu}^{\Omega}\langle\varepsilon_{23}^{p\Omega}\rangle_{\Omega})\right\} \quad , \qquad (14b)
$$

$$
{}^{L(i)}\langle\varepsilon_{12}^{**\Omega}\rangle_{\Omega} = -\frac{2(1-\overline{\nu})}{A_{12}}\left\{A_{12}^{\Gamma}({}^{L(i)}\overline{\varepsilon}_{12}-L_{\mu}^{\Omega}\langle\varepsilon_{12}^{p\Omega}\rangle_{\Omega})-\frac{3}{2}\left(\Delta R_3+\frac{2}{3}\Delta H_1\right)({}^{L(i)}\overline{\varepsilon}_{12}-L_{\mu}^{\Gamma}\langle\varepsilon_{12}^{p\Gamma}\rangle_{\Gamma})\right\} \quad , \qquad (15a)
$$

$$
{}^{L(i)}\langle\varepsilon_{12}^{**\Gamma}\rangle_{\Gamma} = -\frac{2(1-\overline{\nu})}{A_{12}}\left\{A_{12}^{\Omega}({}^{L(i)}\overline{\varepsilon}_{12}-L_{\mu}^{\Gamma}\langle\varepsilon_{12}^{p\Gamma}\rangle_{\Gamma})-\frac{3f}{2(1-f)}\left(\Delta R_3+\frac{2}{3}\Delta H_1\right)({}^{L(i)}\overline{\varepsilon}_{12}-L_{\mu}^{\Omega}\langle\varepsilon_{12}^{p\Omega}\rangle_{\Omega})\right\} \quad , \qquad (15b)
$$

where the coefficients in Eqs. (11) to (15) are summarized in Appendix A.2. From Eqs. (11) to (15), all the components of the equivalent eigenstrains ${}^{L(i)}\langle\varepsilon_{ij}^{**X}\rangle_X$ can be expressed as the strain ${}^{L(i)}\overline{\varepsilon}_{ij}$ in the material due to the applied stress and eigenstrains $\langle\varepsilon_{ij}^{pX}\rangle_X$ ($X=\Omega,\Gamma$). Eq. (12) expresses the difference between the deviatoric strain components 11 and 22. Interestingly, this equation is in perfect agreement with Eqs. (15) for the shear strain components 12 in terms of coefficient of strain. Let us consider the reason for this. The model in Fig. 3 represents that the spheroidal fillers are oriented along the x_3 axis. Thus, the properties of the material are the same as those of the hexagonal material. Due to the symmetry of the elastic constants of the hexagonal material, the difference between the 11 and 22 components of the strain can be expressed as the difference between the 11 and 12 components of the compliance. This difference agrees with the 66 component of the compliance, that is, the component related to the shear component 12 of the strain. Eq. (12) expresses this fact and can be said to be a physically consistent equation. Since the sum of the 11, 22, and 33 components of the deviatoric strain is zero, the deviatoric components 11 and 22 of the equivalent eigenstrain can be obtained from Eqs. (12) and (13). As mentioned above, the coefficients prefixed with Δ that appear in the equations are all zero when the shapes of the Ω and V regions are similar and coaxial. Consequently, the equivalent eigenstrains reduce to a more simple form.

In the analysis of the total strain shown later, the volume average of the equivalent eigenstrains ${}^{L(i)}\langle\varepsilon_{ij}^{**V}\rangle_V$ over the V region, as shown below, is required.

$$
{}^{L(i)}\langle\varepsilon_{ij}^{**V}\rangle_V = f\,{}^{L(i)}\langle\varepsilon_{ij}^{**\Omega}\rangle_{\Omega}+(1-f)\,{}^{L(i)}\langle\varepsilon_{ij}^{**\Gamma}\rangle_{\Gamma} \quad . \qquad (16)
$$

Substituting the equivalent eigenstrain obtained by Eqs. (11) to (15) into Eq. (16) yields ${}^{L(i)}<\varepsilon_{ij}^{**V}>_V$ as follows

$$\begin{aligned}{}^{L(i)}<\boldsymbol{\varepsilon}^{**V}>_V &= -(1-\overline{\nu})\left\langle\left\{f\mathbf{P}^{\Omega}+(1-f)\mathbf{P}^{\Gamma}\right\}{}^{L(i)}\overline{\boldsymbol{\varepsilon}}-\left\{f\mathbf{P}^{\Omega}<^{\mathbf{L}}\boldsymbol{\varepsilon}^{p\Omega}>_{\Omega}+(1-f)\mathbf{P}^{\Gamma}<^{\mathbf{L}}\boldsymbol{\varepsilon}^{p\Gamma}>_{\Gamma}\right\}\right\rangle \\ &= -(1-\overline{\nu})\left\langle\mathbf{P}^{V}\,{}^{L(i)}\overline{\boldsymbol{\varepsilon}}-\left\{f\mathbf{P}^{\Omega}<^{\mathbf{L}}\boldsymbol{\varepsilon}^{p\Omega}>_{\Omega}+(1-f)\mathbf{P}^{\Gamma}<^{\mathbf{L}}\boldsymbol{\varepsilon}^{p\Gamma}>_{\Gamma}\right\}\right\rangle . \end{aligned} \tag{17}$$

In the equation, the quantities denoted in bold notation, such as ${}^{L(i)}<\boldsymbol{\varepsilon}^{**V}>_V$, ${}^{L(i)}\overline{\boldsymbol{\varepsilon}}$, and $<^{\mathbf{L}}\boldsymbol{\varepsilon}^{pX}>_X$ $(X=\Omega,\,\Gamma)$, differ from the usual component order. They are composed of hydrostatic, deviatoric, and shear components in the following order and are given as follows:

$${}^{L(i)}<\boldsymbol{\varepsilon}^{**V}>_V=\left\{{}^{L(i)}<\varepsilon_{ii}^{**V}>_V,{}^{\prime L(i)}<\varepsilon_{11}^{**V}>_V,{}^{\prime L(i)}<\varepsilon_{22}^{**V}>_V,{}^{\prime L(i)}<\varepsilon_{33}^{**V}>_V,{}^{L(i)}<\varepsilon_{23}^{**V}>_V,{}^{L(i)}<\varepsilon_{31}^{**V}>_V,{}^{L(i)}<\varepsilon_{12}^{**V}>_V\right\}^t, \tag{18a}$$

$${}^{L(i)}\overline{\boldsymbol{\varepsilon}}=\left\{{}^{L(i)}\overline{\varepsilon}_{ii},{}^{\prime L(i)}\overline{\varepsilon}_{11},{}^{\prime L(i)}\overline{\varepsilon}_{22},{}^{\prime L(i)}\overline{\varepsilon}_{33},{}^{L(i)}\overline{\varepsilon}_{23},{}^{L(i)}\overline{\varepsilon}_{31},{}^{L(i)}\overline{\varepsilon}_{12}\right\}^t, \tag{18b}$$

$$<^{\mathbf{L}}\boldsymbol{\varepsilon}^{pX}>_X=\left\{L_K^X<\varepsilon_{ii}^{pX}>_X,\,L_\mu^X{}'<\varepsilon_{11}^{pX}>_X,\,L_\mu^X{}'<\varepsilon_{22}^{pX}>_X,\,L_\mu^X{}'<\varepsilon_{33}^{pX}>_X,\,L_\mu^X<\varepsilon_{23}^{pX}>_X,\,L_\mu^X<\varepsilon_{31}^{pX}>_X,\,L_\mu^X<\varepsilon_{12}^{pX}>_X\right\}^t$$
$$(X=\Omega,\,\Gamma)\,, \tag{18c}$$

where ^{t} represents transpose. $\mathbf{P}^X(X=\Omega,\,\Gamma)$ in Eq. (17) is given by

$$\mathbf{P}^X=\begin{bmatrix} {}^nP_{11}^X & 0 & 0 & {}^nP_{12}^X & 0 & 0 & 0 \\ -\frac{{}^nP_{21}^X}{2} & \frac{1}{2}({}^nP_{22}^X+{}^sP_{12}^X) & \frac{1}{2}({}^nP_{22}^X-{}^sP_{12}^X) & 0 & 0 & 0 & 0 \\ -\frac{{}^nP_{21}^X}{2} & \frac{1}{2}({}^nP_{22}^X-{}^sP_{12}^X) & \frac{1}{2}({}^nP_{22}^X+{}^sP_{12}^X) & 0 & 0 & 0 & 0 \\ {}^nP_{21}^X & 0 & 0 & {}^nP_{22}^X & 0 & 0 & 0 \\ 0 & 0 & 0 & 0 & {}^sP_{23}^X & 0 & 0 \\ 0 & 0 & 0 & 0 & 0 & {}^sP_{23}^X & 0 \\ 0 & 0 & 0 & 0 & 0 & 0 & {}^sP_{12}^X \end{bmatrix},\ (X=\Omega,\,\Gamma)\,, \tag{19a}$$

where ${}^nP_{ij}^X$ and ${}^sP_{ij}^X(X=\Omega,\,\Gamma)$ are given in Appendix A.3. ^{n} and ^{s} are attached to the left shoulders of these coefficients to indicate that they are related to the normal and shear components, respectively. $\mathbf{P}^V$ in Eq. (17) is defined as

$$\mathbf{P}^V=f\mathbf{P}^{\Omega}+(1-f)\mathbf{P}^{\Gamma}\,. \tag{19b}$$

From Eq. (19a), the number of independent components of $\mathbf{P}^X(X=\Omega,\,\Gamma)$ is six. On the other hand, the number of independent components of $\mathbf{P}^V$ in Eq. (19b) is reduced to five by Eq. (A.12) in Appendix A.3.

The sequence of components shown in Eq. (18) is nothing but the original, unlike the commonly used sequence of normal and shear components $\{11,22,33,23,31,12\}$. The resolution of stresses and strains into hydrostatic and deviatoric components is based on the physical viewpoint that the deformation of a material can be resolved into deformations related to volume and shape. This resolution is carried out consistently in subsequent analyses, making it easier to understand the physical interpretation and validity of the solutions of macroscopic elastic moduli and thermal expansion coefficients.

2.1.3. Analysis of macroscopic elastic moduli

The stress-strain relations for the hydrostatic and deviatoric (or shear) components of the region $V(i)$ are obtained from Eqs. (1) and (2) as follows:

$$\begin{aligned}{}^{L(i)}\sigma_{ii}^V &= {}^{L(i)}\sigma_{ii}^0+{}^{L(i)}<\sigma_{ii}^{\infty}>_V=f({}^{L(i)}\sigma_{ii}^0+{}^{L(i)}<\sigma_{ii}^{\infty}>_{\Omega})+(1-f)({}^{L(i)}\sigma_{ii}^0+{}^{L(i)}<\sigma_{ii}^{\infty}>_{\Gamma}) \\ &= 3\overline{K}\left\{{}^{L(i)}\overline{\varepsilon}_{ii}+S_{iikl}^V\,{}^{L(i)}<\varepsilon_{kl}^{**V}>_V-{}^{L(i)}<\varepsilon_{ii}^{**V}>_V\right\} \\ &= 3\overline{K}\left\{{}^{L(i)}\varepsilon_{ii}^V-{}^{L(i)}<\varepsilon_{ii}^{**V}>_V\right\}, \end{aligned} \tag{20a}$$

$$\begin{aligned}{}^{\prime L(i)}\sigma_{ij}^V &= {}^{\prime L(i)}\sigma_{ij}^0+{}^{\prime L(i)}<\sigma_{ij}^{\infty}>_V=f({}^{\prime L(i)}\sigma_{ij}^0+{}^{\prime L(i)}<\sigma_{ij}^{\infty}>_{\Omega})+(1-f)({}^{\prime L(i)}\sigma_{ij}^0+{}^{\prime L(i)}<\sigma_{ij}^{\infty}>_{\Gamma}) \\ &= 2\overline{\mu}\left\{{}^{\prime L(i)}\overline{\varepsilon}_{ij}+{}^{\prime}S_{ijkl}^V\,{}^{L(i)}<\varepsilon_{kl}^{**V}>_V-{}^{\prime L(i)}<\varepsilon_{ij}^{**V}>_V\right\} \\ &= 2\overline{\mu}\left\{{}^{\prime L(i)}\varepsilon_{ij}^V-{}^{\prime L(i)}<\varepsilon_{ij}^{**V}>_V\right\}, \end{aligned} \tag{20b}$$

where ${}^{L(i)}\sigma_{ij}^V$ and ${}^{L(i)}\varepsilon_{ij}^V$ is the total stress (elastic stress) and total strain of the region $V(i)$. The hydrostatic and deviatoric (or shear) components of the total strain ${}^{L(i)}\varepsilon_{ij}^V$ are given by

$${}^{L(i)}\varepsilon_{ii}^V={}^{L(i)}\overline{\varepsilon}_{ii}+S_{iikl}^V\,{}^{L(i)}<\varepsilon_{kl}^{**V}>_V\,, \tag{21a}$$

$${}^{\prime L(i)}\varepsilon_{ij}^V={}^{\prime L(i)}\overline{\varepsilon}_{ij}+{}^{\prime}S_{ijkl}^V\,{}^{L(i)}<\varepsilon_{kl}^{**V}>_V\,. \tag{21b}$$

Substituting Eq. (17) into Eq. (21), we obtain the following equation

$$ {}^{L(i)}\boldsymbol{\varepsilon}^{V} = (\mathbf{I} - \mathbf{T}\mathbf{P}^{V})\, {}^{L(i)}\overline{\boldsymbol{\varepsilon}} + \mathbf{T}\left\{ f\mathbf{P}^{\Omega} <^{\mathbf{L}} \boldsymbol{\varepsilon}^{p\Omega} >_{\Omega} + (1-f)\mathbf{P}^{\Gamma} <^{\mathbf{L}} \boldsymbol{\varepsilon}^{p\Gamma} >_{\Gamma} \right\}, \tag{22a} $$

where ${}^{L(i)}\boldsymbol{\varepsilon}^{V}$ is the same sequence of components as Eqs. (18a) and (18b) and $\mathbf{I}$ is the identity matrix of 7×7. $\mathbf{T}$ can be resolved into the normal component ${}^{n}\mathbf{T}$ and the shear component ${}^{s}\mathbf{T}$ as

$$ \mathbf{T} = \begin{bmatrix} {}^{n}\mathbf{T} & \mathbf{0} \\ \mathbf{0} & {}^{s}\mathbf{T} \end{bmatrix}, \tag{23a} $$

$$ {}^{n}\mathbf{T} = \begin{bmatrix} \frac{1+\overline{\nu}}{3} & 0 & 0 & -\frac{1-2\overline{\nu}}{2}\alpha_3^V \\ \frac{1+\overline{\nu}}{18}\alpha_3^V & \frac{3}{4}\left\{\frac{2}{3}H_1^V + \frac{4(1-2\overline{\nu})}{9}\right\} & -\frac{3}{4}R_3^V & 0 \\ \frac{1+\overline{\nu}}{18}\alpha_3^V & -\frac{3}{4}R_3^V & \frac{3}{4}\left\{\frac{2}{3}H_1^V + \frac{4(1-2\overline{\nu})}{9}\right\} & 0 \\ -\frac{1+\overline{\nu}}{9}\alpha_3^V & 0 & 0 & \frac{3}{4}\left\{\frac{2}{3}H_1^V + \frac{4(1-2\overline{\nu})}{9} - R_3^V\right\} \end{bmatrix}, \tag{23b} $$

$$ {}^{s}\mathbf{T} = \begin{bmatrix} -\frac{3}{8}\left\{2H_1^V - \frac{4(5-4\overline{\nu})}{9} + R_3^V\right\} & 0 & 0 \\ 0 & -\frac{3}{8}\left\{2H_1^V - \frac{4(5-4\overline{\nu})}{9} + R_3^V\right\} & 0 \\ 0 & 0 & \frac{3}{4}\left\{\frac{2}{3}H_1^V + \frac{4(1-2\overline{\nu})}{9} + R_3^V\right\} \end{bmatrix}. \tag{23c} $$

Substituting Eqs. (17) and (22a) into Eq. (20), the total stress in the region $V(i)$ becomes

$$ {}^{L(i)}\boldsymbol{\sigma}^{V} = \overline{\mathbf{C}}\left\langle \mathbf{I} - \left\{\mathbf{T} - (1-\overline{\nu})\mathbf{I}\right\}\mathbf{P}^{V} \right\rangle {}^{L(i)}\overline{\boldsymbol{\varepsilon}} + \overline{\mathbf{C}}\left\{\mathbf{T} - (1-\overline{\nu})\mathbf{I}\right\}\left\{ f\mathbf{P}^{\Omega} <^{\mathbf{L}} \boldsymbol{\varepsilon}^{p\Omega} >_{\Omega} + (1-f)\mathbf{P}^{\Gamma} <^{\mathbf{L}} \boldsymbol{\varepsilon}^{p\Gamma} >_{\Gamma} \right\}, \tag{22b} $$

where ${}^{L(i)}\boldsymbol{\sigma}^{V}$ is a sequence of components similar to Eqs. (18a) and (18b), and is given by

$$ {}^{L(i)}\boldsymbol{\sigma}^{V} = \left\{ {}^{L(i)}\sigma_{ii}^{V},\ {}'^{L(i)}\sigma_{11}^{V},\ {}'^{L(i)}\sigma_{22}^{V},\ {}'^{L(i)}\sigma_{33}^{V},\ {}^{L(i)}\sigma_{23}^{V},\ {}^{L(i)}\sigma_{31}^{V},\ {}^{L(i)}\sigma_{12}^{V} \right\}^{t}. \tag{18d} $$

$\overline{\mathbf{C}}$ in Eq. (22b) is given by

$$ \overline{\mathbf{C}} = \begin{bmatrix} 3\overline{K} & 0 & 0 & 0 & 0 & 0 & 0 \\ 0 & 2\overline{\mu} & 0 & 0 & 0 & 0 & 0 \\ 0 & 0 & 2\overline{\mu} & 0 & 0 & 0 & 0 \\ 0 & 0 & 0 & 2\overline{\mu} & 0 & 0 & 0 \\ 0 & 0 & 0 & 0 & 2\overline{\mu} & 0 & 0 \\ 0 & 0 & 0 & 0 & 0 & 2\overline{\mu} & 0 \\ 0 & 0 & 0 & 0 & 0 & 0 & 2\overline{\mu} \end{bmatrix}. \tag{24} $$

Note that the component sequence in Eq. (24) is different from that of the usual Voigt notation.

Next, we consider the coordinate transformation equations for strain and stress from the global coordinate system to the local coordinate one, or vice versa. Let ${}^{L}\boldsymbol{\varepsilon}$ and ${}^{L}\boldsymbol{\sigma}$ denote the strains and stresses in the local coordinate system, and ${}^{G}\boldsymbol{\varepsilon}$ and ${}^{G}\boldsymbol{\sigma}$ in the global coordinate one. The coordinate transformation equations are given by

$$ {}^{L}\boldsymbol{\sigma} = \boldsymbol{l}\,({}^{G}\boldsymbol{\sigma})\,\boldsymbol{l}^{t} \quad , \qquad {}^{L}\boldsymbol{\varepsilon} = \boldsymbol{l}\,({}^{G}\boldsymbol{\varepsilon})\,\boldsymbol{l}^{t}, \tag{25a} $$

$$ {}^{G}\boldsymbol{\sigma} = \boldsymbol{l}^{t}\,({}^{L}\boldsymbol{\sigma})\,\boldsymbol{l} \quad , \qquad {}^{G}\boldsymbol{\varepsilon} = \boldsymbol{l}^{t}\,({}^{L}\boldsymbol{\varepsilon})\,\boldsymbol{l}, \tag{25b} $$

where $\boldsymbol{l}$ in the equation is the coordinate transformation matrix given by Eq. (A.18) in Appendix A.5, and $\boldsymbol{l}^{t}$ is the transposed matrix of $\boldsymbol{l}$. The stress and strain in Eq. (25) are given by

$$ \boldsymbol{\sigma} = \begin{bmatrix} \sigma_{11} & \sigma_{12} & \sigma_{31} \\ & \sigma_{22} & \sigma_{23} \\ sym. & & \sigma_{33} \end{bmatrix}, \qquad \boldsymbol{\varepsilon} = \begin{bmatrix} \varepsilon_{11} & \varepsilon_{12} & \varepsilon_{31} \\ & \varepsilon_{22} & \varepsilon_{23} \\ sym. & & \varepsilon_{33} \end{bmatrix}. \tag{26} $$

Replacing Eq. (26) with the column vectors of hydrostatic, deviatoric, and shear components shown in Eq. (18), the coordinate transformation equation (25) is expressed as follows:

$$ {}^{L}\boldsymbol{\sigma} = \boldsymbol{L}\,({}^{G}\boldsymbol{\sigma}) \quad , \qquad {}^{L}\boldsymbol{\varepsilon} = \boldsymbol{L}\,({}^{G}\boldsymbol{\varepsilon}), \tag{27a} $$

$$ {}^{G}\boldsymbol{\sigma} = \hat{\boldsymbol{L}}\,({}^{L}\boldsymbol{\sigma}) \quad , \qquad {}^{G}\boldsymbol{\varepsilon} = \hat{\boldsymbol{L}}\,({}^{L}\boldsymbol{\varepsilon}), \tag{27b} $$

where the newly defined coordinate transformation matrices $\boldsymbol{L}$ and $\hat{\boldsymbol{L}}$ are shown in Appendix A.5.

Using the relation of Eq. (27), the transformation equations from the local coordinate system to the global coordinate one for ${}^{L(i)}\boldsymbol{\varepsilon}^{V}$ and ${}^{L(i)}\boldsymbol{\sigma}^{V}$ expressed by Eqs. (22a) and (22b) are as follows:

$$ {}^{G}\boldsymbol{\varepsilon}^{V} = \hat{\boldsymbol{L}}(\mathbf{I} - \mathbf{T}\mathbf{P}^{V})\boldsymbol{L}\, {}^{G}\overline{\boldsymbol{\varepsilon}} + \hat{\boldsymbol{L}}\mathbf{T}\left\{ f\mathbf{P}^{\Omega} <^{\mathbf{L}} \boldsymbol{\varepsilon}^{p\Omega} >_{\Omega} + (1-f)\mathbf{P}^{\Gamma} <^{\mathbf{L}} \boldsymbol{\varepsilon}^{p\Gamma} >_{\Gamma} \right\}, \tag{28a} $$

$$ {}^{G}\boldsymbol{\sigma}^{V} = \hat{\boldsymbol{L}}\overline{\mathbf{C}}\left\langle \mathbf{I} - \left\{\mathbf{T} - (1-\overline{\nu})\mathbf{I}\right\}\mathbf{P}^{V} \right\rangle \boldsymbol{L}\, {}^{G}\overline{\boldsymbol{\varepsilon}} + \hat{\boldsymbol{L}}\overline{\mathbf{C}}\left\{\mathbf{T} - (1-\overline{\nu})\mathbf{I}\right\}\left\{ f\mathbf{P}^{\Omega} <^{\mathbf{L}} \boldsymbol{\varepsilon}^{p\Omega} >_{\Omega} + (1-f)\mathbf{P}^{\Gamma} <^{\mathbf{L}} \boldsymbol{\varepsilon}^{p\Gamma} >_{\Gamma} \right\}. \tag{28b} $$

From Eq. (28), taking the summation of the total stress and strain of all coated fillers and the matrix yields the macroscopic total strain ${}^{G}\overline{\boldsymbol{\varepsilon}}$ and stress ${}^{G}\overline{\boldsymbol{\sigma}}$ of the material as follows:

$$
\begin{aligned}
{}^{G}\overline{\boldsymbol{\varepsilon}} &= \sum_{i=1}^{n} f_{V(i)}\,{}^{G}\boldsymbol{\varepsilon}^{V} + \left(1-\sum_{i=1}^{n} f_{V(i)}\right){}^{G}\boldsymbol{\varepsilon}^{m} = \frac{1}{8\pi^2} f_V \int_0^{\pi}\int_0^{2\pi}\int_0^{2\pi} sin\theta\,({}^{G}\boldsymbol{\varepsilon}^{V})\,d\theta\,d\phi\,d\psi + (1-f_V)\,{}^{G}\boldsymbol{\varepsilon}^{m} \\
&= f_V\Big\langle (\mathbf{I}-\mathbf{P}^{\Sigma})\,{}^{G}\overline{\boldsymbol{\varepsilon}} + \left\{ f\mathbf{P}^{p\Sigma\Omega} <^{\mathbf{L}} \boldsymbol{\varepsilon}^{p\Omega} >_{\Omega} + (1-f)\mathbf{P}^{p\Sigma\Gamma} <^{\mathbf{L}} \boldsymbol{\varepsilon}^{p\Gamma} >_{\Gamma} \right\}\Big\rangle + (1-f_V)\,{}^{G}\boldsymbol{\varepsilon}^{m}\,, \qquad (29a)
\end{aligned}
$$

$$
\begin{aligned}
{}^{G}\overline{\boldsymbol{\sigma}} &= \sum_{i=1}^{n} f_{V(i)}\,{}^{G}\boldsymbol{\sigma}^{V} + \left(1-\sum_{i=1}^{n} f_{V(i)}\right){}^{G}\boldsymbol{\sigma}^{m} = \frac{1}{8\pi^2} f_V \int_0^{\pi}\int_0^{2\pi}\int_0^{2\pi} sin\theta\,({}^{G}\boldsymbol{\sigma}^{V})\,d\theta\,d\phi\,d\psi + (1-f_V)\,{}^{G}\boldsymbol{\sigma}^{m} \\
&= f_V\Big\langle (\overline{\mathbf{C}}-\mathbf{Q}^{\Sigma})\,{}^{G}\overline{\boldsymbol{\varepsilon}} + \left\{ f\mathbf{Q}^{p\Sigma\Omega} <^{\mathbf{L}} \boldsymbol{\varepsilon}^{p\Omega} >_{\Omega} + (1-f)\mathbf{Q}^{p\Sigma\Gamma} <^{\mathbf{L}} \boldsymbol{\varepsilon}^{p\Gamma} >_{\Gamma} \right\}\Big\rangle + (1-f_V)\,{}^{G}\boldsymbol{\sigma}^{m}\,. \qquad (29b)
\end{aligned}
$$

Equations (A.12) and (A.19) in Appendix A are used to derive the above equations. ${}^{G}\boldsymbol{\varepsilon}^{m}$ in Eq. (29a) and ${}^{G}\boldsymbol{\sigma}^{m}$ in Eq. (29b) are the total strain and stress in the matrix, and are given as a column vector with the same component arrangement as in Eq. (18).

$\mathbf{P}^{\Sigma}$, $\mathbf{Q}^{\Sigma}$, $\mathbf{P}^{p\Sigma\Omega}$, $\mathbf{P}^{p\Sigma\Gamma}$, $\mathbf{Q}^{p\Sigma\Omega}$, and $\mathbf{Q}^{p\Sigma\Gamma}$ are given in the simple form as

$$
\mathbf{X}^{\Sigma} = \begin{bmatrix} X_h^{\Sigma} & 0 & 0 & 0 & 0 & 0 & 0 \\ 0 & X_d^{\Sigma} & 0 & 0 & 0 & 0 & 0 \\ 0 & 0 & X_d^{\Sigma} & 0 & 0 & 0 & 0 \\ 0 & 0 & 0 & X_d^{\Sigma} & 0 & 0 & 0 \\ 0 & 0 & 0 & 0 & X_d^{\Sigma} & 0 & 0 \\ 0 & 0 & 0 & 0 & 0 & X_d^{\Sigma} & 0 \\ 0 & 0 & 0 & 0 & 0 & 0 & X_d^{\Sigma} \end{bmatrix}, \quad \mathbf{X}^{p\Sigma Y} = \begin{bmatrix} X_h^{p\Sigma Y} & 0 & 0 & X_3^{p\Sigma Y} & 0 & 0 & 0 \\ 0 & 0 & 0 & 0 & 0 & 0 & 0 \\ 0 & 0 & 0 & 0 & 0 & 0 & 0 \\ 0 & 0 & 0 & 0 & 0 & 0 & 0 \\ 0 & 0 & 0 & 0 & 0 & 0 & 0 \\ 0 & 0 & 0 & 0 & 0 & 0 & 0 \\ 0 & 0 & 0 & 0 & 0 & 0 & 0 \end{bmatrix},
$$

$$
(X = P\,, Q)\,,\ (Y = \Omega\,, \Gamma)\,. \qquad (30)
$$

In particular, for $\mathbf{X}^{\Sigma}(X = P\,, Q)$, only the diagonal terms are present and all of the off-diagonal terms are zero. Furthermore, we can see that the number of independent components of $\mathbf{X}^{\Sigma}(X = P\,, Q)$ is two, similar to the elastic moduli of isotropic materials. P_h^{Σ}, P_d^{Σ}, $P_h^{p\Sigma\Omega}$, $P_3^{p\Sigma\Gamma}$, etc. in Eq. (30) are given by

$$
\begin{aligned}
P_h^{\Sigma} &= \frac{1+\overline{\nu}}{3}\left({}^{n}P_{11}^{V} - \frac{1}{3}\alpha_3^{V}\,{}^{n}P_{12}^{V}\right), \\
P_d^{\Sigma} &= \frac{1}{5}\Big\langle -\frac{1+\overline{\nu}}{9}\alpha_3^{V}\,{}^{n}P_{12}^{V} + \frac{3}{4}\left\{\frac{2}{3}H_1^{V} + \frac{4(1-2\overline{\nu})}{9} - R_3^{V}\right\}{}^{n}P_{22}^{V} \\
&\quad + \frac{3}{2}\left\{\frac{2}{3}H_1^{V} + \frac{4(1-2\overline{\nu})}{9} + R_3^{V}\right\}{}^{s}P_{12}^{V} - \frac{3}{4}\left\{2H_1^{V} - \frac{4(5-4\overline{\nu})}{9} + R_3^{V}\right\}{}^{s}P_{23}^{V}\Big\rangle\,, \qquad (31a) \\
P_h^{p\Sigma Y} &= \frac{(1+\overline{\nu})}{3}\,{}^{n}P_{11}^{Y} - \frac{(1-2\overline{\nu})}{2}\alpha_3^{V}\,{}^{n}P_{21}^{Y} \quad , \quad P_3^{p\Sigma Y} = \frac{(1+\overline{\nu})}{3}\,{}^{n}P_{12}^{Y} - \frac{(1-2\overline{\nu})}{2}\alpha_3^{V}\,{}^{n}P_{22}^{Y} \quad , \quad (Y = \Omega\,, \Gamma)\,, \qquad (31b)
\end{aligned}
$$

$$
\begin{aligned}
Q_h^{\Sigma} &= 3\overline{K}\left\{P_h^{\Sigma} - (1-\overline{\nu})\,{}^{n}P_{11}^{V}\right\} \quad , \quad Q_d^{\Sigma} = 2\overline{\mu}\Big\langle P_d^{\Sigma} - \frac{1-\overline{\nu}}{5}\left\{\,{}^{n}P_{22}^{V} + 2({}^{s}P_{23}^{V} + {}^{s}P_{12}^{V})\right\}\Big\rangle\,, \qquad (32a) \\
Q_h^{p\Sigma Y} &= 3\overline{K}\left\{P_h^{p\Sigma Y} - (1-\overline{\nu})\,{}^{n}P_{11}^{Y}\right\} \quad , \quad Q_3^{p\Sigma Y} = 3\overline{K}\left\{P_3^{p\Sigma Y} - (1-\overline{\nu})\,{}^{n}P_{12}^{Y}\right\} \quad , \quad (Y = \Omega\,, \Gamma)\,. \qquad (32b)
\end{aligned}
$$

As can be seen from Eqs. (29) to (30), we find that deviatoric components of ${}^{G}\overline{\boldsymbol{\varepsilon}}$ and ${}^{G}\overline{\boldsymbol{\sigma}}$ are the same as the shear components of them. Therefore, Eq. (29a) and Eq. (29b) can be separated into the hydrostatic component and the deviatoric one, and can be expressed as follows:

$$
\begin{aligned}
{}^{G}\overline{\varepsilon}_{ii} &= f_V\Big\langle (1-P_h^{\Sigma})\,{}^{G}\overline{\varepsilon}_{ii} + \left\{ f\,P_h^{p\Sigma\Omega} L_K^{\Omega} <\varepsilon_{ii}^{p\Omega}>_{\Omega} + (1-f)P_h^{p\Sigma\Gamma} L_K^{\Gamma} <\varepsilon_{ii}^{p\Gamma}>_{\Gamma}\right\} \\
&\qquad + \left\{ f\,P_3^{p\Sigma\Omega} L_{\mu}^{\Omega\,\prime} <\varepsilon_{33}^{p\Omega}>_{\Omega} + (1-f)P_3^{p\Sigma\Gamma} L_{\mu}^{\Gamma\,\prime} <\varepsilon_{33}^{p\Gamma}>_{\Gamma}\right\}\Big\rangle + (1-f_V)^{G}\varepsilon_{ii}^{m}\,, \qquad (33a) \\
{}'^{G}\overline{\varepsilon}_{ij} &= f_V(1-P_d^{\Sigma})\,{}'^{G}\overline{\varepsilon}_{ij} + (1-f_V)\,{}'^{G}\varepsilon_{ij}^{m}\,, \qquad (33b)
\end{aligned}
$$

$$
\begin{aligned}
{}^{G}\overline{\sigma}_{ii} &= 3f_V\overline{K}\Big\langle \left\{1-P_h^{\Sigma} + (1-\overline{\nu})\,{}^{n}P_{11}^{V}\right\}{}^{G}\overline{\varepsilon}_{ii} \\
&\quad + f\left\{P_h^{p\Sigma\Omega} - (1-\overline{\nu})\,{}^{n}P_{11}^{\Omega}\right\}L_K^{\Omega} <\varepsilon_{ii}^{p\Omega}>_{\Omega} + (1-f)\left\{P_h^{p\Sigma\Gamma} - (1-\overline{\nu})\,{}^{n}P_{11}^{\Gamma}\right\}L_K^{\Gamma} <\varepsilon_{ii}^{p\Gamma}>_{\Gamma} \\
&\quad + f\left\{P_3^{p\Sigma\Omega} - (1-\overline{\nu})\,{}^{n}P_{12}^{\Omega}\right\}L_{\mu}^{\Omega\,\prime} <\varepsilon_{33}^{p\Omega}>_{\Omega} + (1-f)\left\{P_3^{p\Sigma\Gamma} - (1-\overline{\nu})\,{}^{n}P_{12}^{\Gamma}\right\}L_{\mu}^{\Gamma\,\prime} <\varepsilon_{33}^{p\Gamma}>_{\Gamma}\Big\rangle + (1-f_V)^{G}\sigma_{ii}^{m}\,, \qquad (34a) \\
{}'^{G}\overline{\sigma}_{ij} &= 2f_V\overline{\mu}\Big\langle 1-P_d^{\Sigma} + \frac{1-\overline{\nu}}{5}\left\{\,{}^{n}P_{22}^{V} + 2({}^{s}P_{23}^{V} + {}^{s}P_{12}^{V})\right\}\Big\rangle\,{}'^{G}\overline{\varepsilon}_{ij} + (1-f_V)\,{}'^{G}\sigma_{ij}^{m}\,. \qquad (34b)
\end{aligned}
$$

The relation between shear stresses and strains is obtained by removing the superscript $'$ from Eqs. (33b) and (34b). The following relations hold between ε_{ij}^{m} and σ_{ij}^{m} in the matrix:

$$ {}^{G}\sigma_{ii}^{m} = 3K\,{}^{G}\varepsilon_{ii}^{m} \quad , \qquad {}'^{G}\sigma_{ij}^{m} = 2\mu\,{}'^{G}\varepsilon_{ij}^{m} \, , \tag{35} $$

where K and μ are bulk modulus and shear modulus of the matrix respectively, as shown in Fig. 1. For Eqs. (33) and (34), by eliminating ε_{ij}^{m} and σ_{ij}^{m} using the relation of Eq. (35), we obtain the relation between ${}^{G}\overline{\varepsilon}_{ij}$ and ${}^{G}\overline{\sigma}_{ij}$ as follows:

$$ \begin{aligned} {}^{G}\overline{\sigma}_{ii} = 3\Big\langle & K - f_V\big\{(K-\overline{K})(1-P_h^{\Sigma}) - (1-\overline{\nu})\overline{K}\,{}^{n}P_{11}^{V}\big\}\Big\rangle\,{}^{G}\overline{\varepsilon}_{ii} \\ & - 3f_V\Big\langle f L_K^{\Omega}\big\{(K-\overline{K})P_h^{p\Sigma\Omega} + (1-\overline{\nu})\overline{K}\,{}^{n}P_{11}^{\Omega}\big\} < \varepsilon_{ii}^{p\Omega} >_{\Omega} + (1-f)L_K^{\Gamma}\big\{(K-\overline{K})P_h^{p\Sigma\Gamma} + (1-\overline{\nu})\overline{K}\,{}^{n}P_{11}^{\Gamma}\big\} < \varepsilon_{ii}^{p\Gamma} >_{\Gamma} \\ & + f L_{\mu}^{\Omega}\big\{(K-\overline{K})P_3^{p\Sigma\Omega} + (1-\overline{\nu})\overline{K}\,{}^{n}P_{12}^{\Omega}\big\}' < \varepsilon_{33}^{p\Omega} >_{\Omega} + (1-f)L_{\mu}^{\Gamma}\big\{(K-\overline{K})P_3^{p\Sigma\Gamma} + (1-\overline{\nu})\overline{K}\,{}^{n}P_{12}^{\Gamma}\big\}' < \varepsilon_{33}^{p\Gamma} >_{\Gamma}\Big\rangle \, , \end{aligned} \tag{36a} $$

$$ {}'^{G}\overline{\sigma}_{ij} = 2\left[\mu - f_V\left\langle(\mu-\overline{\mu})(1-P_d^{\Sigma}) - \frac{1-\overline{\nu}}{5}\overline{\mu}\big\{{}^{n}P_{22}^{V} + 2({}^{s}P_{23}^{V} + {}^{s}P_{12}^{V})\big\}\right\rangle\right]{}'^{G}\overline{\varepsilon}_{ij} \, . \tag{36b} $$

If the eigenstrains $\varepsilon_{ij}^{p\Omega}$ and $\varepsilon_{ij}^{p\Gamma}$ are zero, the total strain ${}^{G}\overline{\varepsilon}_{ij}$ is equal to the elastic strain. Then, the relations between ${}^{G}\overline{\varepsilon}_{ij}$ and ${}^{G}\overline{\sigma}_{ij}$ by using the macroscopic bulk modulus $\overline{K}$ and shear modulus $\overline{\mu}$ are given as follows:

$$ {}^{G}\overline{\sigma}_{ii} = 3\overline{K}\;{}^{G}\overline{\varepsilon}_{ii} \quad , \qquad {}'^{G}\overline{\sigma}_{ij} = 2\overline{\mu}\;{}'^{G}\overline{\varepsilon}_{ij} \, . \tag{37} $$

After substituting $\varepsilon_{ij}^{p\Omega} = \varepsilon_{ij}^{p\Gamma} = 0$ into Eq. (36), we set Eq. (36) equal to Eq. (37). We finally obtain the macroscopic bulk modulus $\overline{K}$ and shear modulus $\overline{\mu}$ as follows:

$$ \overline{K} = K + \frac{f_V(1-\overline{\nu})K\,{}^{n}P_{11}^{V}}{1 - f_V + f_V\big\{P_h^{\Sigma} - (1-\overline{\nu})\,{}^{n}P_{11}^{V}\big\}} \quad , \quad \overline{\mu} = \mu + \frac{\dfrac{f_V(1-\overline{\nu})}{5}\mu\big\{{}^{n}P_{22}^{V} + 2({}^{s}P_{23}^{V} + {}^{s}P_{12}^{V})\big\}}{1 - f_V + f_V\left\langle P_d^{\Sigma} - \dfrac{1-\overline{\nu}}{5}\big\{{}^{n}P_{22}^{V} + 2({}^{s}P_{23}^{V} + {}^{s}P_{12}^{V})\big\}\right\rangle} \, , \tag{38} $$

where $\overline{\nu}$ is the macroscopic Poisson's ratio of the material.

As shown in Eq. (19) and equations in Appendix A.2 and A.3, P_h^{Σ}, P_d^{Σ}, ${}^{n}P_{ij}^{V}$, and ${}^{s}P_{ij}^{V}$ in Eq. (38) contain the unknown macroscopic elastic moduli $\overline{K}$, $\overline{\mu}$, and $\overline{\nu}$. Therefore, Eq. (38) represents equations for determining these unknown moduli. Since the physical properties of the material are isotropic, the following relation holds among $\overline{\mu}$, $\overline{K}$, and $\overline{\nu}$:

$$ \overline{\nu} = \frac{3\overline{K} - 2\overline{\mu}}{6\overline{K} + 2\overline{\mu}} \, . \tag{39} $$

Substituting Eq. (39) into Eq. (38) gives equations for the unknown $\overline{K}$ and $\overline{\mu}$. However, the two equations in Eq. (38) are complicated equations of $\overline{K}$ and $\overline{\mu}$, and it is difficult to solve them explicitly. Therefore, it is necessary to find the values of $\overline{K}$ and $\overline{\mu}$ that satisfy Eq. (38) by numerical calculation.

If the shape of the inner region Ω and the outer region V of the coated filler is spherical, substituting the geometrical factors in Appendix A.1 into the coefficients in Appendix A.2, we obtain $\alpha_i^X = 0$, $R_i^X = 0$ $(X = \Omega, V, \Gamma)$. Therefore, A_3^X, A_{23}^X, A_{12}^X $(X = \Omega, \Gamma)$ in Appendix A.2 are $A_3^X = L_{\mathrm{I}}^X L_{\mathrm{II}}^X$ and $A_{23}^X = A_{12}^X = L_{\mathrm{II}}^X$, respectively. Substituting these into Eqs. (A.9) and (A.10) in Appendix A.3, we obtain the following relations:

$$ {}^{n}P_{11}^{X} = \frac{3}{L_{\mathrm{I}}^X} \quad , \quad {}^{n}P_{22}^{X} = {}^{s}P_{23}^{X} = {}^{s}P_{12}^{X} = \frac{2}{L_{\mathrm{II}}^X} \quad , \quad (X = \Omega\,, \Gamma) \, . \tag{40} $$

Substituting Eq. (40) into Eqs. (19) and (30), we can obtain P_h^{Σ}, P_d^{Σ}, ${}^{n}P_{ij}^{V}$, and ${}^{s}P_{ij}^{V}$. Furthermore, by substituting these into Eq. (38), the macroscopic bulk modulus $\overline{K}$ and shear modulus $\overline{\mu}$ for the case of the spherical shape of coated fillers can be expressed as follows:

$$ \overline{K} = K + \frac{3f_V(1-\overline{\nu})K\left(\dfrac{f}{L_{\mathrm{I}}^{\Omega}} + \dfrac{1-f}{L_{\mathrm{I}}^{\Gamma}}\right)}{1 - f_V - 2(1-2\overline{\nu})f_V\left(\dfrac{f}{L_{\mathrm{I}}^{\Omega}} + \dfrac{1-f}{L_{\mathrm{I}}^{\Gamma}}\right)} \quad , \quad \overline{\mu} = \mu + \frac{30f_V(1-\overline{\nu})\mu\left(\dfrac{f}{L_{\mathrm{II}}^{\Omega}} + \dfrac{1-f}{L_{\mathrm{II}}^{\Gamma}}\right)}{15(1-f_V) + 2(7-5\overline{\nu})f_V\left(\dfrac{f}{L_{\mathrm{II}}^{\Omega}} + \dfrac{1-f}{L_{\mathrm{II}}^{\Gamma}}\right)} \, . \tag{41} $$

When $f = 1$, the region Γ in the coated filler disappears, or when $f = 0$, the region Ω disappears. In these cases, the double inhomogeneous inclusion becomes the single inhomogeneous inclusion. In this limit, Eq. (41) reduces to the following expression

$$ \overline{K} = K + \frac{3f_V(1-\overline{\nu})\,\overline{K}\,(K^X - K)}{3(1-\overline{\nu})\overline{K} + (1+\overline{\nu})(K^X - \overline{K})} \quad , \qquad \overline{\mu} = \mu + \frac{15f_V(1-\overline{\nu})\,\overline{\mu}\,(\mu^X - \mu)}{15(1-\overline{\nu})\overline{\mu} + 2(4-5\overline{\nu})(\mu^X - \overline{\mu})} \quad , $$
$$ (X = \Omega \; when \; f = 1, \; X = \Gamma \; when \; f = 0) \, . \tag{42} $$

These solutions in Eq. (42) agree with those found by Budiansky [30].

2.1.4. Analysis of macroscopic thermal expansion coefficient

For the model shown in Fig. 3, we consider the state where the external stress ${}^{G}\sigma_{ij}^{0}=0$ and only the temperature change ΔT occurs in the material. Then, thermal expansion strains occur in the material due to the difference in the thermal expansion coefficient between the coated filler and the matrix. When the thermal expansion of the homogenized material surrounding the coated filler $V(i)$ is regarded as the reference, the thermal expansion strains $\varepsilon_{ij}^{p\Omega}$ and $\varepsilon_{ij}^{p\Gamma}$ occurred in the coated filler are expressed by

$$<\varepsilon_{ij}^{pX}>_{X}=\delta_{ij}(\alpha^{X}-\overline{\alpha})\Delta T \quad , \quad (X=\Omega\,,\Gamma)\,, \tag{43}$$

where $\alpha^{X}(X=\Omega\,,\Gamma)$ is the thermal expansion coefficient of the region X, and $\overline{\alpha}$ is the unknown macroscopic thermal expansion coefficient of the homogenized material as shown in Fig. 3.

The hydrostatic components of the total strain and stress of the coated filler $V(i)$ are obtained from Eqs. (19) to (23), (31), (32) and (43) as follows:

$$\begin{aligned}{}^{L(i)}\varepsilon_{ii}^{V}&=3\Big\langle f\Big\{\frac{(1+\overline{\nu})}{3}\,{}^{n}P_{11}^{\Omega}-\frac{(1-2\overline{\nu})}{2}\alpha_{3}^{V}\,{}^{n}P_{21}^{\Omega}\Big\}L_{K}^{\Omega}(\alpha^{\Omega}-\overline{\alpha})+(1-f)\Big\{\frac{(1+\overline{\nu})}{3}\,{}^{n}P_{11}^{\Gamma}-\frac{(1-2\overline{\nu})}{2}\alpha_{3}^{V}\,{}^{n}P_{21}^{\Gamma}\Big\}L_{K}^{\Gamma}(\alpha^{\Gamma}-\overline{\alpha})\Big\rangle+3\overline{\alpha}\,\Delta T\\&=3\Big\{f\,P_{h}^{p\Sigma\Omega}L_{K}^{\Omega}(\alpha^{\Omega}-\overline{\alpha})+(1-f)P_{h}^{p\Sigma\Gamma}L_{K}^{\Gamma}(\alpha^{\Gamma}-\overline{\alpha})\Big\}\Delta T+3\overline{\alpha}\,\Delta T\,,\end{aligned} \tag{44a}$$

$${}^{L(i)}\sigma_{ii}^{V}=9\overline{K}\Big\langle f\big\{P_{h}^{p\Sigma\Omega}-(1-\overline{\nu})\,{}^{n}P_{11}^{\Omega}\big\}L_{K}^{\Omega}(\alpha^{\Omega}-\overline{\alpha})+(1-f)\big\{P_{h}^{p\Sigma\Gamma}-(1-\overline{\nu})\,{}^{n}P_{11}^{\Gamma}\big\}L_{K}^{\Gamma}(\alpha^{\Gamma}-\overline{\alpha})\Big\rangle\Delta T\,, \tag{44b}$$

where we note that the thermal expansion strain $3\overline{\alpha}\Delta T$ must be added to the total strain ${}^{L(i)}\varepsilon_{ii}^{V}$, since ${}^{L(i)}\varepsilon_{ii}^{V}$ is solved by referring the thermal expansion of the homogenized material. Transforming Eqs. (44) to the global coordinate system and taking the sum of the total strain and stress in coated fillers and the matrix, the hydrostatic components of the macroscopic total strain and stress of the material are given by the following equations, respectively:

$${}^{G}\overline{\varepsilon}_{ii}=3f_{V}\Big\{f\,P_{h}^{p\Sigma\Omega}L_{K}^{\Omega}(\alpha^{\Omega}-\overline{\alpha})+(1-f)P_{h}^{p\Sigma\Gamma}L_{K}^{\Gamma}(\alpha^{\Gamma}-\overline{\alpha})\Big\}\Delta T+3f_{V}\,\overline{\alpha}\,\Delta T+(1-f_{V})\,{}^{G}\varepsilon_{ii}^{m}=3\overline{\alpha}\Delta T\,, \tag{45a}$$

$${}^{G}\overline{\sigma}_{ii}=9f_{V}\,\overline{K}\Big\langle f\big\{P_{h}^{p\Sigma\Omega}-(1-\overline{\nu})\,{}^{n}P_{11}^{\Omega}\big\}L_{K}^{\Omega}(\alpha^{\Omega}-\overline{\alpha})+(1-f)\big\{P_{h}^{p\Sigma\Gamma}-(1-\overline{\nu})\,{}^{n}P_{11}^{\Gamma}\big\}L_{K}^{\Gamma}(\alpha^{\Gamma}-\overline{\alpha})\Big\rangle\Delta T+(1-f_{V})\,{}^{G}\sigma_{ii}^{m}=0\,, \tag{45b}$$

where ${}^{G}\overline{\varepsilon}_{ii}$ is the thermal expansion strain of the whole material itself, so ${}^{G}\overline{\varepsilon}_{ii}$ is equal to $3\overline{\alpha}\Delta T$ as shown on the right side of Eq. (45a). In addition, ${}^{G}\overline{\sigma}_{ii}$ in Eq. (45b) is the sum of the internal stresses in the material, so ${}^{G}\overline{\sigma}_{ii}$ must be zero. Solving Eq. (45b) for the total stress ${}^{G}\sigma_{ii}^{m}$ in the matrix yields

$${}^{G}\sigma_{ii}^{m}=-\frac{9f_{V}}{1-f_{V}}\overline{K}\Big\langle f\big\{P_{h}^{p\Sigma\Omega}-(1-\overline{\nu})\,{}^{n}P_{11}^{\Omega}\big\}L_{K}^{\Omega}(\alpha^{\Omega}-\overline{\alpha})+(1-f)\big\{P_{h}^{p\Sigma\Gamma}-(1-\overline{\nu})\,{}^{n}P_{11}^{\Gamma}\big\}L_{K}^{\Gamma}(\alpha^{\Gamma}-\overline{\alpha})\Big\rangle\Delta T\,. \tag{46}$$

The total strain ${}^{G}\varepsilon_{ij}^{m}$ of the matrix is given by the sum of the elastic strain ${}^{G}\varepsilon_{ij}^{me}$ and the thermal expansion strain $3\alpha\Delta T$ of the matrix. Therefore, the hydrostatic component of ${}^{G}\varepsilon_{ij}^{m}$ is obtained from Eqs. (35) and (46) as follows:

$$\begin{aligned}{}^{G}\varepsilon_{ii}^{m}&={}^{G}\varepsilon_{ii}^{me}+3\alpha\Delta T=\frac{{}^{G}\sigma_{ii}^{m}}{3K}+3\alpha\Delta T\\&=-\frac{3f_{V}}{1-f_{V}}\frac{\overline{K}}{K}\Big\langle f\big\{P_{h}^{p\Sigma\Omega}-(1-\overline{\nu})\,{}^{n}P_{11}^{\Omega}\big\}L_{K}^{\Omega}(\alpha^{\Omega}-\overline{\alpha})+(1-f)\big\{P_{h}^{p\Sigma\Gamma}-(1-\overline{\nu})\,{}^{n}P_{11}^{\Gamma}\big\}L_{K}^{\Gamma}(\alpha^{\Gamma}-\overline{\alpha})\Big\rangle\Delta T+3\alpha\Delta T\,.\end{aligned} \tag{47}$$

Substituting Eq. (47) into Eq. (45a), the macroscopic thermal expansion coefficient $\overline{\alpha}$ finally becomes to be

$$\overline{\alpha}=\alpha+\frac{f_{V}\Big\{f\mathscr{P}^{\Omega}L_{K}^{\Omega}(\alpha^{\Omega}-\alpha)+(1-f)\mathscr{P}^{\Gamma}L_{K}^{\Gamma}(\alpha^{\Gamma}-\alpha)\Big\}}{(1-f_{V})K+f_{V}\Big\{f\mathscr{P}^{\Omega}L_{K}^{\Omega}+(1-f)\mathscr{P}^{\Gamma}L_{K}^{\Gamma}\Big\}}\,, \tag{48a}$$

$$\mathscr{P}^{X}=(K-\overline{K})P_{h}^{p\Sigma X}+(1-\overline{\nu})\overline{K}\,{}^{n}P_{11}^{X}\,, \quad (X=\Omega,\,\Gamma)\,. \tag{48b}$$

The right-hand side of Eq. (48a) does not include $\overline{\alpha}$ and is a function of macroscopic elastic moduli. Therefore, $\overline{\alpha}$ is automatically determined if the macroscopic elastic moduli of Eq. (38) is obtained.

When the inner region Ω and the outer region V of the coated filler are spherical, by substituting Eq. (40) into Eq. (48), $\overline{\alpha}$ reduces to

$$\overline{\alpha}=\alpha+\frac{f_{V}\big\{(1+\overline{\nu})K+2(1-2\overline{\nu})\overline{K}\big\}\Big\{\dfrac{f}{L_{\mathrm{I}}^{\Omega}}L_{K}^{\Omega}(\alpha^{\Omega}-\alpha)+\dfrac{1-f}{L_{\mathrm{I}}^{\Gamma}}L_{K}^{\Gamma}(\alpha^{\Gamma}-\alpha)\Big\}}{(1-f_{V})K+f_{V}\big\{(1+\overline{\nu})K+2(1-2\overline{\nu})\overline{K}\big\}\Big\{\dfrac{f}{L_{\mathrm{I}}^{\Omega}}L_{K}^{\Omega}(\alpha^{\Omega}-\alpha)+\dfrac{1-f}{L_{\mathrm{I}}^{\Gamma}}L_{K}^{\Gamma}(\alpha^{\Gamma}-\alpha)\Big\}}\,. \tag{49}$$

Furthermore, in the case of a single inhomogeneous inclusion $f=0$ or $f=1$, by substituting Eq. (42) into Eq. (49), $\overline{\alpha}$ becomes

$$\overline{\alpha}=\alpha+\frac{3f_V(1-\overline{\nu})K^X(\alpha^X-\alpha)}{3(1-\overline{\nu})\overline{K}+(1+\overline{\nu})(K^X-\overline{K})}\quad,\quad(X=\Omega\ when\ f=1,\ X=\Gamma\ when\ f=0)\,. \tag{50}$$

The solution in Eq. (50) agrees with that found previously by the author [20].

2.2. Mori-Tanaka theorem

2.2.1. Analysis of macroscopic elastic moduli

In this section, we derive the macroscopic elastic moduli and thermal expansion coefficient of composite materials based on the Mori-Tanaka theorem. In this theorem, the interaction due to the existence of many coated fillers is represented by unknown interaction stresses $\tilde{\sigma}_{ij}$, which act on the whole material. That is, the region surrounding the coated filler $V(i)$ in Fig. 3 is smeared out by unknown interaction stresses $\tilde{\sigma}_{ij}$ instead of unknown elastic moduli $\overline{K}$, $\overline{\mu}$, and the thermal expansion coefficient $\overline{\alpha}$. Therefore, the elastic moduli and thermal expansion coefficient in this region are K, μ, and α of the matrix, respectively. The strains corresponding to the external stress σ^0_{ij} and the interaction stress $\tilde{\sigma}_{ij}$ are represented by ε^0_{ij} and $\tilde{\varepsilon}_{ij}$ respectively. Then, the equivalent equations of the coated filler $V(i)$ are expressed as follows by referring to Eq. (1)
hydrostatic component:

$$\begin{aligned}
&{}^{L(i)}\sigma^0_{ii}+{}^{L(i)}\tilde{\sigma}_{ii}+{}^{L(i)}<\sigma^\infty_{ii}>_\Omega\\
&=3K^\Omega\left\{{}^{L(i)}\varepsilon^0_{ii}+{}^{L(i)}\tilde{\varepsilon}_{ii}+(S^\Omega_{iikl}-I_{iikl})\,{}^{L(i)}<\varepsilon^{**\Omega}_{kl}>_\Omega+(S^V_{iikl}-S^\Omega_{iikl})\,{}^{L(i)}<\varepsilon^{**\Gamma}_{kl}>_\Gamma+{}^{L(i)}<\varepsilon^{*\Omega}_{ii}>_\Omega\right\}\\
&=3K\left\{{}^{L(i)}\varepsilon^0_{ii}+{}^{L(i)}\tilde{\varepsilon}_{ii}+(S^\Omega_{iikl}-I_{iikl})\,{}^{L(i)}<\varepsilon^{**\Omega}_{kl}>_\Omega+(S^V_{iikl}-S^\Omega_{iikl})\,{}^{L(i)}<\varepsilon^{**\Gamma}_{kl}>_\Gamma\right\}\quad in\,\Omega\,,
\end{aligned} \tag{51a}$$

$$\begin{aligned}
&{}^{L(i)}\sigma^0_{ii}+{}^{L(i)}\tilde{\sigma}_{ii}+{}^{L(i)}<\sigma^\infty_{ii}>_\Gamma\\
&=3K^\Gamma\left\{{}^{L(i)}\varepsilon^0_{ii}+{}^{L(i)}\tilde{\varepsilon}_{ii}+(S^V_{iikl}-I_{iikl})\,{}^{L(i)}<\varepsilon^{**\Gamma}_{kl}>_\Gamma+\frac{f}{1-f}(S^V_{iikl}-S^\Omega_{iikl})({}^{L(i)}<\varepsilon^{**\Omega}_{kl}>_\Omega-{}^{L(i)}<\varepsilon^{**\Gamma}_{kl}>_\Gamma)+{}^{L(i)}<\varepsilon^{*\Gamma}_{ii}>_\Gamma\right\}\\
&=3K\left\{{}^{L(i)}\varepsilon^0_{ii}+{}^{L(i)}\tilde{\varepsilon}_{ii}+(S^V_{iikl}-I_{iikl})\,{}^{L(i)}<\varepsilon^{**\Gamma}_{kl}>_\Gamma+\frac{f}{1-f}(S^V_{iikl}-S^\Omega_{iikl})({}^{L(i)}<\varepsilon^{**\Omega}_{kl}>_\Omega-{}^{L(i)}<\varepsilon^{**\Gamma}_{kl}>_\Gamma)\right\}\quad in\,\Gamma\,,
\end{aligned} \tag{51b}$$

deviatoric (or shear) component:

$$\begin{aligned}
&{}'^{L(i)}\sigma^0_{ij}+{}'^{L(i)}\tilde{\sigma}_{ij}+{}'^{L(i)}<\sigma^\infty_{ij}>_\Omega\\
&=2\mu^\Omega\left\{{}'^{L(i)}\varepsilon^0_{ij}+{}'^{L(i)}\tilde{\varepsilon}_{ij}+{}'S^\Omega_{ijkl}\,{}^{L(i)}<\varepsilon^{**\Omega}_{kl}>_\Omega-{}'^{L(i)}<\varepsilon^{**\Omega}_{ij}>_\Omega+({}'S^V_{ijkl}-{}'S^\Omega_{ijkl})\,{}^{L(i)}<\varepsilon^{**\Gamma}_{kl}>_\Gamma+{}'^{L(i)}<\varepsilon^{*\Omega}_{ij}>_\Omega\right\}\\
&=2\overline{\mu}\left\{{}'^{L(i)}\varepsilon^0_{ij}+{}'^{L(i)}\tilde{\varepsilon}_{ij}+{}'S^\Omega_{ijkl}\,{}^{L(i)}<\varepsilon^{**\Omega}_{kl}>_\Omega-{}'^{L(i)}<\varepsilon^{**\Omega}_{ij}>_\Omega+({}'S^V_{ijkl}-{}'S^\Omega_{ijkl})\,{}^{L(i)}<\varepsilon^{**\Gamma}_{kl}>_\Gamma\right\}\quad in\,\Omega\,,
\end{aligned} \tag{52a}$$

$$\begin{aligned}
&{}'^{L(i)}\sigma^0_{ij}+{}'^{L(i)}\tilde{\sigma}_{ij}+{}'^{L(i)}<\sigma^\infty_{ij}>_\Gamma\\
&=2\mu^\Gamma\left\{{}'^{L(i)}\varepsilon^0_{ij}+{}'^{L(i)}\tilde{\varepsilon}_{ij}+{}'S^V_{ijkl}\,{}^{L(i)}<\varepsilon^{**\Gamma}_{kl}>_\Gamma-{}'^{L(i)}<\varepsilon^{**\Gamma}_{ij}>_\Gamma\right.\\
&\qquad\left.+\frac{f}{1-f}({}'S^V_{ijkl}-{}'S^\Omega_{ijkl})({}^{L(i)}<\varepsilon^{**\Omega}_{kl}>_\Omega-{}^{L(i)}<\varepsilon^{**\Gamma}_{kl}>_\Gamma)+{}'^{L(i)}<\varepsilon^{*\Gamma}_{ij}>_\Gamma\right\}\\
&=2\overline{\mu}\left\{{}'^{L(i)}\varepsilon^0_{ij}+{}'^{L(i)}\tilde{\varepsilon}_{ij}+{}'S^V_{ijkl}\,{}^{L(i)}<\varepsilon^{**\Gamma}_{kl}>_\Gamma-{}'^{L(i)}<\varepsilon^{**\Gamma}_{ij}>_\Gamma\right.\\
&\qquad\left.+\frac{f}{1-f}({}'S^V_{ijkl}-{}'S^\Omega_{ijkl})({}^{L(i)}<\varepsilon^{**\Omega}_{kl}>_\Omega-{}^{L(i)}<\varepsilon^{**\Gamma}_{kl}>_\Gamma)\right\}\quad in\,\Gamma\,,
\end{aligned} \tag{52b}$$

where the following relations hold between σ^0_{ij} and ε^0_{ij}, $\tilde{\sigma}_{ij}$ and $\tilde{\varepsilon}_{ij}$, respectively.

$$\sigma^0_{ii}=3K\varepsilon^0_{ii}\quad,\quad{}'\sigma^0_{ij}=2\mu\,{}'\varepsilon^0_{ij}\,, \tag{53a}$$

$$\tilde{\sigma}_{ii}=3K\tilde{\varepsilon}_{ii}\quad,\quad{}'\tilde{\sigma}_{ij}=2\mu\,{}'\tilde{\varepsilon}_{ij}\,. \tag{53b}$$

Comparing Eqs. (1) and (51), Eqs. (2) and (52), we can see that Eqs. (51) and (52) are a simple replacement of Eqs. (1) and (2) as follows:

$$\begin{aligned}
&\sigma^0_{ij}\ \rightarrow\ \sigma^0_{ij}+\tilde{\sigma}_{ij}\quad,\quad\overline{\varepsilon}_{ij}\ \rightarrow\ \varepsilon^0_{ij}+\tilde{\varepsilon}_{ij}\,,\\
&\overline{K}\ \rightarrow\ K\quad,\quad\overline{\mu}\ \rightarrow\ \mu\quad,\quad\overline{\nu}\ \rightarrow\ \nu\,.
\end{aligned} \tag{54}$$

Therefore, the subsequent calculations are performed by replacing the equations in Sec.2.1 with Eq. (54), so the coefficients that appear in the equations have the same form as those used in Sec.2.1. However, it should be noted that the unknown macroscopic

elastic moduli $\overline{K}$, $\overline{\mu}$, and $\overline{\nu}$ appearing in Eqs. (10), (23), (31), and (32) are replaced by the known elastic moduli of the matrix K, μ, and ν.

From the above, the macroscopic total strain ${}^{G}\overline{\varepsilon}_{ij}$ and stress ${}^{G}\overline{\sigma}_{ij}$ are as follows by referring to Eqs. (33) and (34)

$$ {}^{G}\overline{\varepsilon}_{ii} = \left\{ f_V(1-P_h^{\Sigma}) + (1-f_V) \right\} ({}^{G}\varepsilon_{ii}^{0} + {}^{G}\tilde{\varepsilon}_{ii}) + f_V \left\{ f P_h^{p\Sigma\Omega} L_K^{\Omega} < \varepsilon_{ii}^{p\Omega} >_{\Omega} + (1-f) P_h^{p\Sigma\Gamma} L_K^{\Gamma} < \varepsilon_{ii}^{p\Gamma} >_{\Gamma} \right\} $$
$$ + f_V \left\{ f P_3^{p\Sigma\Omega} L_{\mu}^{\Omega\prime} < \varepsilon_{33}^{p\Omega} >_{\Omega} + (1-f) P_3^{p\Sigma\Gamma} L_{\mu}^{\Gamma\prime} < \varepsilon_{33}^{p\Gamma} >_{\Gamma} \right\} , \tag{55a} $$

$$ {}^{\prime G}\overline{\varepsilon}_{ij} = \left\{ f_V(1-P_d^{\Sigma}) + (1-f_V) \right\} ({}^{\prime G}\varepsilon_{ij}^{0} + {}^{\prime G}\tilde{\varepsilon}_{ij}) , \tag{55b} $$

$$ {}^{G}\overline{\sigma}_{ii} = 3K \left\langle f_V \left\{ 1 - P_h^{\Sigma} + (1-\nu)\, {}^{n}P_{11}^{V} \right\} + (1-f_V) \right\rangle ({}^{G}\varepsilon_{ii}^{0} + {}^{G}\tilde{\varepsilon}_{ii}) $$
$$ + 3 f_V K \left\langle f \left\{ P_h^{p\Sigma\Omega} - (1-\nu)\, {}^{n}P_{11}^{\Omega} \right\} L_K^{\Omega} < \varepsilon_{ii}^{p\Omega} >_{\Omega} + (1-f) \left\{ P_h^{p\Sigma\Gamma} - (1-\nu)\, {}^{n}P_{11}^{\Gamma} \right\} L_K^{\Gamma} < \varepsilon_{ii}^{p\Gamma} >_{\Gamma} \right. $$
$$ \left. + f \left\{ P_3^{p\Sigma\Omega} - (1-\nu)\, {}^{n}P_{12}^{\Omega} \right\} L_{\mu}^{\Omega\prime} < \varepsilon_{33}^{p\Omega} >_{\Omega} + (1-f) \left\{ P_3^{p\Sigma\Gamma} - (1-\nu)\, {}^{n}P_{12}^{\Gamma} \right\} L_{\mu}^{\Gamma\prime} < \varepsilon_{33}^{p\Gamma} >_{\Gamma} \right\rangle , \tag{56a} $$

$$ {}^{\prime G}\overline{\sigma}_{ij} = 2\mu \left\langle f_V \left(1 - P_d^{\Sigma} + \frac{1-\nu}{5} \left\{ {}^{n}P_{22}^{V} + 2({}^{s}P_{23}^{V} + {}^{s}P_{12}^{V}) \right\} \right) + (1-f_V) \right\rangle ({}^{\prime G}\varepsilon_{ij}^{0} + {}^{\prime G}\tilde{\varepsilon}_{ij}) , \tag{56b} $$

where ${}^{G}\varepsilon_{ij}^{m}$ and ${}^{G}\sigma_{ij}^{m}$ in Eqs. (33) and (34) are the total strain and stress of the matrix, and given by the sum of the external fields and interaction ones. Between ${}^{G}\varepsilon_{ij}^{m}$ and ${}^{G}\sigma_{ij}^{m}$, the same relation as Eq. (35) holds. That is,

$$ {}^{G}\varepsilon_{ij}^{m} = {}^{G}\varepsilon_{ij}^{0} + {}^{G}\tilde{\varepsilon}_{ij} \quad , \quad {}^{G}\sigma_{ij}^{m} = {}^{G}\sigma_{ij}^{0} + {}^{G}\tilde{\sigma}_{ij} , $$
$$ {}^{G}\sigma_{ii}^{m} = 3K\, {}^{G}\varepsilon_{ii}^{m} \quad , \quad {}^{\prime G}\sigma_{ij}^{m} = 2\mu\, {}^{\prime G}\varepsilon_{ij}^{m} . \tag{57} $$

These relations are used in the derivation of Eqs. (55) and (56).

In Eqs. (55) and (56), by substituting $\varepsilon_{ij}^{p\Omega} = \varepsilon_{ij}^{p\Gamma} = 0$ and eliminating $({}^{G}\varepsilon_{ij}^{0} + {}^{G}\tilde{\varepsilon}_{ij}^{0})$, we can find the relation between ${}^{G}\overline{\varepsilon}_{ij}$ and ${}^{G}\overline{\sigma}_{ij}$. Equating the obtained relation with Eq. (37), the macroscopic bulk modulus $\overline{K}$ and shear modulus $\overline{\mu}$ are given by

$$ \overline{K} = K + \frac{f_V(1-\nu)K\, {}^{n}P_{11}^{V}}{1 - f_V P_h^{\Sigma}} \quad , \quad \overline{\mu} = \mu + \frac{\dfrac{f_V(1-\nu)}{5}\mu \left\{ {}^{n}P_{22}^{V} + 2({}^{s}P_{23}^{V} + {}^{s}P_{12}^{V}) \right\}}{1 - f_V P_d^{\Sigma}} , \tag{58} $$

where ${}^{n}P_{ij}^{V}$, ${}^{s}P_{ij}^{V}$, P_h^{Σ}, and P_d^{Σ} have the same form as Eqs. (19) and (31). However, as previously mentioned, we note that the unknown elastic moduli $\overline{K}$, $\overline{\mu}$, and $\overline{\nu}$ included in these coefficients are replaced by the known elastic moduli of the matrix K, μ, and ν. Interestingly, Eq. (58) contains the same types of coefficients as Eq. (38). This makes it easy to perform calculations using these two solutions simultaneously. Note that Eq. (58), unlike Eq. (38), are explicit solutions. This is the advantage of the Mori-Tanaka theorem.

Next, we consider the case where the inner region Ω and the outer region V of the coated filler are spherical. In this case, by substituting Eq. (40) into Eq. (58), $\overline{K}$ and $\overline{\mu}$ are reduced to

$$ \overline{K} = K + \frac{3f_V(1-\nu)K\left(\dfrac{f}{L_{\mathrm{I}}^{\Omega}} + \dfrac{1-f}{L_{\mathrm{I}}^{\Gamma}} \right)}{1 - f_V(1+\nu)\left(\dfrac{f}{L_{\mathrm{I}}^{\Omega}} + \dfrac{1-f}{L_{\mathrm{I}}^{\Gamma}} \right)} \quad , \quad \overline{\mu} = \mu + \frac{30 f_V(1-\nu)\mu\left(\dfrac{f}{L_{\mathrm{II}}^{\Omega}} + \dfrac{1-f}{L_{\mathrm{II}}^{\Gamma}} \right)}{15 - 4f_V(4-5\nu)\left(\dfrac{f}{L_{\mathrm{II}}^{\Omega}} + \dfrac{1-f}{L_{\mathrm{II}}^{\Gamma}} \right)} . \tag{59} $$

Hashin and Shtirkman have derived upper and lower bounds for the macroscopic bulk modulus K^* and shear modulus μ^* of multiphase composites [15], and these solutions are given by

$$ K_1^* = K_1 + \frac{A_1}{1 + \alpha_1 A_1} \quad , \quad K_2^* = K_n + \frac{A_n}{1 + \alpha_n A_n} , \tag{60a} $$

$$ \mu_1^* = \mu_1 + \frac{B_1}{2(1 + \beta_1 B_1)} \quad , \quad \mu_2^* = \mu_n + \frac{B_n}{2(1 + \beta_n B_n)} , \tag{60b} $$

where K_1^* and μ_1^* are the lower bounds, K_2^* and μ_2^* are the upper bounds, and the coefficients in the equations are given as

$$ A_1 = \sum_{i=2}^{n} \frac{f_i}{\dfrac{1}{K_i - K_1} - \alpha_1} \quad , \quad A_n = \sum_{i=1}^{n-1} \frac{f_i}{\dfrac{1}{K_i - K_n} - \alpha_n} , \tag{61a} $$

$$B_1 = \sum_{i=2}^{n} \frac{f_i}{\dfrac{1}{2(\mu_i - \mu_1)} - \beta_1} \quad , \quad B_n = \sum_{i=1}^{n-1} \frac{f_i}{\dfrac{1}{2(\mu_i - \mu_n)} - \beta_n} \ , \tag{61b}$$

$$\alpha_i = -\frac{3}{3K_i + 4\mu_i} \quad , \quad \beta_i = -\frac{3(K_i + 2\mu_i)}{5\mu_i(3K_i + 4\mu_i)} \quad , \quad (i = 1,\ n) \ . \tag{61c}$$

In Eq. (61), K_i and μ_i are the bulk modulus and shear modulus of the i-th phase respectively. $i = 1$ indicates the minimum elastic modulus, and $i = n$ indicates the maximum. f_i is the volume fraction of the i-th phase.

For Eq. (60), set $n = 3$ and perform the following replacement.

$$K_1 = K \quad , \quad K_2 = K^{\Omega} \quad , \quad K_3 = K^{\Gamma} \ ,$$
$$\mu_1 = \mu \quad , \quad \mu_2 = \mu^{\Omega} \quad , \quad \mu_3 = \mu^{\Gamma} \ ,$$
$$f_1 = 1 - f_V \quad , \quad f_2 = f f_V \quad , \quad f_3 = (1 - f) f_V \ .$$

Hashin's and Shtrikman's lower bounds K_1^* and μ_1^* obtained by this operation completely agree with the present analytical solutions $\overline{K}$ and $\overline{\mu}$ in Eq. (59). Note that this agreement holds even if the subscripts 2 and 3 are exchanged in the above equation.

Furthermore, regarding Eq. (59), in the case of a spherical and single inhomogeneous inclusion with $f = 0$ or $f = 1$, $\overline{K}$ and $\overline{\mu}$ can be simplified as follows:

$$\overline{K} = K + \frac{3f(1-\nu)K(K^X - K)}{3(1-\nu)K + (1-f)(1+\nu)(K^X - K)} \quad , \quad \overline{\mu} = \mu + \frac{15f(1-\nu)\mu(\mu^X - \mu)}{15(1-\nu)\mu + 2(1-f)(4-5\nu)(\mu^X - \mu)} \ ,$$
$$(X = \Omega \ when \ f = 1, \ X = \Gamma \ when \ f = 0) \ . \tag{62}$$

The solutions in Eq. (62) agree with the solutions found by Kanaun et al. [31]. From the above results, it can be seen that these analytical solutions are consistent for the special case that the shape of the coated fillers is spherical.

From this derivation process, it is interesting that the Mori-Tanaka theorem can give directly explicit solutions of macroscopic elastic moduli without obtaining unknown interaction fields $\tilde{\sigma}_{ij}$ and $\tilde{\varepsilon}_{ij}$. The interaction stress $\tilde{\sigma}_{ij}$ can be obtained from the condition that the total internal stress in the whole material is zero. Since ${}^{G}\overline{\sigma}_{ij}$ in Eq. (56) is given by the sum of the external stress ${}^{G}\sigma_{ij}^{0}$ and the total internal stress, subtracting the stress ${}^{G}\sigma_{ij}^{0}$ from ${}^{G}\overline{\sigma}_{ij}$ yields zero. Therefore, from Eqs. (56) and (53), the interaction strain $\tilde{\varepsilon}_{ij}$ can be obtained as

$$\begin{aligned}
&{}^{G}\overline{\sigma}_{ij} - {}^{G}\sigma_{ij}^{0} = 0 \ , \\
&\therefore {}^{G}\tilde{\varepsilon}_{ii} = \frac{f_V}{1 - f_V\left\{P_h^{\Sigma} - (1-\nu)\,{}^{n}P_{11}^{V}\right\}} \Big\langle \left\{P_h^{\Sigma} - (1-\nu)\,{}^{n}P_{11}^{V}\right\} {}^{G}\varepsilon_{ii}^{0} \\
&\qquad - \Big[f\left\{P_h^{p\Sigma\Omega} - (1-\nu)\,{}^{n}P_{11}^{\Omega}\right\} L_K^{\Omega} < \varepsilon_{ii}^{p\Omega} >_{\Omega} + (1-f)\left\{P_h^{p\Sigma\Gamma} - (1-\nu)\,{}^{n}P_{11}^{\Gamma}\right\} L_K^{\Gamma} < \varepsilon_{ii}^{p\Gamma} >_{\Gamma} \\
&\qquad + f\left\{P_3^{p\Sigma\Omega} - (1-\nu)\,{}^{n}P_{12}^{\Omega}\right\} L_{\mu}^{\Omega\,\prime} < \varepsilon_{33}^{p\Omega} >_{\Omega} + (1-f)\left\{P_3^{p\Sigma\Gamma} - (1-\nu)\,{}^{n}P_{12}^{\Gamma}\right\} L_{\mu}^{\Gamma\,\prime} < \varepsilon_{33}^{p\Gamma} >_{\Gamma} \Big] \Big\rangle \ ,
\end{aligned} \tag{63a}$$

$$\therefore {}^{\prime G}\tilde{\varepsilon}_{ij} = \frac{f_V\left\langle P_d^{\Sigma} - \dfrac{1-\nu}{5}\left\{ {}^{n}P_{22}^{V} + 2({}^{s}P_{23}^{V} + {}^{s}P_{12}^{V})\right\}\right\rangle}{1 - f_V\left\langle P_d^{\Sigma} - \dfrac{1-\nu}{5}\left\{ {}^{n}P_{22}^{V} + 2({}^{s}P_{23}^{V} + {}^{s}P_{12}^{V})\right\}\right\rangle} {}^{\prime G}\varepsilon_{ij}^{0} \ . \tag{63b}$$

The interaction stress $\tilde{\sigma}_{ij}$ is obtained by substituting Eq. (63) into Eq. (53).

2.2.2. Analysis of macroscopic thermal expansion coefficient

Next, we derive the macroscopic thermal expansion coefficient $\overline{\alpha}$ of the material. Similar to the previous section, we consider the state where only the temperature change ΔT is applied, with the external stress $\sigma_{ij}^{0} = 0$. Therefore, we substitute $\varepsilon_{ij}^{0} = 0$ into Eqs. (55) and (56). In the same way as Eq. (43), when the thermal expansion of the matrix is regarded as the reference, the thermal expansion strains $< \varepsilon_{ij}^{p\Omega} >_{\Omega}$ and $< \varepsilon_{ij}^{p\Gamma} >_{\Gamma}$ that occur in the coated filler can be expressed by

$$< \varepsilon_{ij}^{pX} >_X = \delta_{ij}(\alpha^X - \alpha)\Delta T \quad , \quad (X = \Omega \ , \Gamma) \ . \tag{64}$$

From Eq. (64), the hydrostatic components in Eqs. (55) and (56) are as follows:

$${}^{G}\overline{\varepsilon}_{ii} = \left\{ f_V(1 - P_h^{\Sigma}) + (1 - f_V)\right\} {}^{G}\tilde{\varepsilon}_{ii} + 3f_V\left\{ f P_h^{p\Sigma\Omega} L_K^{\Omega}(\alpha^{\Omega} - \alpha) + (1-f) P_h^{p\Sigma\Gamma} L_K^{\Gamma}(\alpha^{\Gamma} - \alpha)\right\}\Delta T + 3\alpha\Delta T = 3\overline{\alpha}\Delta T \ , \tag{65a}$$

$$\begin{aligned}
{}^{G}\overline{\sigma}_{ii} &= 3K\Big\langle f_V\left\{1 - P_h^{\Sigma} + (1-\nu)\,{}^{n}P_{11}^{V}\right\} + (1 - f_V)\Big\rangle {}^{G}\tilde{\varepsilon}_{ii} \\
&\quad + 9f_V K\Big\langle f\left\{P_h^{p\Sigma\Omega} - (1-\nu)\,{}^{n}P_{11}^{\Omega}\right\} L_K^{\Omega}(\alpha^{\Omega} - \alpha) + (1-f)\left\{P_h^{p\Sigma\Gamma} - (1-\nu)\,{}^{n}P_{11}^{\Gamma}\right\} L_K^{\Gamma}(\alpha^{\Gamma} - \alpha)\Big\rangle \Delta T = 0 \ ,
\end{aligned} \tag{65b}$$

where we note that $3\alpha\Delta T$ is added to the total strain ${}^{G}\overline{\varepsilon}_{ii}$ because of the same reason as the derivation of Eq. (44a). Similar to Eq. (45a), ${}^{G}\overline{\varepsilon}_{ii}$ is the thermal expansion strain of the whole material, that is $3\overline{\alpha}\Delta T$. Eq. (65b) is the sum of the internal stresses in the material and becomes to be zero. Solving this equation for the interaction strain ${}^{G}\tilde{\varepsilon}_{ii}$ yields

$$ {}^{G}\tilde{\varepsilon}_{ii} = -\frac{3f_V\left\langle f\left\{P_h^{p\Sigma\Omega} - (1-\nu)\,{}^{n}P_{11}^{\Omega}\right\}L_K^{\Omega}(\alpha^{\Omega}-\alpha) + (1-f)\left\{P_h^{p\Sigma\Gamma} - (1-\nu)\,{}^{n}P_{11}^{\Gamma}\right\}L_K^{\Gamma}(\alpha^{\Gamma}-\alpha)\right\rangle\Delta T}{1 - f_V\left\{P_h^{\Sigma} - (1-\nu)\,{}^{n}P_{11}^{V}\right\}} . \tag{66} $$

Substituting Eq. (66) into Eq. (65a) and solving for the macroscopic thermal expansion coefficient $\overline{\alpha}$ yields

$$ \begin{aligned} \overline{\alpha} = \alpha + \frac{f_V(1-\nu)}{1 - f_V\left\{P_h^{\Sigma} - (1-\nu)\,{}^{n}P_{11}^{V}\right\}}\Big\langle & f\left\{(1-f_V P_h^{\Sigma})\,{}^{n}P_{11}^{\Omega} + f_V P_h^{p\Sigma\Omega}\,{}^{n}P_{11}^{V}\right\}L_K^{\Omega}(\alpha^{\Omega}-\alpha) \\ & + (1-f)\left\{(1-f_V P_h^{\Sigma})\,{}^{n}P_{11}^{\Gamma} + f_V P_h^{p\Sigma\Gamma}\,{}^{n}P_{11}^{V}\right\}L_K^{\Gamma}(\alpha^{\Gamma}-\alpha)\Big\rangle . \end{aligned} \tag{67} $$

Unlike $\overline{\alpha}$ in Eq. (48) obtained by the self-consistent method, $\overline{\alpha}$ in Eq. (67) is not directly related to $\overline{K}$ in Eq. (58) obtained by the Mori-Tanaka theorem. However, $\overline{\alpha}$ contains the same coefficients used in $\overline{K}$, so $\overline{\alpha}$ and $\overline{K}$ are closely related.

In the case where the inner region Ω and the outer region V of the coated filler are spherical, the same relation as Eq. (40) holds. Substituting this relation into Eq. (67), the macroscopic thermal expansion coefficient $\overline{\alpha}$ becomes

$$ \overline{\alpha} = \alpha + \frac{3f_V(1-\nu)}{1 - 2f_V(1-2\nu)\left(\dfrac{f}{L_{\mathrm{I}}^{\Omega}} + \dfrac{1-f}{L_{\mathrm{I}}^{\Gamma}}\right)}\left\{\frac{f}{L_{\mathrm{I}}^{\Omega}}L_K^{\Omega}(\alpha^{\Omega}-\alpha) + \frac{1-f}{L_{\mathrm{I}}^{\Gamma}}L_K^{\Gamma}(\alpha^{\Gamma}-\alpha)\right\} . \tag{68} $$

Schapery derived the solutions for the lower bound α_1^* and upper bound α_2^* of the macroscopic thermal expansion coefficient of multiphase composites that exhibit isotropy, and these solutions are given by the following equations [32].

$$ \alpha_1^* = \overline{\alpha} + \left(\frac{\overline{K\alpha}}{\overline{K}} - \overline{\alpha}\right)\frac{\left(\dfrac{1}{K_L} - \dfrac{1}{\hat{K}}\right)}{\left(\dfrac{1}{K_L} - \dfrac{1}{\overline{K}}\right)} - \Delta\hat{\alpha}_v \quad , \quad \alpha_2^* = \overline{\alpha} + \left(\frac{\overline{K\alpha}}{\overline{K}} - \overline{\alpha}\right)\frac{\left(\dfrac{1}{K_L} - \dfrac{1}{\hat{K}}\right)}{\left(\dfrac{1}{K_L} - \dfrac{1}{\overline{K}}\right)} + \Delta\hat{\alpha}_v , \tag{69a} $$

$$ \Delta\hat{\alpha}_v = \frac{\left(\dfrac{1}{\hat{K}} - \dfrac{1}{\overline{K}}\right)^{\frac{1}{2}}\left(\dfrac{1}{K_L} - \dfrac{1}{\hat{K}}\right)^{\frac{1}{2}}}{\left(\dfrac{1}{K_L} - \dfrac{1}{\overline{K}}\right)}\left\{\left(\overline{K\alpha^2} - \frac{\overline{K\alpha}^2}{\overline{K}}\right)\left(\frac{1}{K_L} - \frac{1}{\overline{K}}\right) - \left(\frac{\overline{K\alpha}}{\overline{K}} - \overline{\alpha}\right)^2\right\}^{\frac{1}{2}} , \tag{69b} $$

where $\hat{K}$ is the macroscopic bulk modulus. $\overline{\alpha}$, $\overline{K}$, $1/K_L$, $\overline{K\alpha}$, and $\overline{K\alpha^2}$ are expressed as

$$ \overline{\alpha} = \sum_{i=1}^{n} f_i\alpha_i \quad , \quad \overline{K} = \sum_{i=1}^{n} f_i K_i \quad , \quad \frac{1}{K_L} = \sum_{i=1}^{n} f_i\left(\frac{1}{K_i}\right) \quad , \quad \overline{K\alpha} = \sum_{i=1}^{n} f_i K_i\alpha_i \quad , \quad \overline{K\alpha^2} = \sum_{i=1}^{n} f_i K_i\alpha_i^2 , \tag{70} $$

where α_i, K_i, μ_i, and f_i in Eq. (70) are the bulk modulus, shear modulus, thermal expansion coefficient, and volume fraction of the i-th phase. The same solution is also found by Rosen and Hashin, but in a slightly different form than Shapery's solution of Eq. (69) [33]. It should be noted that the equations described in Rosen et al.'s paper contain some mistakes in their descriptions. The analytical solution Eq. (68) when the coated filler is spherical does not agree with Eq. (69). A detailed comparison of these two solutions will be given in Chapter 4.

Regarding Eq. (68), if $f = 0$ or $f = 1$, it reduces to

$$ \overline{\alpha} = \alpha + \frac{3f(1-\nu)K^X(\alpha^X - \alpha)}{3(1-\nu)K^X - 2(1-f)(1-2\nu)(K^X - K)} \quad , \quad (X = \Omega \ when \ f = 1, \ X = \Gamma \ when \ f = 0) . \tag{71} $$

The solution in Eq. (71) agrees with that found by Kanaun et al. [31].

2.3. Christenen's method

Christensen proposed a method for deriving the solutions for the macroscopic elastic moduli when the fibers are oriented randomly in the material using the solutions when the fibers are oriented unidirectionally [24]. The author extends this method to the case where the shape of the filler is ellipsoidal, and derives the solutions for the macroscopic elastic moduli and thermal expansion coefficient [34]. This method assumes that the stress fields in the case of randomly oriented fillers are equal to the average of the known stress fields in the case of unidirectional aligned fillers integrated over all orientations. When the shape of the fillers is spheroidal, the solutions for the macroscopic elastic moduli and the thermal expansion coefficient are given as follows:

$$ \overline{K} = \frac{1}{9}\left\{\overline{E}_{33} + 4(1+\overline{\nu}_{23})^2\,\overline{B}\right\} \quad , \quad \overline{\mu} = \frac{1}{15}\left\{\overline{E}_{33} + 6(\overline{\mu}_{23} + \overline{\mu}_{12}) + (1-2\overline{\nu}_{23})^2\,\overline{B}\right\} \quad , \tag{72a} $$

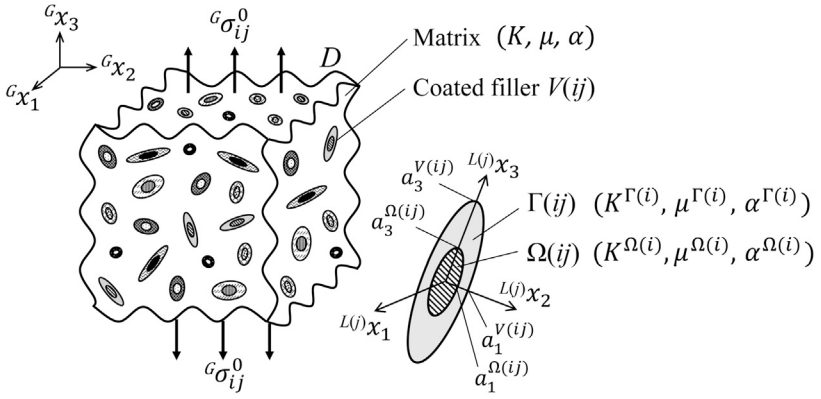

Fig. 4. Composite material containing various types of spheroidal-coated fillers with different physical properties and shapes oriented randomly.

$$\overline{\alpha} = \frac{\overline{E}_{33}\overline{\alpha}_{33} + 4(1+\overline{\nu}_{23})\overline{B}(\overline{\alpha}_{11} + \overline{\nu}_{23}\overline{\alpha}_{33})}{\overline{E}_{33} + 4(1+\overline{\nu}_{23})^2\,\overline{B}} \quad , \tag{73}$$

where $\overline{E}_{ij}$, $\overline{\nu}_{ij}$, $\overline{\mu}_{ij}$, and $\overline{\alpha}_{ij}$ are the macroscopic Young's modulus, Poisson's ratio, shear modulus, and thermal expansion coefficient when the spheroidal fillers are oriented so that their rotational symmetry axes coincide with the x_3 axis. $\overline{B}$ is the plane strain bulk modulus in the plane strain state where the macroscopic total strain in the x_3 direction is zero, and is given by the following equation

$$\frac{1}{\overline{B}} = 2\left\{ \frac{1-\overline{\nu}_{12}}{\overline{E}_{11}} - \frac{2(\overline{\nu}_{23})^2}{\overline{E}_{33}} \right\} \quad . \tag{72b}$$

The author derived explicit solutions for the macroscopic elastic moduli and thermal expansion coefficient when spheroidal-coated fillers are oriented unidirectionally [11]. These solutions are shown in Appendix A.3.

The research groups of Wenxiang et al. and Pin et al. also analyzed using Christensen's method [25] [26]. They derived the solutions as macroscopic Ramè constants. We can easily confirm that the solutions of $\overline{K}$ and $\overline{\mu}$ obtained from their solutions are the same as Eq. (72a). However, we should note that in their analyses, the axis of rotational symmetry of the spheroidal-coated filler is the x_1 axis. Christensen's method is an approximate method of simply superposition of solutions for the unidirectional oriented fillers. Therefore, in this method, interactions between fillers with different orientations are not considered.

3. Analysis of macroscopic elastic moduli and thermal expansion coefficient for composite materials containing various types of coated fillers oriented randomly

3.1. Analytical model

Fig. 4 shows a composite material in which various types of spheroidal-coated fillers with different physical properties and shapes are oriented randomly in the material. Similar to the model in Fig. 1, we assume that the interfaces between the constituents are completely bonded. The coated fillers are classified by (i) in terms of their physical properties and shapes. Therefore, as shown in Fig. 4, we add the superscript (i) to the right shoulder of the elastic moduli and thermal expansion coefficient of the Ω and Γ regions in the coated filler, and assume that there are n kinds of coated fillers. Although not shown in the figure, the eigenstrain is similarly classified by (i) and expressed by $\varepsilon_{ij}^{p\Omega(i)}$ and $\varepsilon_{ij}^{p\Gamma(i)}$. The orientation is classified by (j), and it is assumed that there are m types of orientations. Since all fillers are oriented randomly, there are m types of orientations for every (i)-th coated filler. Let $V(ij)$ denote the region of the coated filler with physical properties and shape (i) and orientation (j), and $f_{V(ij)}$ denote the volume fraction of $V(ij)$. The total volume fraction of the coated fillers, denoted by f_V, is calculated as $f_V = \sum_{i=1}^{n}\sum_{j=1}^{m} f_{V(ij)}$. Let $f_{(i)}$ be the volume fraction of the region $\Omega(ij)$ occupied in the region $V(ij)$.

3.2. Self-consistent method

As shown in Chap.2, the region surrounding a coated filler $V(ij)$ is smeared out with a material with unknown macroscopic elastic moduli $\overline{K}$, $\overline{\mu}$, and thermal expansion coefficient $\overline{\alpha}$. Solving the equivalent equation in the local coordinate system ${}^{L(j)}x_i$ taken along the direction of the principal semi-axis of $V(ij)$ and referring to Eq. (22a), (22b), the total strain and stress of $V(ij)$ can be obtained as follows:

$${}^{L(j)}\boldsymbol{\varepsilon}^{V} = (\mathbf{I} - \mathbf{T}^{(i)}\mathbf{P}^{V(i)})\,{}^{L(j)}\overline{\boldsymbol{\varepsilon}} + \mathbf{T}^{(i)}\left\{ f_{(i)}\mathbf{P}^{\Omega(i)} <^{\mathbf{L}} \boldsymbol{\varepsilon}^{p\Omega(i)} >_{\Omega(i)} + (1-f_{(i)})\mathbf{P}^{\Gamma(i)} <^{\mathbf{L}} \boldsymbol{\varepsilon}^{p\Gamma(i)} >_{\Gamma(i)} \right\}, \tag{74a}$$

$${}^{L(j)}\boldsymbol{\sigma}^{V} = \overline{\mathbf{C}}\left\langle \mathbf{I} - \left\{ \mathbf{T}^{(i)} - (1-\overline{\nu})\mathbf{I} \right\}\mathbf{P}^{V(i)} \right\rangle {}^{L(j)}\overline{\boldsymbol{\varepsilon}} + \overline{\mathbf{C}}\left\{ \mathbf{T}^{(i)} - (1-\overline{\nu})\mathbf{I} \right\}\left\{ f_{(i)}\mathbf{P}^{\Omega(i)} <^{\mathbf{L}} \boldsymbol{\varepsilon}^{p\Omega(i)} >_{\Omega(i)} + (1-f_{(i)})\mathbf{P}^{\Gamma(i)} <^{\mathbf{L}} \boldsymbol{\varepsilon}^{p\Gamma(i)} >_{\Gamma(i)} \right\}, \tag{74b}$$

where $\mathbf{P}^{\Omega(i)}$, $\mathbf{P}^{\Gamma(i)}$, and $\mathbf{P}^{V(i)}$ have the same matrix form as Eq. (19), and their components have the same form as Eqs. (A.9) and (A.10) in Appendix A.3. However, it should be noted that the coefficients related to the shape and physical properties of the coated fillers containing in $\mathbf{P}^{\Omega(i)}$, $\mathbf{P}^{\Gamma(i)}$, and $\mathbf{P}^{V(i)}$ are represented by $\alpha_3^{X(i)}$, $R_3^{X(i)}$, $H_{\mathrm{I}}^{X(i)}$, $L_{\mathrm{I}}^{X(i)}$, and $L_{\mathrm{II}}^{X(i)}$ $(X=\Omega,\ \Gamma)$ classified by (i).

Referring to Eq. (28), the transforming Eq. (74) to the global coordinate system yields following equations

$$ {}^{G}\boldsymbol{\varepsilon}^{V} = \hat{\boldsymbol{L}}^{(j)}(\mathbf{I}-\mathbf{T}^{(i)}\mathbf{P}^{V(i)})\boldsymbol{L}^{(j)}\,{}^{G}\overline{\boldsymbol{\varepsilon}} + \hat{\boldsymbol{L}}^{(j)}\mathbf{T}^{(i)}\Big\{ f_{(i)}\mathbf{P}^{\Omega(i)} <^{\mathbf{L}} \boldsymbol{\varepsilon}^{p\Omega(i)} >_{\Omega(i)} + (1-f_{(i)})\mathbf{P}^{\Gamma(i)} <^{\mathbf{L}} \boldsymbol{\varepsilon}^{p\Gamma(i)} >_{\Gamma(i)} \Big\}, \tag{75a} $$

$$ \begin{aligned} {}^{G}\boldsymbol{\sigma}^{V} &= \hat{\boldsymbol{L}}^{(j)}\overline{\mathbf{C}}\Big\langle \mathbf{I} - \big\{\mathbf{T}^{(i)} - (1-\overline{\nu})\mathbf{I}\big\}\mathbf{P}^{V(i)} \Big\rangle \boldsymbol{L}^{(j)}\,{}^{G}\overline{\boldsymbol{\varepsilon}} \\ &\quad + \hat{\boldsymbol{L}}^{(j)}\overline{\mathbf{C}}\big\{\mathbf{T}^{(i)} - (1-\overline{\nu})\mathbf{I}\big\}\Big\{ f_{(i)}\mathbf{P}^{\Omega(i)} <^{\mathbf{L}} \boldsymbol{\varepsilon}^{p\Omega(i)} >_{\Omega(i)} + (1-f_{(i)})\mathbf{P}^{\Gamma(i)} <^{\mathbf{L}} \boldsymbol{\varepsilon}^{p\Gamma(i)} >_{\Gamma(i)} \Big\}. \end{aligned} \tag{75b} $$

Using the total strains and stresses in Eq. (75) and referring to Eq. (29), the total macroscopic strain ${}^{G}\overline{\boldsymbol{\varepsilon}}$ and stress ${}^{G}\overline{\boldsymbol{\sigma}}$ of the material are obtained as

$$ \begin{aligned} {}^{G}\overline{\boldsymbol{\varepsilon}} &= \sum_{i=1}^{n}\sum_{j=1}^{m} f_{V(ij)}\,{}^{G}\boldsymbol{\varepsilon}^{V} + \Big(1-\sum_{i=1}^{n}\sum_{j=1}^{m} f_{V(ij)}\Big)\,{}^{G}\boldsymbol{\varepsilon}^{m} = \sum_{i=1}^{n}\frac{f_{V(i)}}{8\pi^2}\int_0^{\pi}\int_0^{2\pi}\int_0^{2\pi} sin\theta\,({}^{G}\boldsymbol{\varepsilon}^{V})\,d\theta\,d\phi\,d\psi + (1-f_V)\,{}^{G}\boldsymbol{\varepsilon}^{m} \\ &= \sum_{i=1}^{n} f_{V(i)}\Big\langle (\mathbf{I}-\mathbf{P}^{\Sigma(i)})\,{}^{G}\overline{\boldsymbol{\varepsilon}} + \big\{ f_{(i)}\mathbf{P}^{p\Sigma\Omega(i)} <^{\mathbf{L}} \boldsymbol{\varepsilon}^{p\Omega(i)} >_{\Omega(i)} + (1-f_{(i)})\mathbf{P}^{p\Sigma\Gamma(i)} <^{\mathbf{L}} \boldsymbol{\varepsilon}^{p\Gamma(i)} >_{\Gamma(i)} \big\}\Big\rangle + (1-f_V)\,{}^{G}\boldsymbol{\varepsilon}^{m}, \end{aligned} \tag{76a} $$

$$ \begin{aligned} {}^{G}\overline{\boldsymbol{\sigma}} &= \sum_{i=1}^{n}\sum_{j=1}^{m} f_{V(ij)}\,{}^{G}\boldsymbol{\sigma}^{V} + \Big(1-\sum_{i=1}^{n}\sum_{j=1}^{m} f_{V(ij)}\Big)\,{}^{G}\boldsymbol{\sigma}^{m} = \sum_{i=1}^{n}\frac{f_{V(i)}}{8\pi^2}\int_0^{\pi}\int_0^{2\pi}\int_0^{2\pi} sin\theta\,({}^{G}\boldsymbol{\sigma}^{V})\,d\theta\,d\phi\,d\psi + (1-f_V)\,{}^{G}\boldsymbol{\sigma}^{m} \\ &= \sum_{i=1}^{n} f_{V(i)}\Big\langle (\overline{\mathbf{C}}-\mathbf{Q}^{\Sigma(i)})\,{}^{G}\overline{\boldsymbol{\varepsilon}} + \big\{ f_{(i)}\mathbf{Q}^{p\Sigma\Omega(i)} <^{\mathbf{L}} \boldsymbol{\varepsilon}^{p\Omega(i)} >_{\Omega(i)} + (1-f_{(i)})\mathbf{Q}^{p\Sigma\Gamma(i)} <^{\mathbf{L}} \boldsymbol{\varepsilon}^{p\Gamma(i)} >_{\Gamma(i)} \big\}\Big\rangle + (1-f_V)\,{}^{G}\boldsymbol{\sigma}^{m}. \end{aligned} \tag{76b} $$

$\mathbf{P}^{\Sigma(i)}$, $\mathbf{P}^{p\Sigma X(i)}$, $\mathbf{Q}^{\Sigma(i)}$, and $\mathbf{Q}^{p\Sigma X(i)}$ $(X=\Omega,\ \Gamma)$ have the same matrix form as Eq. (30), and their components have the same form as Eqs. (31) and (32).

Similar to Eqs. (33) and (34), Eq. (76) can be expressed as equations for the hydrostatic component and the deviatoric one as follows:

$$ \begin{aligned} {}^{G}\overline{\varepsilon}_{ii} &= \sum_{i=1}^{n} f_{V(i)}\Big\langle (1-P_h^{\Sigma(i)})\,{}^{G}\overline{\varepsilon}_{ii} + \big\{ f_{(i)}P_h^{p\Sigma\Omega(i)}L_K^{\Omega(i)} < \varepsilon_{ii}^{p\Omega(i)} >_{\Omega(i)} + (1-f_{(i)})P_h^{p\Sigma\Gamma(i)}L_K^{\Gamma(i)} < \varepsilon_{ii}^{p\Gamma(i)} >_{\Gamma(i)} \big\} \\ &\qquad + \big\{ f_{(i)}P_3^{p\Sigma\Omega(i)}L_\mu^{\Omega(i)\prime} < \varepsilon_{33}^{p\Omega(i)} >_{\Omega(i)} + (1-f_{(i)})P_3^{p\Sigma\Gamma(i)}L_\mu^{\Gamma(i)\prime} < \varepsilon_{33}^{p\Gamma(i)} >_{\Gamma(i)} \big\}\Big\rangle + (1-f_V)\,{}^{G}\varepsilon_{ii}^{m}, \end{aligned} \tag{77a} $$

$$ {}^{\prime G}\overline{\varepsilon}_{ij} = \sum_{i=1}^{n} f_{V(i)}(1-P_d^{\Sigma(i)})\,{}^{\prime G}\overline{\varepsilon}_{ij} + (1-f_V)\,{}^{\prime G}\varepsilon_{ij}^{m}, \tag{77b} $$

$$ \begin{aligned} {}^{G}\overline{\sigma}_{ii} &= 3\overline{K}\sum_{i=1}^{n} f_{V(i)}\Big\langle \big\{1-P_h^{\Sigma(i)} + (1-\overline{\nu})\,{}^{n}P_{11}^{V(i)}\big\}\,{}^{G}\overline{\varepsilon}_{ii} + f_{(i)}\big\{P_h^{p\Sigma\Omega(i)} - (1-\overline{\nu})\,{}^{n}P_{11}^{\Omega(i)}\big\}L_K^{\Omega(i)} < \varepsilon_{ii}^{p\Omega(i)} >_{\Omega(i)} \\ &\qquad + (1-f_{(i)})\big\{P_h^{p\Sigma\Gamma(i)} - (1-\overline{\nu})\,{}^{n}P_{11}^{\Gamma(i)}\big\}L_K^{\Gamma(i)} < \varepsilon_{ii}^{p\Gamma(i)} >_{\Gamma(i)} + f_{(i)}\big\{P_3^{p\Sigma\Omega(i)} - (1-\overline{\nu})\,{}^{n}P_{12}^{\Omega(i)}\big\}L_\mu^{\Omega(i)\prime} < \varepsilon_{33}^{p\Omega(i)} >_{\Omega(i)} \\ &\qquad + (1-f_{(i)})\big\{P_3^{p\Sigma\Gamma(i)} - (1-\overline{\nu})\,{}^{n}P_{12}^{\Gamma(i)}\big\}L_\mu^{\Gamma(i)\prime} < \varepsilon_{33}^{p\Gamma(i)} >_{\Gamma(i)} \Big\rangle + (1-f_V)\,{}^{G}\sigma_{ii}^{m}, \end{aligned} \tag{78a} $$

$$ {}^{\prime G}\overline{\sigma}_{ij} = 2\overline{\mu}\sum_{i=1}^{n} f_{V(i)}\Big\langle 1-P_d^{\Sigma(i)} + \frac{1-\overline{\nu}}{5}\big\{\,{}^{n}P_{22}^{V(i)} + 2(\,{}^{s}P_{23}^{V(i)} + \,{}^{s}P_{12}^{V(i)})\big\}\Big\rangle\,{}^{\prime G}\overline{\varepsilon}_{ij} + (1-f_V)\,{}^{\prime G}\sigma_{ij}^{m}. \tag{78b} $$

The relation between shear stresses and strains is obtained by removing subscript $\prime$ from Eqs. (77b) and (78b). From Eqs. (77), (78), and (35), the relation between ${}^{G}\overline{\varepsilon}_{ij}$ and ${}^{G}\overline{\sigma}_{ij}$ can be obtained. Substituting $\varepsilon_{ij}^{p\Omega(i)} = \varepsilon_{ij}^{p\Gamma(i)} = 0$ in this relation and equating it with Eq. (37), the macroscopic bulk modulus $\overline{K}$ and shear modulus $\overline{\mu}$ are finally obtained as

$$ \begin{aligned} \overline{K} &= K + \frac{(1-\overline{\nu})K\sum_{i=1}^{n} f_{V(i)}\,{}^{n}P_{11}^{V(i)}}{1-f_V+\sum_{i=1}^{n} f_{V(i)}\big\{P_h^{\Sigma(i)} - (1-\overline{\nu})\,{}^{n}P_{11}^{V(i)}\big\}}, \\ \overline{\mu} &= \mu + \frac{\frac{(1-\overline{\nu})}{5}\mu\sum_{i=1}^{n} f_{V(i)}\big\{\,{}^{n}P_{22}^{V(i)} + 2(\,{}^{s}P_{23}^{V(i)} + \,{}^{s}P_{12}^{V(i)})\big\}}{1-f_V+\sum_{i=1}^{n} f_{V(i)}\Big\langle P_d^{\Sigma(i)} - \frac{(1-\overline{\nu})}{5}\big\{\,{}^{n}P_{22}^{V(i)} + 2(\,{}^{s}P_{23}^{V(i)} + \,{}^{s}P_{12}^{V(i)})\big\}\Big\rangle}. \end{aligned} \tag{79} $$

Next, the macroscopic thermal expansion coefficient of the material is considered. As shown in Subsec.2.1.4, we consider the state where the external stress $\sigma_{ij}^0 = 0$ and only the temperature change ΔT occurs. When the thermal expansion of the homogenized material surrounding the coated fillers is regarded as the reference, the thermal expansion strains $\varepsilon_{ij}^{p\Omega(i)}$ and $\varepsilon_{ij}^{p\Gamma(i)}$ occurred in the coated fillers are given by

$$\varepsilon_{ij}^{pX(i)} = \delta_{ij}(\alpha^{X(i)} - \overline{\alpha})\Delta T \quad , \quad (X = \Omega\,, \Gamma)\,, \tag{80}$$

where $\alpha^{X(i)}$ $(X = \Omega,\ \Gamma)$ in Eq. (80) is the thermal expansion coefficient of the region X. The hydrostatic components of the total strain and stress of the coated filler $V(ij)$ are given as follows by referring to Eq. (44)

$$\begin{aligned}
{}^{L(j)}\varepsilon_{ii}^{V} &= 3\Big\langle f_{(i)}\Big\{\frac{(1+\overline{\nu})}{3}\,{}^{n}P_{11}^{\Omega(i)} - \frac{(1-2\overline{\nu})}{2}\alpha_3^{V(i)}\,{}^{n}P_{21}^{\Omega(i)}\Big\}L_K^{\Omega(i)}(\alpha^{\Omega(i)} - \overline{\alpha}) \\
&\quad + (1-f_{(i)})\Big\{\frac{(1+\overline{\nu})}{3}\,{}^{n}P_{11}^{\Gamma(i)} - \frac{(1-2\overline{\nu})}{2}\alpha_3^{V(i)}\,{}^{n}P_{21}^{\Gamma(i)}\Big\}L_K^{\Gamma(i)}(\alpha^{\Gamma(i)} - \overline{\alpha})\Big\rangle + 3\overline{\alpha}\,\Delta T \\
&= 3\Big\{f\,P_h^{p\Sigma\Omega}L_K^{\Omega}(\alpha^{\Omega} - \overline{\alpha}) + (1-f)P_h^{p\Sigma\Gamma}L_K^{\Gamma}(\alpha^{\Gamma} - \overline{\alpha})\Big\}\Delta T + 3\overline{\alpha}\,\Delta T\,,
\end{aligned} \tag{81a}$$

$${}^{L(j)}\sigma_{ii}^{V} = 9\overline{K}\Big\langle f_{(i)}\big\{P_h^{p\Sigma\Omega(i)} - (1-\overline{\nu})\,{}^{n}P_{11}^{\Omega(i)}\big\}L_K^{\Omega}(\alpha^{\Omega(i)} - \overline{\alpha}) + (1-f_{(i)})\big\{P_h^{p\Sigma\Gamma(i)} - (1-\overline{\nu})\,{}^{n}P_{11}^{\Gamma(i)}\big\}L_K^{\Gamma}(\alpha^{\Gamma(i)} - \overline{\alpha})\Big\rangle\Delta T\,. \tag{81b}$$

Transforming Eq. (81) to the global coordinate system and taking the sum of the total strain and stress in coated fillers and the matrix, the hydrostatic components of the macroscopic total strain and stress of the material are given as follows by referring to Eq. (45)

$${}^{G}\overline{\varepsilon}_{ii} = 3\sum_{i=1}^{n} f_{V(i)}\Big\{f_{(i)}P_h^{p\Sigma\Omega(i)}L_K^{\Omega(i)}(\alpha^{\Omega(i)} - \overline{\alpha}) + (1-f_{(i)})P_h^{p\Sigma\Gamma(i)}L_K^{\Gamma(i)}(\alpha^{\Gamma(i)} - \overline{\alpha})\Big\}\Delta T + 3f_V\,\overline{\alpha}\,\Delta T + (1-f_V)^{G}\varepsilon_{ii}^{m} = 3\overline{\alpha}\Delta T\,, \tag{82a}$$

$$\begin{aligned}
{}^{G}\overline{\sigma}_{ii} &= 9\overline{K}\sum_{i=1}^{n} f_{V(i)}\Big\langle f_{(i)}\big\{P_h^{p\Sigma\Omega(i)} - (1-\overline{\nu})\,{}^{n}P_{11}^{\Omega(i)}\big\}L_K^{\Omega(i)}(\alpha^{\Omega(i)} - \overline{\alpha}) \\
&\quad + (1-f_{(i)})\big\{P_h^{p\Sigma\Gamma(i)} - (1-\overline{\nu})\,{}^{n}P_{11}^{\Gamma(i)}\big\}L_K^{\Gamma(i)}(\alpha^{\Gamma(i)} - \overline{\alpha})\Big\rangle\Delta T + (1-f_V)\,{}^{G}\sigma_{ii}^{m} = 0\,.
\end{aligned} \tag{82b}$$

We can obtain the total stress ${}^{G}\sigma_{ii}^{m}$ in the matrix from Eq. (82b), and derive the total strain ${}^{G}\varepsilon_{ii}^{m}$ in the matrix, similar to Eq. (47). Substituting obtained ${}^{G}\varepsilon_{ii}^{m}$ into Eq. (80) and solving for the macroscopic thermal expansion coefficient $\overline{\alpha}$, we have

$$\overline{\alpha} = \alpha + \frac{\displaystyle\sum_{i=1}^{n} f_{V(i)}\Big\{f_{(i)}\mathscr{P}^{\Omega(i)}L_K^{\Omega(i)}(\alpha^{\Omega(i)} - \alpha) + (1-f_{(i)})\mathscr{P}^{\Gamma(i)}L_K^{\Gamma(i)}(\alpha^{\Gamma(i)} - \alpha)\Big\}}{(1-f_V)K + \displaystyle\sum_{i=1}^{n} f_{V(i)}\Big\{f_{(i)}\mathscr{P}^{\Omega(i)}L_K^{\Omega(i)} + (1-f_{(i)})\mathscr{P}^{\Gamma(i)}L_K^{\Gamma(i)}\Big\}}\,, \tag{83a}$$

$$\mathscr{P}^{X(i)} = (K - \overline{K})P_h^{p\Sigma X(i)} + (1-\overline{\nu})\overline{K}\,{}^{n}P_{11}^{X(i)} \quad , \quad (X = \Omega,\ \Gamma)\,. \tag{83b}$$

By comparing Eqs. (38) and (79), and Eqs. (48) and (83), it can be observed that the solutions for the macroscopic properties of materials with various types of coated fillers can be obtained by summing the terms related to the shape, properties, and volume fraction of the coated fillers included in the solutions for the macroscopic properties of materials with a single kind of coated filler. In this way, it is possible to express the solutions in a simple form. However, it is anticipated that numerically determining the values of $\overline{K}$ and $\overline{\mu}$ that satisfy Eq. (79) will be difficult in practice. As a method to avoid this difficulty, a method of repeating homogenization in multiple stages can be considered. In this method, first, the macroscopic elastic moduli and the thermal expansion coefficient when only one kind of coated filler is included in the material are derived by using Eqs. (38) and (48). Furthermore, by repeating homogenization by adding another type of coated fillers to the matrix with macroscopic elastic moduli obtained in the previous homogenization, the macroscopic elastic moduli and the thermal expansion coefficient can be obtained. It is an interesting question how the macroscopic physical properties obtained differ between this method and the direct solutions of Eqs. (79) and (83). Since this discussion is beyond the scope of this paper, it is left for future study.

3.3. The Mori-Tanaka theorem

Similar to Sec.2.2, the solution of macroscopic elastic moduli can be obtained by replacing the solutions obtained in the previous section with Eqs. (54) and (57). Therefore, referring to Eqs. (77) and (78), the total macroscopic strain ${}^{G}\overline{\varepsilon}$ and stress ${}^{G}\overline{\sigma}$ of the material are given as follows:

$$\begin{aligned}
{}^{G}\overline{\varepsilon}_{ii} &= \Big\{\sum_{i=1}^{n} f_{V(i)}(1 - P_h^{\Sigma(i)}) + (1-f_V)\Big\}({}^{G}\varepsilon_{ii}^{0} + {}^{G}\tilde{\varepsilon}_{ii}) \\
&\quad + \sum_{i=1}^{n} f_{V(i)}\Big\langle\big\{f_{(i)}P_h^{p\Sigma\Omega(i)}L_K^{\Omega(i)} < \varepsilon_{ii}^{p\Omega(i)} >_{\Omega(i)} + (1-f_{(i)})P_h^{p\Sigma\Gamma(i)}L_K^{\Gamma(i)} < \varepsilon_{ii}^{p\Gamma(i)} >_{\Gamma(i)}\big\}
\end{aligned}$$

$$+\left\{ f_{(i)} P_3^{p\Sigma\Omega(i)} L_\mu^{\Omega(i)\prime} < \varepsilon_{33}^{p\Omega(i)} >_{\Omega(i)} + (1-f_{(i)}) P_3^{p\Sigma\Gamma(i)} L_\mu^{\Gamma(i)\prime} < \varepsilon_{33}^{p\Gamma(i)} >_{\Gamma(i)} \right\} \Big\rangle , \tag{84a}$$

$${}'^G\overline{\varepsilon}_{ij} = \Big\{ \sum_{i=1}^{n} f_{V(i)} (1 - P_d^{\Sigma(i)}) + (1-f_V) \Big\} ({}'^G\varepsilon_{ij}^0 + {}'^G\tilde{\varepsilon}_{ij}) , \tag{84b}$$

$${}^G\overline{\sigma}_{ii} = 3K \Big\langle \sum_{i=1}^{n} f_{V(i)} \left\{ 1 - P_h^{\Sigma(i)} + (1-\nu)\, {}^n P_{11}^{V(i)} \right\} + (1-f_V) \Big\rangle ({}^G\varepsilon_{ii}^0 + {}^G\tilde{\varepsilon}_{ii})$$
$$+ \sum_{i=1}^{n} f_{V(i)} \Big\langle f_{(i)} \left\{ P_h^{p\Sigma\Omega(i)} - (1-\nu)\, {}^n P_{11}^{\Omega(i)} \right\} L_K^{\Omega(i)} < \varepsilon_{ii}^{p\Omega(i)} >_{\Omega(i)} + (1-f_{(i)}) \left\{ P_h^{p\Sigma\Gamma(i)} - (1-\nu)\, {}^n P_{11}^{\Gamma(i)} \right\} L_K^{\Gamma(i)} < \varepsilon_{ii}^{p\Gamma(i)} >_{\Gamma(i)}$$
$$+ f_{(i)} \left\{ P_3^{p\Sigma\Omega(i)} - (1-\nu)\, {}^n P_{12}^{\Omega(i)} \right\} L_\mu^{\Omega(i)\prime} < \varepsilon_{33}^{p\Omega(i)} >_{\Omega(i)} + (1-f_{(i)}) \left\{ P_3^{p\Sigma\Gamma(i)} - (1-\nu)\, {}^n P_{12}^{\Gamma(i)} \right\} L_\mu^{\Gamma(i)\prime} < \varepsilon_{33}^{p\Gamma(i)} >_{\Gamma(i)} \Big\rangle , \tag{85a}$$

$${}'^G\overline{\sigma}_{ij} = 2\mu \Big\{ \sum_{i=1}^{n} f_{V(i)} (1 - P_d^{\Sigma(i)}) + (1-f_V) \Big\} ({}'^G\varepsilon_{ij}^0 + {}'^G\tilde{\varepsilon}_{ij}) + \frac{1-\nu}{5} \sum_{i=1}^{n} f_{V(i)} \left\{ {}^n P_{22}^{V(i)} + 2({}^s P_{23}^{V(i)} + {}^s P_{12}^{V(i)}) \right\} . \tag{85b}$$

Substituting $\varepsilon_{ij}^{p\Omega(i)} = \varepsilon_{ij}^{p\Gamma(i)} = 0$ and eliminating $({}^G\varepsilon_{ij}^0 + {}^G\tilde{\varepsilon}_{ij})$ in Eqs. (84) and (85), we can find the relation between ${}^G\overline{\varepsilon}_{ij}$ and ${}^G\overline{\sigma}_{ij}$. Equating the obtained relation with Eq. (37), the macroscopic bulk modulus $\overline{K}$ and shear modulus $\overline{\mu}$ are given by

$$\overline{K} = K + \frac{(1-\nu) K \sum_{i=1}^{n} f_{V(i)}\, {}^n P_{11}^{V(i)}}{1 - \sum_{i=1}^{n} f_{V(i)} P_h^{\Sigma}} \quad , \quad \overline{\mu} = \mu + \frac{\frac{(1-\nu)}{5} \mu \sum_{i=1}^{n} f_{V(i)} \left\{ {}^n P_{22}^{V(i)} + 2({}^s P_{23}^{V(i)} + {}^s P_{12}^{V(i)}) \right\}}{1 - \sum_{i=1}^{n} f_{V(i)} P_d^{\Sigma(i)}} . \tag{86}$$

Next, we consider the macroscopic thermal expansion coefficient of the material. As mentioned in the previous section, we consider the state where the external stress $\sigma_{ij}^0 = 0$ and only the temperature change ΔT occurs. In the same way as Eq. (64), when the thermal expansion of the matrix is regarded as the reference, the thermal expansion strains $\varepsilon_{ij}^{p\Omega(i)}$ and $\varepsilon_{ij}^{p\Gamma(i)}$ that occur in the coated filler $V(ij)$ are expressed by

$$\varepsilon_{ij}^{pX(i)} = \delta_{ij} (\alpha^{X(i)} - \alpha) \Delta T \quad , \quad (X = \Omega\, , \Gamma) . \tag{87}$$

From Eq. (87), the hydrostatic components in Eqs. (84) and (85) are given by

$${}^G\overline{\varepsilon}_{ii} = \Big\{ \sum_{i=1}^{n} f_{V(i)} (1 - P_h^{\Sigma(i)}) + (1-f_V) \Big\}\, {}^G\tilde{\varepsilon}_{ii}$$
$$+ 3 \sum_{i=1}^{n} f_{V(i)} \Big\{ f_{(i)} P_h^{p\Sigma\Omega(i)} L_K^{\Omega(i)} (\alpha^{\Omega(i)} - \alpha) + (1-f_{(i)}) P_h^{p\Sigma\Gamma(i)} L_K^{\Gamma(i)} (\alpha^{\Gamma(i)} - \alpha) \Big\} \Delta T + 3\alpha \Delta T = 3\overline{\alpha} \Delta T , \tag{88a}$$

$${}^G\overline{\sigma}_{ii} = 3K \Big\langle \sum_{i=1}^{n} f_{V(i)} \left\{ 1 - P_h^{\Sigma(i)} + (1-\nu)\, {}^n P_{11}^{V(i)} \right\} + (1-f_V) \Big\rangle\, {}^G\tilde{\varepsilon}_{ii} \tag{88b}$$
$$+ 9K \sum_{i=1}^{n} f_{V(i)} \Big\langle f_{(i)} \left\{ P_h^{p\Sigma\Omega(i)} - (1-\nu)\, {}^n P_{11}^{\Omega(i)} \right\} L_K^{\Omega(i)} (\alpha^{\Omega(i)} - \alpha) + (1-f_{(i)}) \left\{ P_h^{p\Sigma\Gamma(i)} - (1-\nu)\, {}^n P_{11}^{\Gamma(i)} \right\} L_K^{\Gamma(i)} (\alpha^{\Gamma(i)} - \alpha) \Big\rangle \Delta T = 0 .$$

The interaction strain ${}^G\tilde{\varepsilon}_{ii}$ can be obtained from Eq. (88b). Substituting this into Eq. (88a), the macroscopic thermal expansion coefficient $\overline{\alpha}$ is obtained as

$$\overline{\alpha} = \alpha + \frac{1-\nu}{1 - \sum_{i=1}^{n} f_{V(i)} \left\{ P_h^{\Sigma(i)} - (1-\nu)\, {}^n P_{11}^{V(i)} \right\}}$$
$$\Big\langle \Big\{ 1 - \sum_{i=1}^{n} f_{V(i)} P_h^{\Sigma(i)} \Big\} \sum_{i=1}^{n} f_{V(i)} \left\{ f_{(i)}\, {}^n P_{11}^{\Omega(i)} L_K^{\Omega(i)} (\alpha^{\Omega(i)} - \alpha) + (1-f_{(i)})\, {}^n P_{11}^{\Gamma(i)} L_K^{\Gamma(i)} (\alpha^{\Gamma(i)} - \alpha) \right\}$$
$$+ \sum_{i=1}^{n} f_{V(i)}\, {}^n P_{11}^{V(i)} \sum_{i=1}^{n} f_{V(i)} \left\{ f_{(i)} P_h^{p\Sigma\Omega(i)} L_K^{\Omega(i)} (\alpha^{\Omega(i)} - \alpha) + (1-f_{(i)}) P_h^{p\Sigma\Gamma(i)} L_K^{\Gamma(i)} (\alpha^{\Gamma(i)} - \alpha) \right\} \Big\rangle . \tag{89}$$

By comparing Eqs. (58) and (86), it can be found that the solutions for the macroscopic elastic moduli of materials with various types of coated fillers can be obtained by summing the terms related to the shape, properties, and volume fraction of the coated fillers included in the solutions for the macroscopic elastic moduli of materials with a single kind of coated filler. However, when comparing Eqs. (67) and (89), it should be noted that the macroscopic thermal expansion coefficient is not such a simple summation.

Table 1
Elastic constants and thermal expansion coefficient of constituents and aspect ratios of the coated filler.

	Young's modulus (GPa)	Poisson's ratio	Thermal expansion coefficient $\times 10^{-6}(1/K)$	Aspect ratio
Matrix	1	0.35	10	-
Filler	25	0.25	1	10 ($=\omega_3^{\Omega}$)
Interface	5	0.30	5	5 ($=\omega_3^{V}$)

As described in the summary of the self-consistent method in the previous section, a method of repeating homogenization in multiple stages by using the Mori-Tanaka theorem can be considered. The difference between the direct summation method (Eqs. (86) and (89)) and stepwise homogenization is expected to appear as a difference in the evaluation of the interaction between the coated fillers. This point is also a topic for future study.

4. Numerical calculations and discussions

In this chapter, we utilize the solutions obtained in Chap.2 to perform numerical calculations. First, we confirm whether the macroscopic elastic moduli and the thermal expansion coefficient based on the self-consistent method, the Mori-Tanaka theorem, and Christensen's method satisfy the boundary condition for the volume fraction f_V of the coated fillers. After this confirmation, as composite materials considered for practical use, we assume a material CNT/Al impregnated with carbon nanotubes (CNT) into an Al matrix. This material is designed to improve the rigidity and reduce the thermal expansion of the Al matrix simultaneously. In this material, an interfacial layer consisting of aluminum carbide (Al_4C_3) is formed on the surface of CNT fillers through the chemical reaction between CNT and the Al matrix. It has been clarified that this interfacial layer significantly influences the macroscopic Young's modulus and thermal expansion coefficient of the material.

He et al. fabricated CNT/Al materials containing CNT fillers with various volume fractions using a powder metallurgy method. They experimentally obtained the macroscopic Young's modulus of this material [6]. Similarly, Aborkin et al. fabricated the same material as He et al. They confirmed the formation of the Al_4C_3 interfacial layer on the surface of CNT fillers and experimentally obtained the macroscopic thermal expansion coefficient of the material [5]. Comparing with these experimental results, we verify the applicability of the analytical solutions to real materials.

On the other hand, Shi et al. conducted a numerical analysis of CNT/Al using the finite element method. They investigated the effect of the volume fraction of the CNT fillers and the thickness of the Al_4C_3 interfacial layer on the macroscopic thermal expansion coefficient of the material [35]. By comparing with the results of this numerical calculation, we will verify the accuracy of the solutions of the macroscopic thermal expansion coefficient of the material. Furthermore, we will examine the effect of the shape of the CNT fillers, which was not considered in the aforementioned experiments and finite element analyses, and explore design guidelines for this material.

4.1. Boundary conditions of macroscopic physical properties for volume fraction of the coated fillers and this confirmation

The solutions for the macroscopic elastic modulus, Eqs. (38), (58), and (72a, 72b) and the macroscopic thermal expansion coefficient, Eqs. (48), (67), and (73) must become those of the matrix when the volume fraction f_V of the coated fillers is zero. We can immediately see from these equations that this boundary condition is satisfied, though some calculations are required to confirm this for Eqs. (72a), (72b) and (73). However, when the material is filled with coated filler, that is $f_V = 1$, it is unclear what values these physical properties should converge to. When the volume fraction f of the filler in the coated filler V is zero, the filler region disappears. On the other hand, when $f = 1$, the coating layer disappears. Under these conditions, the solutions of the macroscopic physical properties should agree with those for the single-phase filler that the author has already derived [20]. This comparison requires a very complicated expansion of the equations, so we will confirm it through numerical calculations. Table 1 shows the physical properties of the constituents used in the calculations. The aspect ratios of the inner region Ω and outer region V of the coated filler are $\omega_3^{\Omega} = 10$ and $\omega_3^{V} = 5$, respectively. Although these physical properties are not based on actual materials, all values are given to be different from each other without loss of generality.

Fig. 5 shows the change in the macroscopic bulk modulus $\overline{K}$ with f_V. The vertical axis of the figure is $\overline{K}/K$ nondimensionalized by the bulk modulus K of the matrix. Fig. 5(a) shows the result when $f = 0$, that is, the filler in the coated filler disappears and the filler is a single-phase region with the physical properties of the coating layer. On the other hand, Fig. 5(b) shows the result when the coating layer disappears. In the latter case, we should note that simply substituting $f = 1$ into the solutions shown in Chapter 2 is a mistake. This is because if the inner and outer shapes of the coated fillers are not similar and their aspect ratios are different from each other, the two regions cannot overlap in the condition of $f = 1$. Therefore, in this condition, the inner and outer shapes of the coated fillers must be similar, that is, $\omega_3^{\Omega} = \omega_3^{V}$. In this case, all coefficients associated with Δ, which represents the difference in shape between the inner and outer regions of the coated filler, disappear, and all terms including $f/(1-f)$ in the coefficients shown in Appendices A.2 and A.3 also disappear. This automatically avoids the divergence at $f = 1$.

The solid red, blue, and green lines in Fig. 5 are the results of the solutions based on the self-consistent method (SC), the Mori-Tanaka theorem (MT), and Christensen's method (CM) obtained in Chap.2. The black solid lines are the solutions of the upper and lower bounds of Hashin et al. When $f = 0$ and $f_V = 1$, the value of $\overline{K}/K$ must be $K^{\Gamma}/K = 3.75$ from the values in Table 1. Similarly,

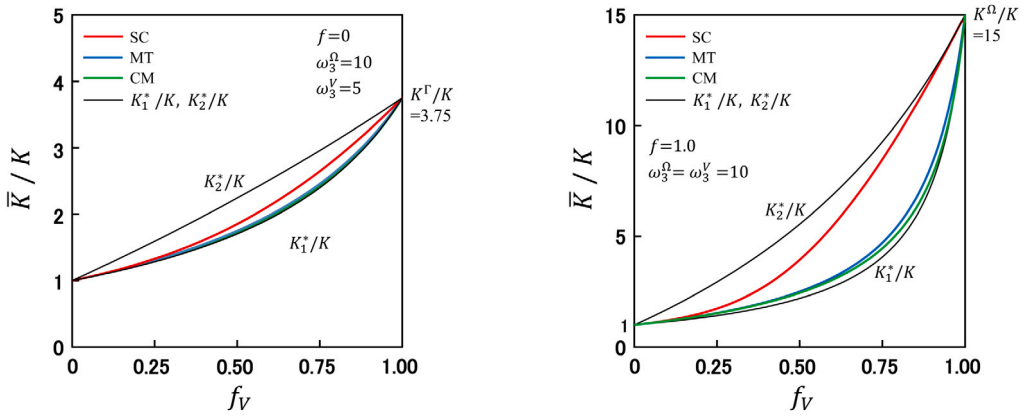

Fig. 5. Change in macroscopic bulk modulus $\overline{K}/K$ with the volume fraction f_V of the coated fillers.

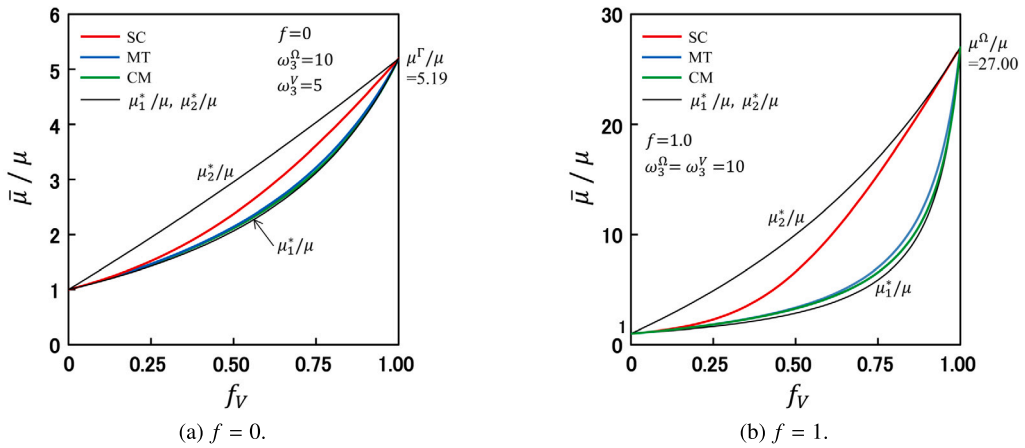

Fig. 6. Change in macroscopic shear modulus $\overline{K}/K$ with the volume fraction f_V of the coated fillers.

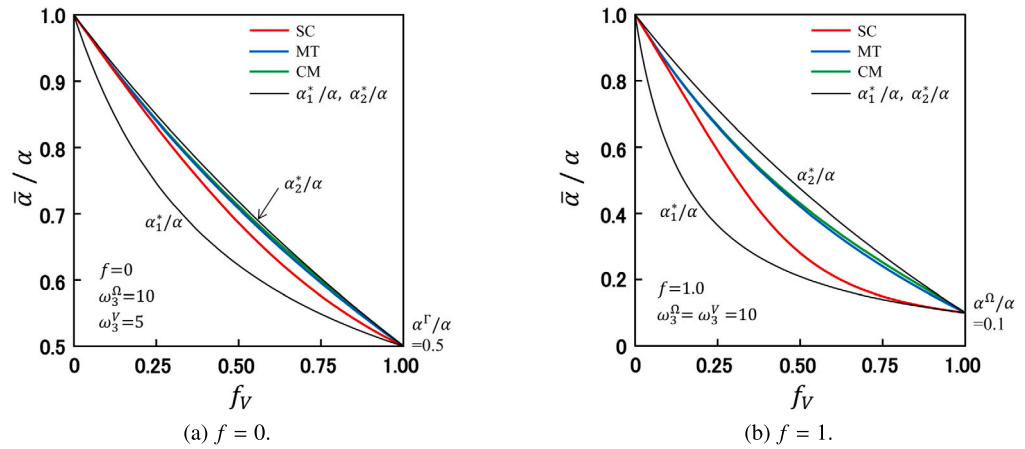

Fig. 7. Change in macroscopic thermal expansion coefficient $\overline{\alpha}/\alpha$ with the volume fraction f_V of the coated fillers.

when $f = 1$ and $f_V = 1$, the value of $\overline{K}/K$ must be $K^\Omega/K = 15$. We can see from Figs. 5(a) and 5(b) that these conditions are satisfied. We can also confirm that the results of SC, MT, and CM fall between the upper and lower bounds and are valid from the viewpoint of energy. Figs. 6(a) and 6(b) show the results of the macroscopic shear modulus $\overline{\mu}$, while Figs. 7(a) and 7(b) the results for the macroscopic thermal expansion coefficient $\overline{\alpha}$. The line types in the figures are the same as in Fig. 5. Similar to $\overline{K}$, these results also satisfy the conditions at $f_V = 1$, and the results of SC, MT, and CM fall between the upper and lower bounds. The results of SC

Table 2
Elastic constants, thermal expansion coefficient, and density of constituents.

	Material	Young's modulus (GPa)	Poisson's ratio	Thermal expansion coefficient $\times 10^{-6}(1/K)$	Density (g/cm^3)
Matrix	Al	71.1 (He et al.)	0.33	21.40	2.69
		67.6 (Aborkin et al.)			
Filler	CNT	1280.0	0.20	0.85	2.10
Interface	Al_4C_3	289.8	0.20	3.60	-

He et al.(2009), Aborkin et al.(2021), Ahmadi et al.(2019)

Table 3
Dimensions of CNT and Al_4C_3, aspect ratios, and volume fraction used in experiments by He et al.(2009).

Diameter of CNT	Length of CNT	Thickness of Al_4C_3	Aspect ratio of CNT	Aspect ratio of $(CNT + Al_4C_3)$	Volume fraction of CNT in $(CNT + Al_4C_3)$
$d_{CNT}(nm)$	$L_{CNT}(nm)$	$t_{Al_4C_3}(nm)$	ω_3^{Ω}	ω_3^{V}	f
15	1800	3	120.0	86.0	0.51

Table 4
Dimensions of CNT and Al_4C_3, aspect ratios, and volume fraction used in experiments by Aborkin et al.(2021).

Diameter of CNT	Length of CNT	Thickness of Al_4C_3	Aspect ratio of CNT	Aspect ratio of $(CNT + Al_4C_3)$	Volume fraction of CNT in $(CNT + Al_4C_3)$
$d_{CNT}(nm)$	$L_{CNT}(nm)$	$t_{Al_4C_3}(nm)$	ω_3^{Ω}	ω_3^{V}	f
80	800	27.5	10	6.33	0.33

and MT agree with those of the solutions obtained by the author for the single-phase fillers [20]. In Figs. 5 to 7, we can find that the results of CM are close to those of MT, regardless of the value of f_V. The slight difference between the two methods is because CM does not take into account the interaction between the fillers with different orientations, as mentioned in Sec.2.3. We can also see that the results of MT and CM deviate significantly from that of SC as f_V increases. This behavior is a well-known fact, and MT and CM have poor accuracy when the fillers are included in the material at high concentrations.

This calculation result is only an example. However, the analytical solutions will give valid results even for combinations of other constituents, since the solutions are continuous in terms of physical properties, shapes, and volume fractions of the constituents.

4.2. Comparison with experimental results

In this section, the experimental results of He et al. and Aborkin et al. for the macroscopic Young's modulus and thermal expansion coefficient of CNT/Al are compared with the analytical results. Table 2 shows the Young's modulus, Poisson's ratio, thermal expansion coefficient, and density of the constituents used in the analysis. Since the paper by He et al. does not describe physical properties other than the Young's modulus and the density of the Al matrix, the physical properties given in the papers by Aborkin et al. and Ahmadi et al. [5] [36] will be used. As indicated in Table 2, since He et al. and Aborkin et al. employed different Young's modulus for the Al matrix, we will compare the experimental results using the corresponding Young's moduli for each Al matrix. Tables 3 and 4 show the dimensions of the CNT fiber and interfacial layer Al_4C_3 used in the experiments by He et al. and Aborkin et al. From these values, the aspect ratio of the CNT fiber, $\omega_3^{\Omega} = L_{CNT}/d_{CNT}$, the aspect ratio of the region V consisting of the CNT fiber and the interfacial layer Al_4C_3, $\omega_3^{V} = (L_{CNT} + 2t_{Al_4C_3})/(d_{CNT} + 2t_{Al_4C_3})$, and the volume fraction f of the CNT region occupied in the region V are also listed in each table. The values listed in these tables are used in comparisons with the experimental results of He et al. and Aborkin et al.

Fig. 8 shows the change in the macroscopic Young's modulus $\overline{E}$ with the volume fraction f_{CNT} of the CNT fillers excluding interfacial layer Al_4C_3. The vertical axis of the figure is $\overline{E}/E$, which is dimensionless with the Young's modulus E of the matrix. The dashed red, blue, and green lines in the figure indicate the results of the self-consistent method (SC), the Mori-Tanaka theorem (MT), and Christensen's method (CM) when the interface layer Al_4C_3 does not exist. The solid red, blue, and green lines are the results of SC, MT, and CM in the presence of the interfacial layer Al_4C_3 with the thickness shown in Table 3. The black dots in the figure indicate the experimental results of He et al. In the experiment by He et al., the results for the macroscopic Young's modulus versus the weight fraction of the CNT fillers are obtained. Therefore, in the figure, we have plotted the data converted from weight fraction to volume fraction using the densities in Table 2.

First, comparing the analytical results of the dashed lines and the solid lines, we observe that regardless of the value of f_{CNT}, the value of $\overline{E}/E$ when the interfacial layer is present is higher than that when the interfacial layer is not present. This is a reasonable result because the Young's modulus of the interfacial layer is higher than that of the Al matrix, as shown in Table 2. Comparing the results of SC, MT, and CM, we can see that the difference between the three methods is small within the range of f_{CNT} shown

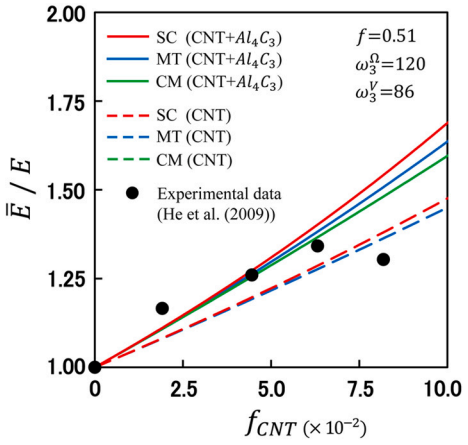

Fig. 8. Change in macroscopic Young's modulus $\overline{E}/E$ with the volume fraction f_{CNT}.

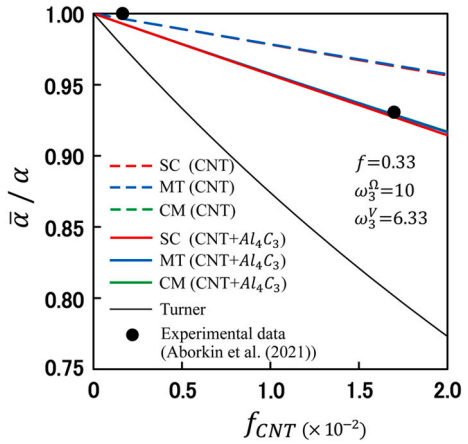

Fig. 9. Change in macroscopic thermal expansion coefficient $\overline{\alpha}/\alpha$ with the volume fraction f_{CNT}.

in the figure. In particular, the results of CM and MT shown by the dashed lines almost overlap, and there is almost no difference between them. This result is consistent with the general observation that, although the evaluation for the interaction among fillers is different between these methods, there is little difference between the results of these methods at low volume fraction of the fillers. Comparing these analytical results with the experimental ones, we find that the analytical results shown by the solid line agree well with the experimental results within the range where the value of f_{CNT} is less than 0.075. The reason why $\overline{E}/E$ decreases when f_{CNT} exceeds 0.075 is considered to be due to aggregations of the CNT fillers. The CNT/Al composites used in He et al.'s experiment are formed and fabricated using a powder metallurgy method. They reported that CNT fillers gather together to form spherical aggregations within the Al matrix [6]. In addition, it has been confirmed that CNT fillers exist in a wavy shape within the aggregations. Since such a CNT aggregation can be approximately regarded as a spherical filler, the aspect ratio of the CNT filler appears to decrease. It is considered that this causes the macroscopic Young's modulus to decrease. Mohammad et al. and Mojtaba et al. performed the micromechanical analyses that take into account the presence of such aggregations and the wavy shape of CNT fillers [37] [38]. These structural factors are the subject of future research.

Fig. 9 shows the change in the macroscopic thermal expansion coefficient $\overline{\alpha}$ with the volume fraction f_{CNT}. The vertical axis of the figure is $\overline{\alpha}/\alpha$, which is dimensionless with the thermal expansion coefficient α of the matrix. The line types in the figure are the same as in Fig. 8, and the black dots are the experimental results of Aborkin et al. The solid black line in the figure shows Turner's empirical law, and the solution for the macroscopic thermal expansion coefficient of the composite material consisting of the n phase is given as

$$\overline{\alpha} = \left\{ \sum_{i=1}^{n} f_i K_i \alpha_i \right\} \Big/ \left\{ \sum_{i=1}^{n} f_i K_i \right\} \quad , \tag{90}$$

where α_i, K_i, and f_i are the thermal expansion coefficient, bulk modulus, and volume fraction of the i-th phase.

First, comparing the analytical results of the dashed lines and the solid lines, we observe that regardless of the value of f_{CNT}, the value of $\overline{\alpha}/\alpha$ when the interfacial layer is present is lower than that when the interfacial layer is not present. This is a reasonable result because the thermal expansion coefficient of the interfacial layer is lower than that of the Al matrix, as shown in Table 2.

Table 5
Elastic constants and thermal expansion coefficient of constituents used by Shi et al.(2019).

	Material	Young's modulus (GPa)	Poisson's ratio	Thermal expansion coefficient $\times 10^{-6}(1/K)$
Matrix	Al	77	0.33	23.6
Filler	CNT	680	0.27	1.0
Interface	Al_4C_3	309	0.20	5.0

Similar to Fig. 8, we can see that the results of SC, MT, and CM take almost the same value regardless of the value of f_{CNT}. In particular, since the lines of MT overlap with those of CM, the lines of CM do not appear in the figure. Comparing these analytical results with the experimental ones, we find that the analytical results indicated by the solid line agree well with the experimental results, although the number of data points is small. On the other hand, we can see that the Tuner's results obtained from Eq. (90) are significantly different from the experimental results. This means that it is impossible to predict the macroscopic thermal expansion coefficient with the simple sum of the physical properties shown in the above equation.

From the above results, it is considered that the analytical results of the macroscopic Young's modulus have sufficient accuracy in the range of the volume fraction of the CNT fillers less than 7.5%, indicating that CNT fillers are uniformly dispersed in the material. However, for the thermal expansion coefficient, there are few experimental data points to be compared, and the volume fraction of the CNT fillers is less than 5%, so the accuracy verification is not sufficient. Therefore, in the next section, we will compare the analytical results with the numerically calculated results obtained by the finite element method for the macroscopic thermal expansion coefficient.

4.3. Comparison of macroscopic thermal expansion coefficient with numerically calculated results using the finite element method

In this section, we compare the analytical results with numerically calculated results obtained by Shi et al. using the finite element method for the macroscopic thermal expansion coefficient of CNT/Al. Shi et al. calculated the macroscopic thermal expansion coefficients of CNT/Al for cases where CNT fibers with interfacial layers are randomly oriented in two dimensions (2D) and three dimensions (3D) within the material, and compared the results of both cases [35]. According to their calculations, in the case of 3D random orientation, the number of elements is approximately four times larger than that of 2D random orientation, and the calculation time for a certain condition is shown to be about 230 times longer than that of 2D random orientation. However, the difference between the macroscopic thermal expansion coefficients obtained for each case is about 1.6%, so they approximate the calculation of 3D random orientation with 2D random orientation, which is good computational efficiency. The physical properties of the constituents used in Shi et al.'s analysis are presented in Table 5, while the dimensions of the CNT filler and the interfacial layer Al_4C_3 are shown in Table 6. The aspect ratios and volume fractions in Table 6 are calculated from the dimensions of the CNT filler and the interfacial layer Al_4C_3, similar to Tables 3 and 4. In this analysis, the values in these tables are used for comparison with the results of Shi et al.

Fig. 10 shows the change in the macroscopic thermal expansion coefficient $\overline{\alpha}$ with the volume fraction f_{CNT}. The red, blue, and green lines in the figure are the results of SC, MT, and CM, respectively, as in the previous figures. The black and white circular markers in the figure represent Shi et al.'s analytical results for the cases with and without the Al_4C_3 interfacial layer, respectively. The results with and without the Al_4C_3 interfacial layer show that $\overline{\alpha}$ decreases linearly as f_{CNT} increases. As shown in Table 5, the thermal expansion coefficients of the CNT filler and the Al_4C_3 interfacial layer are smaller than that of the Al matrix, so this is a natural result. When the value of f_{CNT} is constant, the value of $\overline{\alpha}$ with the interface layer is approximately 10% lower than that without the interface layer. This reduction rate appears higher than that due to the effect of only CNT fillers without the Al_4C_3 interface layer, when compared to the thermal expansion coefficients of CNT and Al_4C_3 as shown in Table 5. As indicated in Eqs. (48) and (67), this behavior is due to a synergistic effect arising from the product of their thermal expansion coefficients and elastic moduli. Comparing the dashed lines with the white circular markers, we can observe that they generally show good quantitative agreement. On the other hand, comparing the solid line with the black circular markers representing the case with the interfacial layer, we can find that the results of the solid line are slightly lower than the black circular markers. Furthermore, as f_{CNT} increases, the difference between them also increases. However, the difference between them at $f_{CNT} = 0.1$ is about 5%.

Fig. 11 shows the change in the macroscopic thermal expansion coefficient $\overline{\alpha}$ with the diameter d_{CNT} of the CNT filler. As an analytical condition, the volume fraction f_{CNT} is constant at 0.05. The dimensions other than the diameter d_{CNT} shown in Table 6 are also constant. Therefore, it should be noted that the volume fraction f and the aspect ratios ω_3^{Ω} and ω_3^{V} change simultaneously with the change of d_{CNT}. The types of lines and markers in the figure are the same as in Fig. 10. The results of SC, MT, CM, and FEM show that $\overline{\alpha}$ increases as d_{CNT} increases. This is because when d_{CNT} increases, the aspect ratio of CNT decreases and the shape of the CNT fillers approaches to be spherical, which increases the thermal expansion strain of the whole material. This tendency is independent of the presence or absence of the interfacial layer, so it is a valid result.

Next, comparing the results of SC, MT, CM, and FEM for the case without the interface layer, we can see that the results of SC, MT, and CM are almost the same. The difference between these analytical results and the FEM result is only a few % at most. Similarly, when considering the interfacial layer, this difference decreases as d_{CNT} increases. However, when d_{CNT} becomes smaller than 30(nm), that is, when the aspect ratio of the CNT filler increases and the shape of the fillers approaches to be long fibrous, the difference becomes more than 10%. Therefore, when the aspect ratio of the CNT filler becomes large in the calculation considering

Table 6
Dimensions of CNT and Al_4C_3, aspect ratios, and volume fraction used by Shi et al.(2019).

Diameter of CNT	Length of CNT	Thickness of Al_4C_3	Aspect ratio of CNT	Aspect ratio of $(CNT + Al_4C_3)$	Volume fraction of CNT in $(CNT + Al_4C_3)$
$d_{CNT}(nm)$	$L_{CNT}(nm)$	$t_{Al_4C_3}(nm)$	ω_3^{Ω}	ω_3^{V}	f
70	1000	15	14.3	10.3	0.48

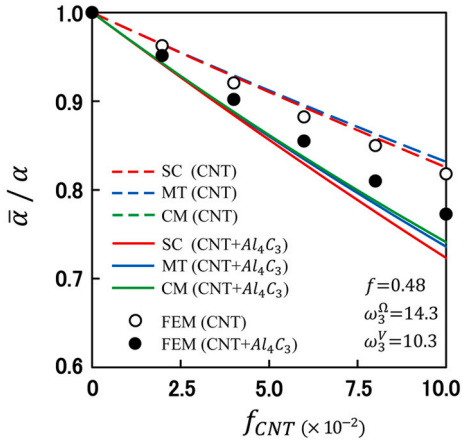

Fig. 10. Change in macroscopic thermal expansion coefficient $\overline{\alpha}/\alpha$ with the volume fraction f_{CNT}.

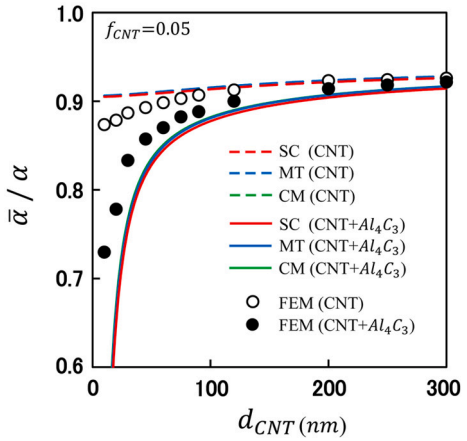

Fig. 11. Change in macroscopic thermal expansion coefficient $\overline{\alpha}/\alpha$ with the diameter $d_{CNT}(nm)$.

the interfacial layer, it is possible that approximating of 2D random orientation by FEM may cause a large error. It is necessary to pay attention to this point.

Fig. 12 shows the change in the macroscopic thermal expansion coefficient $\overline{\alpha}$ with the thickness $t_{Al_4C_3}$ of the interfacial layer. These are the results when f_{CNT} is 0.01, 0.03, and 0.05. The black-filled triangle, circle, and square markers in the figure represent the FEM analytical results by Shi et al. In this analysis, the aspect ratio ω_3^{Ω} of the CNT filler uses a constant value of 14.3 in Table 6. From the figure, we can see that regardless of the value of f_{CNT}, the results of SC, MT, CM, and FEM gradually decrease as $t_{Al_4C_3}$ increases. This is a reasonable result because the region of the interfacial layer with smaller thermal expansion coefficient than that of the matrix increases. As $t_{Al_4C_3}$ increases, the difference between the analytical results and the FEM results becomes larger. When $t_{Al_4C_3}$ is constant, this difference increases as f_{CNT} increases. In this figure, the difference between them remains approximately 7% even under the condition where it reaches to be maximum at $f_{CNT} = 0.05$ and $t_{Al_4C_3} = 25(nm)$. However, the difference occurred by increasing the volume fraction of the CNT fillers and the thickness of the interfacial layer suggests that the approximation of 2D random orientation by FEM may cause large errors.

From the above, we find that the results of this analysis quantitatively agree with those of the FEM analysis. However, we should note that the compared FEM analysis is not an actual calculation of 3D random orientation model. Therefore, when the volume fraction of the CNT fillers exceeds 10% or when the interfacial layer becomes approximately one-third or more of the diameter of the CNT filler, caution must be exercised regarding the guarantee of accuracy. As shown in Eqs. (48) and (67), the solution for the

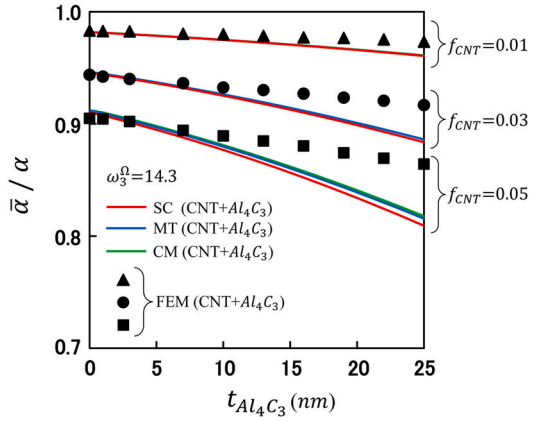

Fig. 12. Change in macroscopic thermal expansion coefficient $\overline{\alpha}/\alpha$ with the thickness $t_{Al_4C_3}$ (parameter : $f_{CNT} = 0.01$, 0.03, and 0.05).

macroscopic thermal expansion coefficient is closely related to that of the macroscopic bulk modulus. From this, we expect that the same results as the macroscopic thermal expansion coefficient can be obtained for the macroscopic bulk modulus.

4.4. Changes in macroscopic elastic modulus and thermal expansion coefficient with changing the shape of fillers

In this section, we calculate the macroscopic Young's modulus $\overline{E}$ and thermal expansion coefficient $\overline{\alpha}$ when the shape of the CNT fillers is continuously changed. Figs. 13 and 14 show the results of $\overline{E}$ and $\overline{\alpha}$, respectively. The horizontal axis of these figures is the aspect ratio ω_3^Ω of the CNT filler, and the vertical axis is the dimensionless macroscopic quantity based on the physical properties of the matrix. In this calculation, only the shape of the CNT fillers is continuously changed while keeping both the volume fraction $f_{CNT} = 0.05$ and the thickness t_{Al_4C3} of the interfacial layer constant. (a), (b), and (c) in each figure are the results for $t_{Al_4C3} = 5$, 10, and 20(nm), respectively. The physical properties of constituents shown in Table 5 are used. Assuming that the diameter of the CNT filler is constant at 70(nm), which is the same as Table 6. ω_3^V and f are given by the following equations

$$\omega_3^V = \frac{70\,\omega_3^\Omega + 2t_{Al_4C_3}}{70 + 2t_{Al_4C_3}} \quad , \quad f = \frac{\omega_3^\Omega}{\left(1 + \dfrac{2t_{Al_4C_3}}{70}\right)^3 \omega_3^V} \, .$$

The solid color lines in the figures are the analytical results (SC, MT, and CM) considering the existence of the interfacial layer. As with the previous results, the results of MT are almost the same as those of CM, so the green lines of CM are almost invisible in the figures. For comparison, the results without the interfacial layer are also shown by dashed lines in all figures. The black solid lines in Fig. 13 represent the lower bound E_1^* and the upper bound E_2^* of the macroscopic Young's modulus. E_1^* and E_2^* are given by

$$E_1^* = \frac{9K_1^*\,\mu_1^*}{\mu_1^* + 3K_1^*} \quad , \quad E_2^* = \frac{9K_2^*\,\mu_2^*}{\mu_2^* + 3K_2^*} \, , \tag{91}$$

where K_1^*, K_2^*, μ_1^*, and μ_2^* are given by Eq. (60). The black solid lines in Fig. 14 show the results of the lower bound α_1^* and the upper bound α_2^* of the macroscopic thermal expansion coefficient obtained by Shapery shown in Eq. (69).

Comparing the dashed lines and the solid lines in Fig. 13, we can see that the value of $\overline{E}$ with the interfacial layer is higher than that without the interfacial layer regardless of the shape of the CNT fillers. Next, we compare the results of SC, MT, and CM (solid lines) when the thickness of the interfacial layer $t_{Al_4C_3}$ is changed. By comparing Figs. 13(a), (b), and (c), we observe that the value of $\overline{E}$ increases with increasing $t_{Al_4C_3}$. This is due to the increasing region of the interfacial layer, which has a higher elastic modulus than the Al matrix. Furthermore, in these figures, we can see that the value of $\overline{E}$ is remarkably higher when the shape of the CNT fillers is closer to the flattened shape than the long fibrous one. This is because, in the case of the fibrous shape, the deformation of the material is constrained only in the longitudinal direction of the fiber, but in the case of the flattened shape, the deformation of the material is constrained in any direction along the flat surface of the filler. As shown in Fig. 13(c), it is interesting that as the thickness of the interfacial layer increases, the value of $\overline{E}$ when the shape of the CNT fillers is spherical ($\omega_3^\Omega = 1$) is higher than that when the shape is fibrous ($\omega_3^\Omega > 10^2$). This result indicates that if the interfacial layer can be made thicker, it is better to cut the CNT fillers into a length as short as its diameter. In all the figures of Fig. 13, it can be confirmed that the solid color lines always fall between the lower bound E_1^* and upper bound E_2^* obtained from Eq. (91), regardless of the value of ω_3^Ω.

The Young's modulus and thermal expansion coefficient of the constituents in Table 4 exhibit an inverse relationship in terms of their relative magnitudes. Therefore, the results of the macroscopic thermal expansion coefficient $\overline{\alpha}$ in Figs. 14(a), (b), and (c) are also inversely related to the results of the macroscopic Young's modulus $\overline{E}$ in Figs. 13(a), (b), and (c). Therefore, the results of $\overline{\alpha}$ with the interfacial layer are lower than those without the interfacial layer, and we observe that this decrease becomes more

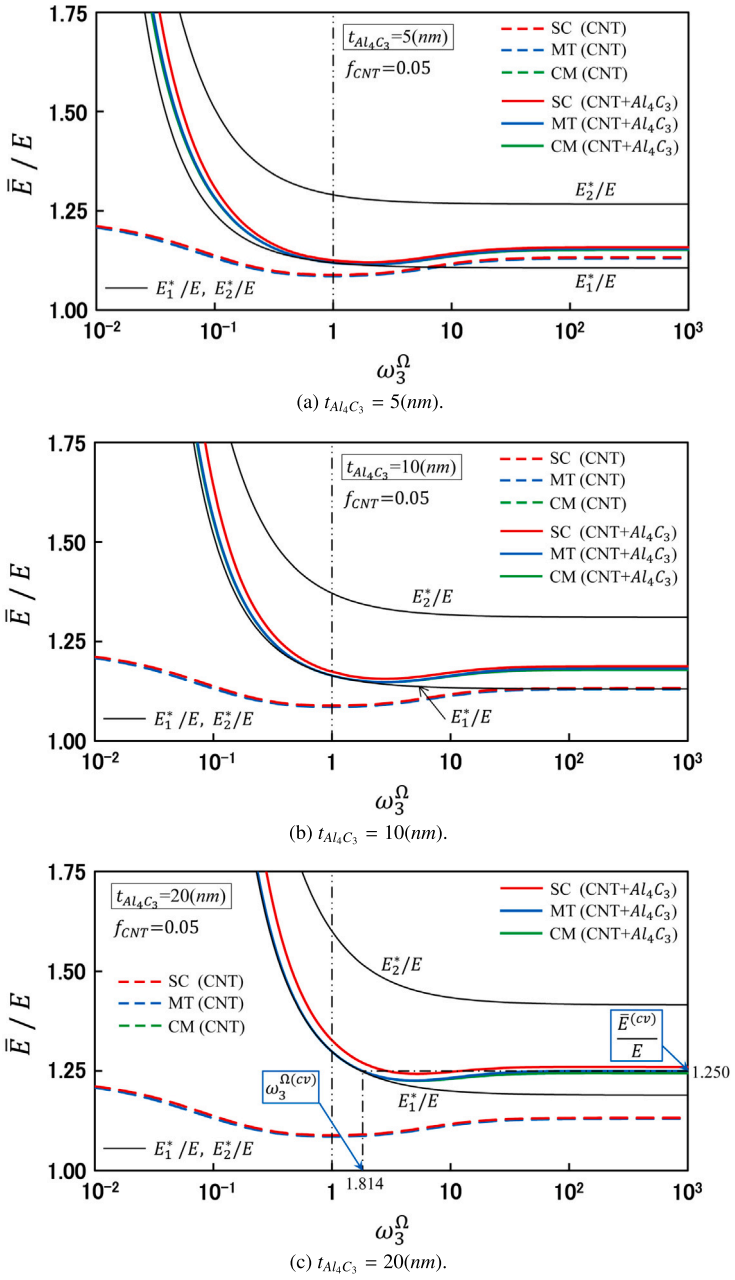

Fig. 13. Change in macroscopic Young's modulus $\overline{E}/E$ with the aspect ratio ω_3^Ω of the CNT fillers.

pronounced as $t_{Al_4C_3}$ increases. The same tendency applies to the dependence on the shape of the CNT fillers, and we also observe that approaching a more flattened shape for the CNT filler leads to a significantly greater decrease in $\overline{\alpha}$ compared to the long fibrous shape. Furthermore, similar to Fig. 13, we can confirm that in Fig. 14 the solid color lines always fall between Schapery's lower bound α_1^* and upper bound α_2^*, regardless of the value of ω_3^Ω.

From the above results, we can conclude that in CNT/Al composites with the Al_4C_3 interfacial layer, from a design perspective aiming for an improvement in the macroscopic elastic modulus and a reduction in the macroscopic thermal expansion coefficient, it is more favorable to use the CNT fillers with flattened-shape rather than long fibrous-shape.

$\overline{E}^{(cv)}$ shown in Fig. 13(c) indicates the asymptotic value when the shape of the CNT fillers is long fibrous. In this figure, the value of $\overline{E}^{(cv)}/E$ is 1.250 for the result of the Mori-Tanaka theorem. In the case of the fibrous shape of the filler, $\overline{E}/E$ never exceeds this value, so this is defined as the critical value. As the aspect ratio ω_3^Ω of the CNT filler decreases from 10^3, $\overline{E}/E$ decreases more than $\overline{E}^{(cv)}/E$. However, it turns to increase and reaches $\overline{E}^{(cv)}/E$ again at $\omega_3^\Omega = 1.814$ as shown in Fig. 13(c). The aspect ratio at this

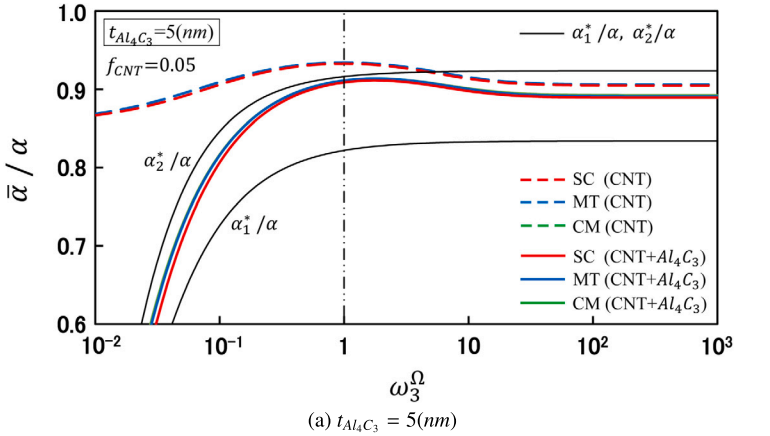

(a) $t_{Al_4C_3} = 5(nm)$

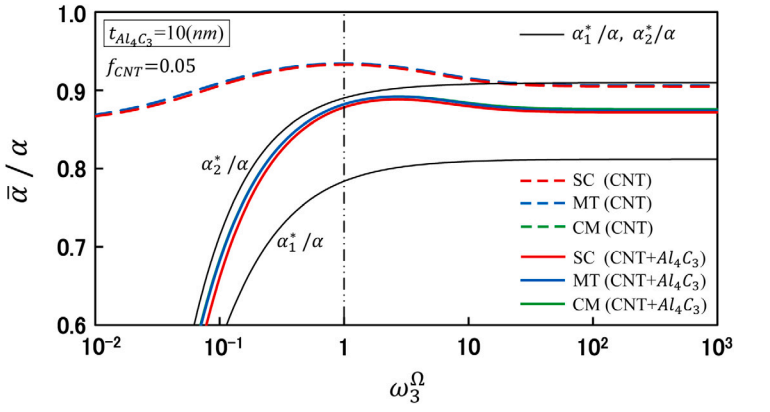

(b) $t_{Al_4C_3} = 10(nm)$.

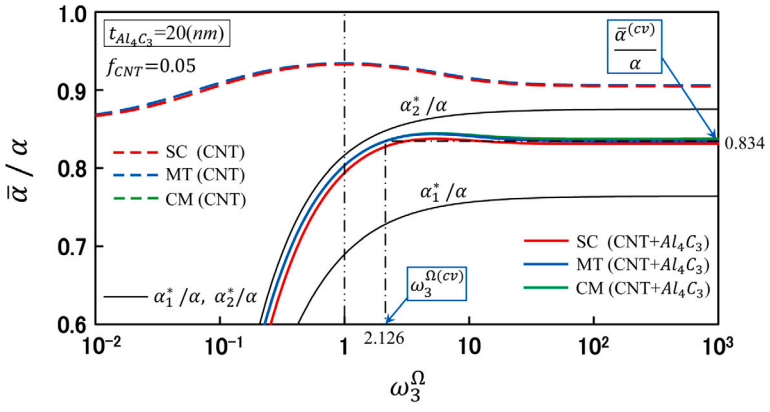

(c) $t_{Al_4C_3} = 20(nm)$.

Fig. 14. Change in macroscopic thermal expansion coefficient $\overline{\alpha}/\alpha$ with the aspect ratio ω_3^Ω of the CNT fillers.

point is defined as the critical aspect ratio $\omega_3^{\Omega(cv)}$. If the aspect ratio of the CNT filler decreases below $\omega_3^{\Omega(cv)}$, $\overline{E}/E$ can be expected to be higher than $\overline{E}^{(cv)}/E$. Similarly, in Fig. 14(c), $\overline{\alpha}^{(cv)}$ is the critical value of the macroscopic thermal expansion coefficient and $\omega_3^{\Omega(cv)}$ is the corresponding aspect ratio. The values of $\omega_3^{\Omega(cv)}$ in Figs. 13(c) and 14(c) are different from each other, but these values are close.

Figs. 15 and 16 show the relationship between the critical aspect ratio $\omega_3^{\Omega(cv)}$ and the thickness of the interfacial layer $t_{Al_4C_3}$. The results in these figures are shown for the values of f_{CNT} at 0.025, 0.050, and 0.075. The solid black line in these figures represent $\omega_3^{\Omega(cv)}$, while the solid blue line indicates the critical value of $\overline{E}^{(cv)}/E$ or $\overline{\alpha}^{(cv)}/\alpha$. The dot-dashed line in Fig. 15 indicates the combination of ω_3^Ω and $t_{Al_4C_3}$ that can effectively increase the macroscopic Young's modulus of the material when $f_{CNT} = 0.050$ and $t_{Al_4C_3} = 20$. Reducing the aspect ratio of the CNT fillers smaller than $\omega_3^{\Omega(cv)} = 1.814$, we can obtain the Young's modulus higher than

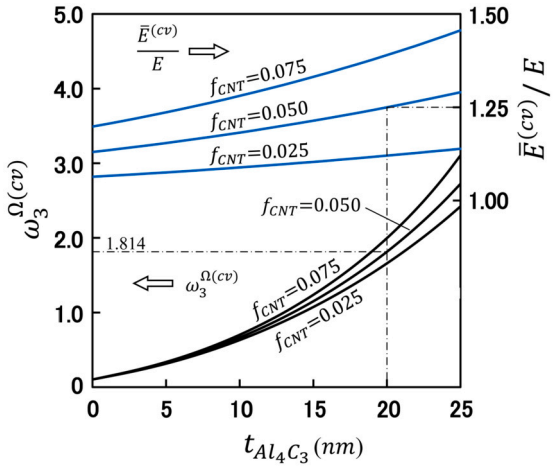

Fig. 15. Relationship between the thickness $t_{Al_4C_3}$ and the critical value $\omega_3^{\Omega(cv)}$ of the aspect ratio obtained from $\overline{E}/E$ in Fig. 13 (parameter: $f_{CNT} = 0.025$, 0.050, and 0.075).

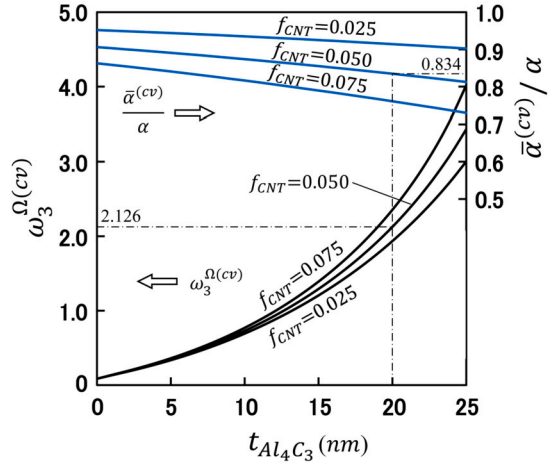

Fig. 16. Relationship between the thickness $t_{Al_4C_3}$ and the critical value $\omega_3^{\Omega(cv)}$ of the aspect ratio obtained from $\overline{\alpha}/\alpha$ in Fig. 14 (parameter: $f_{CNT} = 0.025$, 0.050, and 0.075).

the critical value $\overline{E}^{(cv)}/E = 1.25$. The same can be said for the thermal expansion coefficient in Fig. 16. From these figures, when the thickness of the interfacial layer is small, the value of $\omega_3^{\Omega(cv)}$ is almost the same regardless of the value of the volume fraction of the CNT fillers. Therefore, these results serve as a guide for determining the shape of the CNT fillers. We should note that when using long fibrous CNT fillers at high volume fractions, problems such as wavy structures and aggregations of the fillers can arise during the blending of CNT fillers with the matrix [6]. However, if CNT fillers can be thinly sliced, these problems may be avoided and the properties of CNT/Al can be expected to be significantly improved.

5. Conclusions

In this study, the solutions of the macroscopic elastic moduli and thermal expansion coefficient for composite materials containing spheroidal-coated fillers oriented randomly can be derived explicitly. In this derivation, the double inclusion method is used in combination with the self-consistent method or the Mori-Tanaka theorem. By extending these solutions, the solutions of the macroscopic physical properties are also obtained explicitly for the composite materials containing many types of coated fillers with different physical properties and shapes. To verify the validity of the solutions, the analytical results are compared with the experimental results and the numerical results using the finite element method (FEM) for the composite material containing the CNT fillers with interfacial layer Al_4C_3 in the Al matrix. As a result, the changes in macroscopic Young's modulus and thermal expansion coefficient within a certain range of the volume fraction of the CNT fillers and the thickness of the interfacial layer are quantitatively consistent with the experimental results and the FEM numerical results.

Furthermore, the changes in these macroscopic physical properties of the CNT/Al composite are investigated when the shape of the CNT fillers is continuously changed. As a result, it is found that to obtain high stiffness and low thermal expansion for the CNT/Al composite material, the shape of the CNT fillers should be flattened rather than long fibrous. In addition, a design

guideline for the shape of the CNT fillers and the thickness of the interfacial layer can be shown for a given volume fraction of the CNT fillers.

The motives and prospects that this study provides for future research are given as follows:

· In this analysis, the results of Christensen's method are also indicated. In the analysis of CNT/Al composite materials, the results of this method are almost in agreement with that of the Mori-Tanaka theorem. Furthermore, these results are not significantly different from those of the self-consistent method. This is because the volume fraction of the CNT fillers is limited to a relatively low value in accordance with the actual material. The differences between these homogenization methods require a more detailed examination.

· In CNT/Al composite materials, the aggregations of the CNT fillers tend to occur as the volume fraction of the fillers increases. It is necessary to construct a general and rigorous analytical model that can take such aggregations into account.

· Fillers such as carbon fibers are anisotropic, meaning that their longitudinal and transverse properties differ from each other. Analysis considering such anisotropic characteristics is one of the future research.

· In recent years, ellipsoidal thin flake-shaped fillers such as montmorillonite have been used in composite materials. In this way, the shape of fillers becomes more diverse. Therefore, it is important to model the fillers as ellipsoids to accommodate a wide range of shapes.

CRediT authorship contribution statement

Hiroyuki Ono: Writing – review & editing, Writing – original draft, Visualization, Validation, Supervision, Software, Resources, Project administration, Methodology, Investigation, Funding acquisition, Formal analysis, Data curation, Conceptualization.

Declaration of competing interest

The authors declare the following financial interests/personal relationships which may be considered as potential competing interests:

Hiroyuki ONO reports financial support was provided by Kyoto Institute of Technology.

Data availability

All data supporting the findings of this study are either included within the article or are available from the referenced sources in the article.

Appendix A. Various coefficients in equations

A.1. Geometrical factors

Fig. A.1 shows various shapes of spheroidal filler. Fig. A.1(a) is a prolate spheroid whose longitudinal direction is the x_3 axis, Fig. A.1(b) is a sphere and Fig. A.1(c) is an oblate spheroid and thin in the direction of the x_3 axis. The nonzero components of the geometrical factors H_i and H_{ij} for these spheroidal shapes are expressed as follows [39]:

(a) Prolate spheroid ($\omega_3 > 1$, $\omega_2 = 1$)

$$H_3 = 1 - \frac{\omega_3}{(\omega_3^2-1)^{3/2}}\left\{\omega_3(\omega_3^2-1)^{1/2} - \cosh^{-1}\omega_3\right\} \quad , \quad H_1 = H_2 = \frac{1}{2}(1-H_3) \, ,$$

$$H_{12} = \frac{1}{4}\left(1-H_{31}\right) \quad , \quad H_{23} = \frac{1}{2}(1-3H_3) + H_{31} = \omega_3^2 H_{31} \quad , \quad H_{31} = \frac{1-3H_3}{2(\omega_3^2-1)} = \frac{H_1-H_3}{\omega_3^2-1} \, , \tag{A.1a}$$

(b) Sphere ($\omega_3 = \omega_2 = 1$)

$$H_3 = H_1 = H_2 = \frac{1}{3} \quad , \quad H_{12} = H_{23} = H_{31} = \frac{1}{5} \, , \tag{A.1b}$$

(c) oblate spheroid ($\omega_3 < 1$, $\omega_2 = 1$)

$$H_3 = 1 - \frac{\omega_3}{(1-\omega_3^2)^{3/2}}\left\{\cos^{-1}\omega_3 - \omega_3(1-\omega_3^2)^{1/2}\right\} \quad , \quad H_1 = H_2 = \frac{1}{2}(1-H_3) \, ,$$

$$H_{12} = \frac{1}{4}\left(1-H_{31}\right) \quad , \quad H_{23} = \frac{1}{2}(1-3H_3) + H_{31} = \omega_3^2 H_{31} \quad , \quad H_{31} = -\frac{1-3H_3}{2(1-\omega_3^2)} = \frac{H_1-H_3}{\omega_3^2-1} \, , \tag{A.1c}$$

where ω_3 is the aspect ratio of the filler, given by $\omega_3 = a_3/a_1$ as shown in Fig. A.1. From Eq. (A.1), it can be seen that the geometrical factor is a function expressed only by the aspect ratio ω_3.

Using these geometrical factors, the nonzero components of the Eshelby tensor S_{ijkl} are expressed as follows [39]:

$$S_{1111} = S_{2222} = \frac{5-4\nu}{8(1-\nu)}(1-H_3) + \frac{3(H_3-H_{31})}{8(1-\nu)} \quad , \quad S_{3333} = H_3 + \frac{(H_3-H_{31})}{(1-\nu)} \, ,$$

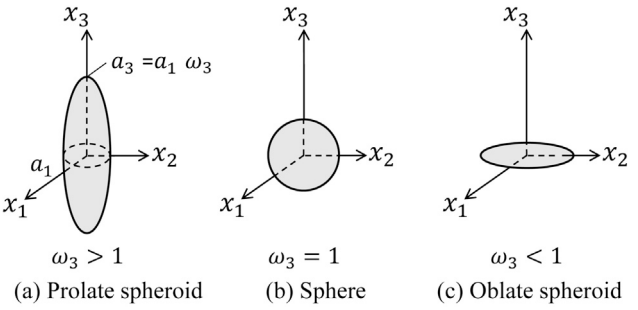

Fig. A.1. Various shapes of spheroidal filler.

$$S_{1122} = S_{2211} = -\frac{1-4\nu}{8(1-\nu)}(1-H_3) + \frac{(H_3 - H_{31})}{8(1-\nu)} \quad , \tag{A.2}$$

$$S_{2233} = S_{1133} = \frac{\nu}{2(1-\nu)}(1-H_3) - \frac{(H_3 - H_{31})}{2(1-\nu)} \quad , \quad S_{3311} = S_{3322} = \frac{\nu}{1-\nu}H_3 - \frac{(H_3 - H_{31})}{2(1-\nu)} \, ,$$

$$S_{2323} = S_{3131} = \frac{1}{4}(1+H_3) - \frac{(H_3 - H_{31})}{2(1-\nu)} \quad , \quad S_{1212} = \frac{1}{2}(S_{1111} - S_{1122}) \, . \tag{A.3}$$

Therefore, the number of independent components of S_{ijkl} in Eqs. (A.2) and (A.3) is six, which consist of only two geometrical factors H_3 and H_{31} and the Poisson's ratio of the matrix. Note that we need to replace ν with the macroscopic unknown Poisson's ratio of the material $\overline{\nu}$ when using this Eshelby tensor in the analysis of the self-consistent method.

A.2. Coefficients appearing in equations of equivalent eigenstrains in the Ω and Γ regions

The coefficients A_3, A_{12}, and A_{23} appearing in the denominator of the equivalent eigenstrain in the Ω and Γ regions obtained in Sec.2.1 are given by

$$A_3 = A_3^{\Omega} A_3^{\Gamma} - \left\{ \frac{f(1+\overline{\nu})(1-2\overline{\nu})}{3(1-f)}(\Delta\alpha_3)^2 \right\}^2 - \frac{f}{6(1-f)} \left\{ 2(1+\overline{\nu})(1-2\overline{\nu})\Delta\alpha_3(\Delta P_{\mathrm{III}} + \Delta P_{\mathrm{IV}}) + 9\left(\Delta R_3 - \frac{2}{3}\Delta H_{\mathrm{I}}\right)\Delta P_{\mathrm{I}} \right\} , \tag{A.4a}$$

$$A_{23} = A_{31} = A_{23}^{\Omega} A_{23}^{\Gamma} - \frac{9f}{16(1-f)}(\Delta R_3 + 2\Delta H_{\mathrm{I}})^2 \quad , \quad A_{12} = A_{12}^{\Omega} A_{12}^{\Gamma} - \frac{9f}{4(1-f)}\left(\Delta R_3 + \frac{2}{3}\Delta H_{\mathrm{I}}\right)^2 . \tag{A.4b}$$

Coefficients prefixed with Δ are expressed as

$$\Delta F_3^X = \frac{2}{3}(1+\overline{\nu})(1-2\overline{\nu})\alpha_3^X \Delta\alpha_3 + 3L_{\mathrm{I}}^X \left(\Delta R_3 - \frac{2}{3}\Delta H_{\mathrm{I}}\right) \quad , \quad (X = \Omega, \, \Gamma) \, , \tag{A.5a}$$

$$\Delta G_3^X = \left(L_{\mathrm{II}}^X - \frac{3}{2}R_3^X\right)\Delta\alpha_3 + \frac{3}{2}\alpha_3^X \left(\Delta R_3 - \frac{2}{3}\Delta H_{\mathrm{I}}\right) \quad , \quad (X = \Omega, \, \Gamma) \, , \tag{A.5b}$$

$$\Delta P_{\mathrm{I}} = \frac{1}{3}(1+\overline{\nu})(1-2\overline{\nu})(L_{\mathrm{I}}^{\Omega}\alpha_3^{\Gamma} + L_{\mathrm{I}}^{\Gamma}\alpha_3^{\Omega})\Delta\alpha_3 + \frac{3}{2}L_{\mathrm{I}}^{\Omega}L_{\mathrm{I}}^{\Gamma}\left(\Delta R_3 - \frac{2}{3}\Delta H_{\mathrm{I}}\right) , \tag{A.6a}$$

$$\Delta P_{\mathrm{II}} = \left\{ \alpha_3^{\Omega}\left(L_{\mathrm{II}}^{\Gamma} - \frac{3}{2}R_3^{\Gamma}\right) + \alpha_3^{\Gamma}\left(L_{\mathrm{II}}^{\Omega} - \frac{3}{2}R_3^{\Omega}\right) \right\}\Delta\alpha_3 + \frac{3}{2}\left(\Delta R_3 - \frac{2}{3}\Delta H_{\mathrm{I}}\right)\left\{ \alpha_3^{\Omega}\alpha_3^{\Gamma} + \frac{f}{1-f}(\Delta\alpha_3)^2 \right\} , \tag{A.6b}$$

$$\Delta P_{\mathrm{III}} = L_{\mathrm{I}}^{\Gamma}\left(L_{\mathrm{II}}^{\Omega} - \frac{3}{2}R_3^{\Omega}\right)\Delta\alpha_3 + \frac{1}{3}(1+\overline{\nu})(1-2\overline{\nu})\Delta\alpha_3 \left\{ \alpha_3^{\Omega}\alpha_3^{\Gamma} - \frac{f}{1-f}(\Delta\alpha_3)^2 \right\} + \frac{3}{2}L_{\mathrm{I}}^{\Gamma}\alpha_3^{\Omega}\left(\Delta R_3 - \frac{2}{3}\Delta H_{\mathrm{I}}\right) , \tag{A.6c}$$

$$\Delta P_{\mathrm{IV}} = L_{\mathrm{I}}^{\Omega}\left(L_{\mathrm{II}}^{\Gamma} - \frac{3}{2}R_3^{\Gamma}\right)\Delta\alpha_3 + \frac{1}{3}(1+\overline{\nu})(1-2\overline{\nu})\Delta\alpha_3 \left\{ \alpha_3^{\Omega}\alpha_3^{\Gamma} - \frac{f}{1-f}(\Delta\alpha_3)^2 \right\} + \frac{3}{2}L_{\mathrm{I}}^{\Omega}\alpha_3^{\Gamma}\left(\Delta R_3 - \frac{2}{3}\Delta H_{\mathrm{I}}\right) , \tag{A.6d}$$

where $\Delta\alpha_3$, ΔR_3, and ΔH_{I} are the coefficients representing the shape difference between the Ω and V regions and are given by Eq. (14). As mentioned in Chap.2, when the shapes of the Ω and V regions are similar and coaxial, $\Delta\alpha_3$, ΔR_3 and ΔH_{I} become zero, and as a result the coefficients of Eqs. (A.5) and (A.6) are all zero. The coefficients appearing in Eqs. (A.4) to (A.6) are given as

$$\alpha_3^{\Gamma} = \alpha_3^V - \frac{f}{1-f}\Delta\alpha_3 \quad , \quad R_3^{\Gamma} = R_3^V - \frac{f}{1-f}\Delta R_3 + \frac{2f}{3(1-f)}\Delta H_{\mathrm{I}} \quad , \quad H_{\mathrm{I}}^{\Gamma} = H_{\mathrm{I}}^V - \frac{4f}{5(1-f)}\Delta H_{\mathrm{I}} \, , \tag{A.7}$$

$$A_3^X = L_{\mathrm{I}}^X \left(L_{\mathrm{II}}^X - \frac{3}{2}R_3^X\right) - \frac{1}{3}(1+\overline{\nu})(1-2\overline{\nu})(\alpha_3^X)^2 \quad , \quad (X = \Omega, \, \Gamma) \, , \tag{A.8a}$$

$$A_{23}^X = A_{31}^X = L_{\mathrm{II}}^X - \frac{3}{4}R_3^X - \frac{1}{2}(5H_{\mathrm{I}}^X - 2) \quad , \quad (X = \Omega, \, \Gamma) \, , \tag{A.8b}$$

$$A_{12}^{\Omega} = L_{\mathrm{II}}^{\Omega} + \frac{3}{2}R_3^{\Omega} \quad , \quad A_{12}^{\Gamma} = L_{\mathrm{II}}^{\Gamma} + \frac{3}{2}R_3^{\Gamma} - \frac{2f}{1-f}\Delta H_{\mathrm{I}} \, . \tag{A.8c}$$

A.3. Coefficients appearing in equations of equivalent eigenstrains in the V region

The coefficients ${}^{n}P_{ij}^{\Omega}$, ${}^{n}P_{ij}^{\Gamma}$, ${}^{s}P_{ij}^{\Omega}$, and ${}^{s}P_{ij}^{\Gamma}$ appearing in the equivalent eigenstrains of the V region obtained in Sec.2.1 are given as follows, using the coefficients shown in Eqs. (A.4) to (A.8):

$$ {}^{n}P_{11}^{\Omega} = \frac{1}{A_3}\left\langle 3A_3^{\Gamma}\left(L_{\mathrm{II}}^{\Omega} - \frac{3}{2}R_3^{\Omega}\right) - \frac{f}{2(1-f)}\left\{\frac{9}{2}\left(\Delta R_3 - \frac{2}{3}\Delta H_{\mathrm{I}}\right)\Delta F_3^{\Gamma} + 2(1+\overline{\nu})(1-2\overline{\nu})\Delta\alpha_3\Delta G_3^{\Gamma}\right\} + (1+\overline{\nu})(1-2\overline{\nu})\Delta P_{\mathrm{II}}\right\rangle , \tag{A.9a} $$

$$ {}^{n}P_{11}^{\Gamma} = \frac{1}{A_3}\left\langle 3A_3^{\Omega}\left(L_{\mathrm{II}}^{\Gamma} - \frac{3}{2}R_3^{\Gamma}\right) - \frac{f}{2(1-f)}\left\{\frac{9}{2}\left(\Delta R_3 - \frac{2}{3}\Delta H_{\mathrm{I}}\right)\Delta F_3^{\Omega} + 2(1+\overline{\nu})(1-2\overline{\nu})\Delta\alpha_3\Delta G_3^{\Omega}\right\} + \frac{f}{(1-f)}(1+\overline{\nu})(1-2\overline{\nu})\Delta P_{\mathrm{II}}\right\rangle , \tag{A.9b} $$

$$ {}^{n}P_{12}^{\Omega} = \frac{3(1-2\overline{\nu})}{A_3}\left\{A_3^{\Gamma}\alpha_3^{\Omega} + \frac{f}{2(1-f)}\Delta\alpha_3\Delta F_3^{\Gamma} + \Delta P_{\mathrm{IV}}\right\} , \tag{A.9c} $$

$$ {}^{n}P_{12}^{\Gamma} = \frac{3(1-2\overline{\nu})}{A_3}\left\{A_3^{\Omega}\alpha_3^{\Gamma} + \frac{f}{2(1-f)}\Delta\alpha_3\Delta F_3^{\Omega} + \frac{f}{1-f}\Delta P_{\mathrm{III}}\right\} , \tag{A.9d} $$

$$ {}^{n}P_{21}^{\Omega} = \frac{2(1+\overline{\nu})}{3A_3}\left\{A_3^{\Gamma}\alpha_3^{\Omega} + \frac{f}{2(1-f)}\Delta\alpha_3\Delta F_3^{\Gamma} + \Delta P_{\mathrm{III}}\right\} , \tag{A.9e} $$

$$ {}^{n}P_{21}^{\Gamma} = \frac{2(1+\overline{\nu})}{3A_3}\left\{A_3^{\Omega}\alpha_3^{\Gamma} + \frac{f}{2(1-f)}\Delta\alpha_3\Delta F_3^{\Omega} + \frac{f}{1-f}\Delta P_{\mathrm{IV}}\right\} , \tag{A.9f} $$

$$ {}^{n}P_{22}^{\Omega} = \frac{2}{A_3}\left\{A_3^{\Gamma}L_1^{\Omega} - \frac{f}{3(1-f)}(1+\overline{\nu})(1-2\overline{\nu})L_1^{\Gamma}(\Delta\alpha_3)^2 + \Delta P_{\mathrm{I}}\right\} , \tag{A.9g} $$

$$ {}^{n}P_{22}^{\Gamma} = \frac{2}{A_3}\left\{A_3^{\Omega}L_1^{\Gamma} - \frac{f}{3(1-f)}(1+\overline{\nu})(1-2\overline{\nu})L_1^{\Omega}(\Delta\alpha_3)^2 + \frac{f}{1-f}\Delta P_{\mathrm{I}}\right\} , \tag{A.9h} $$

$$ {}^{s}P_{23}^{\Omega} = {}^{s}P_{31}^{\Omega} = \frac{1}{A_{23}}\left\{2A_{23}^{\Gamma} + \frac{3}{2}(\Delta R_3 + 2\Delta H_{\mathrm{I}})\right\} , \tag{A.10a} $$

$$ {}^{s}P_{23}^{\Gamma} = {}^{s}P_{31}^{\Gamma} = \frac{1}{A_{23}}\left\{2A_{23}^{\Omega} + \frac{3f}{2(1-f)}(\Delta R_3 + 2\Delta H_{\mathrm{I}})\right\} , \tag{A.10b} $$

$$ {}^{s}P_{12}^{\Omega} = \frac{1}{A_{12}}\left\{2A_{12}^{\Gamma} - 3\left(\Delta R_3 + \frac{2}{3}\Delta H_{\mathrm{I}}\right)\right\} , \tag{A.10c} $$

$$ {}^{s}P_{12}^{\Gamma} = \frac{1}{A_{12}}\left\{2A_{12}^{\Omega} - \frac{3f}{1-f}\left(\Delta R_3 + \frac{2}{3}\Delta H_{\mathrm{I}}\right)\right\} . \tag{A.10d} $$

The coefficients included in the right-hand side of Eqs. (A.9) and (A.10) involve coefficients related to the Ω and Γ regions. However, when the shapes of the Ω and V regions are similar and coaxial, all coefficients prefixed with Δ become zero. Then, A_3, A_{23}, and A_{12} appearing in the denominator on the right side of Eqs. (A.9) and (A.10) are given by Eq. (A.4) as follows:

$$ A_3 = A_3^{\Omega}A_3^{\Gamma} \quad , \quad A_{23} = A_{23}^{\Omega}A_{23}^{\Gamma} \quad , \quad A_{12} = A_{12}^{\Omega}A_{12}^{\Gamma} . \tag{A.11} $$

By substituting Eq. (A.11) into Eqs. (A.9) and (A.10), it is immediately found that ${}^{n}P_{ij}^{X}$ and ${}^{s}P_{ij}^{X}(X = \Omega, \Gamma)$ reduce to coefficients that involve only the same region X on the right side of these equations. In this way, the coefficients in Eqs. (A.9) and (A.10) are designed such that when the Ω region and the V region are similar and coaxial, the regions indicated as a superscript on both sides of Eqs. (A.9) and (A.10) match each other. Furthermore, the following relationship holds between ${}^{n}P_{ij}^{X}(X = \Omega, ; \Gamma)$:

$$ \left\{f\,{}^{n}P_{21}^{\Omega} + (1-f)\,{}^{n}P_{21}^{\Gamma}\right\} - \frac{2(1+\overline{\nu})}{9(1-2\overline{\nu})}\left\{f\,{}^{n}P_{12}^{\Omega} + (1-f)\,{}^{n}P_{12}^{\Gamma}\right\} = 0 . \tag{A.12} $$

This relation is used for the simplification of the coefficients in the calculation of the integral in Eq. (29).

A.4. Solutions of macroscopic elastic moduli and thermal expansion coefficient for composite materials containing spheroidal coated fillers oriented unidirectionally

The macroscopic elastic moduli and the thermal expansion coefficient for composite materials containing spheroidal coated fillers oriented unidirectionally have the same properties as hexagonal crystal materials. These solutions are given as follows [11]:

$$ \frac{\overline{E}_{33}}{E} = \frac{9}{3(1-2\nu)({}^{n}\overline{D}_{11}) + 2(1+\nu)(2\,{}^{n}\overline{D}_{12} + 3\,{}^{n}\overline{D}_{22})} , \quad \frac{\overline{E}_{11}}{E} = \frac{9}{3(1-2\nu)({}^{n}\overline{D}_{11}) + (1+\nu)\left\{\frac{3}{2}(3\,{}^{s}\overline{D}_{12} + {}^{n}\overline{D}_{22}) - 2({}^{n}\overline{D}_{12})\right\}} , \tag{A.13a} $$

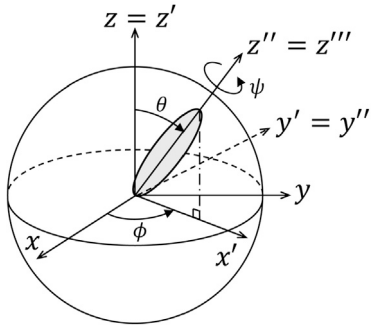

Fig. A.2. Spherical coordinate system expressed by Euler angles.

$$\overline{\nu}_{23} = -\frac{3(1-2\nu)({}^{n}\overline{D}_{11}) + (1+\nu)({}^{n}\overline{D}_{12} - 3\,{}^{n}\overline{D}_{22})}{3(1-2\nu)({}^{n}\overline{D}_{11}) + 2(1+\nu)(2\,{}^{n}\overline{D}_{12} + 3\,{}^{n}\overline{D}_{22})}\ ,\ \overline{\nu}_{12} = -\frac{3(1-2\nu)({}^{n}\overline{D}_{11}) - (1+\nu)\left\{\frac{3}{2}(3\,{}^{s}\overline{D}_{12} - {}^{n}\overline{D}_{22}) + 2({}^{n}\overline{D}_{12})\right\}}{3(1-2\nu)({}^{n}\overline{D}_{11}) + (1+\nu)\left\{\frac{3}{2}(3\,{}^{s}\overline{D}_{12} + {}^{n}\overline{D}_{22}) - 2({}^{n}\overline{D}_{12})\right\}}\ , \tag{A.13b}$$

$$\frac{B}{\overline{B}} = \frac{1}{1-2\nu}\left\{3\,{}^{n}\overline{D}_{22} - \frac{2(1+\nu)({}^{n}\overline{D}_{12} + 3\,{}^{n}\overline{D}_{22})^2}{3(1-2\nu)({}^{n}\overline{D}_{11}) + 2(1+\nu)(2\,{}^{n}\overline{D}_{12} + 3\,{}^{n}\overline{D}_{22})}\right\}, \tag{A.13c}$$

$$\frac{\overline{\mu}_{23}}{\mu} = \frac{1}{{}^{s}\overline{D}_{23}}\quad,\quad \frac{\overline{\mu}_{12}}{\mu} = \frac{1}{{}^{s}\overline{D}_{12}}\ , \tag{A.13d}$$

$$\left\{\begin{matrix}\frac{\overline{\alpha}_{11}}{\alpha}\\ \frac{\overline{\alpha}_{33}}{\alpha}\end{matrix}\right\} = \left\{\begin{matrix}1\\ 1\end{matrix}\right\} + 3(1-\nu)f_V\mathbf{J}\left\{\mathbf{I} - (\mathbf{I} - {}^{n}\overline{\mathbf{D}})({}^{n}\mathbf{T})\right\}\left\{\begin{matrix}fL_K^{\Omega}({}^{n}P_{11}^{\Omega})\left(\frac{\alpha^{\Omega}}{\alpha} - 1\right) + (1-f)L_K^{\Gamma}({}^{n}P_{11}^{\Gamma})\left(\frac{\alpha^{\Gamma}}{\alpha} - 1\right)\\ fL_K^{\Omega}({}^{n}P_{21}^{\Omega})\left(\frac{\alpha^{\Omega}}{\alpha} - 1\right) + (1-f)L_K^{\Gamma}({}^{n}P_{21}^{\Gamma})\left(\frac{\alpha^{\Gamma}}{\alpha} - 1\right)\end{matrix}\right\}, \tag{A.14}$$

where $B = \mu/(1-2\nu)$ in Eq. (A.13) is the plane strain bulk modulus. In Eq. (A.14), $\mathbf{I}$ is a 2×2 identity matrix, and $\mathbf{J}$, ${}^{n}\mathbf{T}$, and ${}^{n}\overline{\mathbf{D}}$ are given as

$$\mathbf{J} = \begin{bmatrix}\frac{1}{3} & -\frac{1}{2}\\ \frac{1}{3} & 1\end{bmatrix}\quad,\quad {}^{n}\mathbf{T} = \frac{(1-2\nu)}{2(1-\nu)}\begin{bmatrix}\frac{4}{3} & \alpha_3^V\\ \frac{2(1+\nu)}{9(1-2\nu)}\alpha_3^V & \frac{3}{2(1-2\nu)}\left\{R_3^V + \frac{4}{9}(2-\nu) - \frac{2}{3}H_1^V\right\}\end{bmatrix}, \tag{A.15}$$

$${}^{n}\overline{\mathbf{D}} = \begin{bmatrix}{}^{n}\overline{D}_{11} & {}^{n}\overline{D}_{12}\\ \frac{2(1+\nu)}{9(1-2\nu)}({}^{n}\overline{D}_{12}) & {}^{n}\overline{D}_{22}\end{bmatrix} = \mathbf{I} - (1-\nu)f_V\left\{f({}^{n}\mathbf{P}^{\Omega}) + (1-f)({}^{n}\mathbf{P}^{\Gamma})\right\}\left\{\mathbf{I} + (1-\nu)f_V({}^{n}\mathbf{T})\left\{f({}^{n}\mathbf{P}^{\Omega}) + (1-f)({}^{n}\mathbf{P}^{\Gamma})\right\}\right\}^{-1}, \tag{A.16a}$$

$${}^{s}\overline{D}_{23} = 1 - \frac{(1-\nu)f_V\left\{f({}^{s}P_{23}^{\Omega}) + (1-f)({}^{s}P_{23}^{\Gamma})\right\}}{1 + \frac{3}{8}f_V\left\{R_3^V + \frac{4}{9}(1-2\nu) + 2H_1^V\right\}\{f({}^{s}P_{23}^{\Omega}) + (1-f)({}^{s}P_{23}^{\Gamma})\}}\ , \tag{A.16b}$$

$${}^{s}\overline{D}_{12} = 1 - \frac{(1-\nu)f_V\left\{f({}^{s}P_{12}^{\Omega}) + (1-f)({}^{s}P_{12}^{\Gamma})\right\}}{1 - \frac{3}{4}f_V\left\{R_3^V - \frac{4}{9}(2-\nu) + \frac{2}{3}H_1^V\right\}\{f({}^{s}P_{12}^{\Omega}) + (1-f)({}^{s}P_{12}^{\Gamma})\}}\ . \tag{A.16c}$$

In Eq. (A.16a), ${}^{n}\mathbf{P}^{\Omega}$ and ${}^{n}\mathbf{P}^{\Gamma}$ are given by

$${}^{n}\mathbf{P}^{X} = \begin{bmatrix}{}^{n}P_{11}^{X} & {}^{n}P_{12}^{X}\\ {}^{n}P_{21}^{X} & {}^{n}P_{22}^{X}\end{bmatrix}\quad,\quad (X = \Omega,\ \Gamma)\quad. \tag{A.17}$$

${}^{n}P_{ij}^{X}$ and ${}^{s}P_{ij}^{X}$ $(X = \Omega,\ \Gamma)$ in Eqs. (A.13) to (A.17) are given by Eqs. (A.9) and (A.10). Also, the other coefficients are the same as those shown so far. However, note that the elastic moduli such as $\overline{K}$, $\overline{\mu}$, and $\overline{\nu}$ included in these coefficients need to be replaced as shown in Eq. (54).

A.5. Matrix of coordinate transformation

Fig. A.2 shows the spherical coordinate system expressed by Euler angles, where θ, ϕ and ψ are the zenith, azimuth, and rotation angles of a filler. In the case of the y-convention, the coordinate transformation is performed by first rotating an azimuth angle ϕ

around the z-axis, then a zenith angle θ around the y-axis, and finally a rotation angle ψ around the z-axis again. The matrix of coordinate transformation in the y-convention $\boldsymbol{l}$ is given by [40],

$$\begin{aligned}\boldsymbol{l} &= \begin{bmatrix} l_{11} & l_{12} & l_{13} \\ l_{21} & l_{22} & l_{23} \\ l_{31} & l_{32} & l_{33} \end{bmatrix} = \begin{bmatrix} \cos\psi & \sin\psi & 0 \\ -\sin\psi & \cos\psi & 0 \\ 0 & 0 & 1 \end{bmatrix} \begin{bmatrix} \cos\theta & 0 & -\sin\theta \\ 0 & 1 & 0 \\ \sin\theta & 0 & \cos\theta \end{bmatrix} \begin{bmatrix} \cos\phi & \sin\phi & 0 \\ -\sin\phi & \cos\phi & 0 \\ 0 & 0 & 1 \end{bmatrix} \\ &= \begin{bmatrix} \cos\theta\cos\phi\cos\psi - \sin\phi\sin\psi & \cos\theta\sin\phi\cos\psi + \cos\phi\sin\psi & -\sin\theta\cos\psi \\ -\cos\theta\cos\phi\sin\psi - \sin\phi\cos\psi & -\cos\theta\sin\phi\sin\psi + \cos\phi\cos\psi & \sin\theta\sin\psi \\ \sin\theta\cos\phi & \sin\theta\sin\phi & \cos\theta \end{bmatrix}. \end{aligned} \tag{A.18}$$

The matrices of coordinate transformation $\boldsymbol{L}$ and $\hat{\boldsymbol{L}}$ used in Eq. (27) are expressed as

$$\boldsymbol{L} = \begin{bmatrix} \frac{1}{3}L^{\Sigma} & L_1^{\Sigma\prime} & L_2^{\Sigma\prime} & L_3^{\Sigma\prime} & 2L_{23}^{\Sigma\prime} & 2L_{31}^{\Sigma\prime} & 2L_{12}^{\Sigma\prime} \\ \frac{1}{3}(L_1^{\Sigma} - \frac{L^{\Sigma}}{3}) & l_{11}^2 - \frac{L_1^{\Sigma\prime}}{3} & l_{12}^2 - \frac{L_2^{\Sigma\prime}}{3} & l_{13}^2 - \frac{L_3^{\Sigma\prime}}{3} & 2(l_{12}l_{13} - \frac{L_{23}^{\Sigma\prime}}{3}) & 2(l_{13}l_{11} - \frac{L_{31}^{\Sigma\prime}}{3}) & 2(l_{11}l_{12} - \frac{L_{12}^{\Sigma\prime}}{3}) \\ \frac{1}{3}(L_2^{\Sigma} - \frac{L^{\Sigma}}{3}) & l_{21}^2 - \frac{L_1^{\Sigma\prime}}{3} & l_{22}^2 - \frac{L_2^{\Sigma\prime}}{3} & l_{23}^2 - \frac{L_3^{\Sigma\prime}}{3} & 2(l_{22}l_{23} - \frac{L_{23}^{\Sigma\prime}}{3}) & 2(l_{23}l_{21} - \frac{L_{31}^{\Sigma\prime}}{3}) & 2(l_{21}l_{22} - \frac{L_{12}^{\Sigma\prime}}{3}) \\ \frac{1}{3}(L_3^{\Sigma} - \frac{L^{\Sigma}}{3}) & l_{31}^2 - \frac{L_1^{\Sigma\prime}}{3} & l_{32}^2 - \frac{L_2^{\Sigma\prime}}{3} & l_{33}^2 - \frac{L_3^{\Sigma\prime}}{3} & 2(l_{32}l_{33} - \frac{L_{23}^{\Sigma\prime}}{3}) & 2(l_{33}l_{31} - \frac{L_{31}^{\Sigma\prime}}{3}) & 2(l_{31}l_{32} - \frac{L_{12}^{\Sigma\prime}}{3}) \\ \frac{1}{3}L_{23}^{\Sigma} & l_{21}l_{31} & l_{22}l_{32} & l_{23}l_{33} & l_{22}l_{33} + l_{32}l_{23} & l_{23}l_{31} + l_{33}l_{21} & l_{21}l_{32} + l_{31}l_{22} \\ \frac{1}{3}L_{31}^{\Sigma} & l_{31}l_{11} & l_{32}l_{12} & l_{33}l_{13} & l_{32}l_{13} + l_{12}l_{33} & l_{33}l_{11} + l_{13}l_{31} & l_{31}l_{12} + l_{11}l_{32} \\ \frac{1}{3}L_{12}^{\Sigma} & l_{11}l_{21} & l_{12}l_{22} & l_{13}l_{23} & l_{12}l_{23} + l_{22}l_{13} & l_{13}l_{21} + l_{23}l_{11} & l_{11}l_{22} + l_{21}l_{12} \end{bmatrix}, \tag{A.19a}$$

$$\hat{\boldsymbol{L}} = \begin{bmatrix} \frac{1}{3}L^{\Sigma} & L_1^{\Sigma} & L_2^{\Sigma} & L_3^{\Sigma} & 2L_{23}^{\Sigma} & 2L_{31}^{\Sigma} & 2L_{12}^{\Sigma} \\ \frac{1}{3}(L_1^{\Sigma\prime} - \frac{L^{\Sigma}}{3}) & l_{11}^2 - \frac{L_1^{\Sigma}}{3} & l_{21}^2 - \frac{L_2^{\Sigma}}{3} & l_{31}^2 - \frac{L_3^{\Sigma}}{3} & 2(l_{21}l_{31} - \frac{L_{23}^{\Sigma}}{3}) & 2(l_{31}l_{11} - \frac{L_{31}^{\Sigma}}{3}) & 2(l_{11}l_{21} - \frac{L_{12}^{\Sigma}}{3}) \\ \frac{1}{3}(L_2^{\Sigma\prime} - \frac{L^{\Sigma}}{3}) & l_{12}^2 - \frac{L_1^{\Sigma}}{3} & l_{22}^2 - \frac{L_2^{\Sigma}}{3} & l_{32}^2 - \frac{L_3^{\Sigma}}{3} & 2(l_{22}l_{32} - \frac{L_{23}^{\Sigma}}{3}) & 2(l_{32}l_{12} - \frac{L_{31}^{\Sigma}}{3}) & 2(l_{12}l_{22} - \frac{L_{12}^{\Sigma}}{3}) \\ \frac{1}{3}(L_3^{\Sigma\prime} - \frac{L^{\Sigma}}{3}) & l_{13}^2 - \frac{L_1^{\Sigma}}{3} & l_{23}^2 - \frac{L_2^{\Sigma}}{3} & l_{33}^2 - \frac{L_3^{\Sigma}}{3} & 2(l_{23}l_{33} - \frac{L_{23}^{\Sigma}}{3}) & 2(l_{33}l_{13} - \frac{L_{31}^{\Sigma}}{3}) & 2(l_{13}l_{23} - \frac{L_{12}^{\Sigma}}{3}) \\ \frac{1}{3}L_{23}^{\Sigma\prime} & l_{12}l_{13} & l_{22}l_{23} & l_{32}l_{33} & l_{22}l_{33} + l_{23}l_{32} & l_{32}l_{13} + l_{33}l_{12} & l_{12}l_{23} + l_{13}l_{22} \\ \frac{1}{3}L_{31}^{\Sigma\prime} & l_{13}l_{11} & l_{23}l_{21} & l_{33}l_{31} & l_{23}l_{31} + l_{21}l_{33} & l_{33}l_{11} + l_{31}l_{13} & l_{13}l_{21} + l_{11}l_{23} \\ \frac{1}{3}L_{12}^{\Sigma\prime} & l_{11}l_{12} & l_{21}l_{22} & l_{31}l_{32} & l_{21}l_{32} + l_{22}l_{31} & l_{31}l_{12} + l_{32}l_{11} & l_{11}l_{22} + l_{12}l_{21} \end{bmatrix}, \tag{A.19b}$$

where

$$\begin{aligned} &L^{\Sigma} = L_1^{\Sigma} + L_2^{\Sigma} + L_3^{\Sigma} = L_1^{\Sigma\prime} + L_2^{\Sigma\prime} + L_3^{\Sigma\prime}, \\ &L_1^{\Sigma} = l_{11}^2 + l_{12}^2 + l_{13}^2 \quad , \quad L_2^{\Sigma} = l_{21}^2 + l_{22}^2 + l_{23}^2 \quad , \quad L_3^{\Sigma} = l_{31}^2 + l_{32}^2 + l_{33}^2 \quad , \\ &L_1^{\Sigma\prime} = l_{11}^2 + l_{21}^2 + l_{31}^2 \quad , \quad L_2^{\Sigma\prime} = l_{12}^2 + l_{22}^2 + l_{32}^2 \quad , \quad L_3^{\Sigma\prime} = l_{13}^2 + l_{23}^2 + l_{33}^2 , \\ &L_{23}^{\Sigma} = l_{21}l_{31} + l_{22}l_{32} + l_{23}l_{33} \quad , \quad L_{31}^{\Sigma} = l_{31}l_{11} + l_{32}l_{12} + l_{33}l_{13} \quad , \quad L_{12}^{\Sigma} = l_{11}l_{21} + l_{12}l_{22} + l_{13}l_{23} , \\ &L_{23}^{\Sigma\prime} = l_{12}l_{13} + l_{22}l_{23} + l_{32}l_{33} \quad , \quad L_{31}^{\Sigma\prime} = l_{13}l_{11} + l_{23}l_{21} + l_{33}l_{31} \quad , \quad L_{12}^{\Sigma\prime} = l_{11}l_{12} + l_{21}l_{22} + l_{31}l_{32} . \end{aligned} \tag{A.20}$$

The components l_{ij} in Eq. (A.20) are as shown on the right side of Eq. (A.18).

References

[1] S.M.A.K. Mohammed, D.L. Chen, Carbon nanotube-reinforced aluminum matrix composites, Adv. Eng. Mater. 22 (2022) 1901176, https://doi.org/10.1002/adem.201901176.

[2] A. Sayam, A.M. Rahman, M. Rahman, S. Smriti, F. Ahmed, M. Rabbi, M. Hossain, M. Faruque, A review on carbon fiber-reinforced hierarchical composites: mechanical performance, manufacturing process, structural applications and allied challenges, Carbon Lett. 32 (2022) 1173–1205, https://doi.org/10.1007/s42823-022-00358-2.

[3] F. Li, Y. Liu, C.B. Qu, H.M. Xiao, Y. Hua, G. Sui, S. Fu, Enhanced mechanical properties of short carbon fiber reinforced polyethersulfone composites by graphene oxide coating, Polymer 59 (2015) 155–165, https://doi.org/10.1016/j.polymer.2014.12.067.

[4] T. Rajan, R. Pillai, B. Pai, Reinforcement coatings and interfaces in aluminium metal matrix composites, J. Mater. Sci. 33 (1998) 3491–3503, https://doi.org/10.1023/A:1004674822751.

[5] A. Aborkin, A. Elkin, V. Reshetniak, A. Ob'edkov, A. Sytschev, V. Leontiev, D. Titov, M. Alymov, Thermal expansion of aluminum matrix composites reinforced by carbon nanotubes with in-situ and ex-situ designed interfaces ceramics layers, J. Alloys Compd. 872 (15) (2021) 159593, https://doi.org/10.1016/j.jallcom.2021.159593.

[6] C. He, N. Zhao, S. Song, Mechanical properties and microstructures of carbon nanotube-reinforced al matrix composite fabricated by in situ chemical vapor deposition, J. Alloys Compd. 487 (2009) 258–262, https://doi.org/10.1016/j.jallcom.2009.07.099.

[7] T. Mura, Micromechanics of Defects in Solids, second revised edition, Kluwer Academic Publishers, 1987.

[8] S. Nemat-Nasser, M. Hori, Micromechanics: Overall Properties of Heterogeneous Materials, North-Holland, 1993.

[9] S. Araki, H. Ono, S. Kenji, Approximate analysis of stress fields in and around a thin-coated fiber by means of double inclusion method, Theor. Appl. Mech. Jpn 51 (2002) 75–90, https://doi.org/10.11345/nctam.51.75.

[10] Y. Mikata, M. Taya, Stress field in a coated continuous fiber composite subjected to thermo-mechanical loadings, J. Compos. Mater. 19 (1985) 554–578, https://doi.org/10.1177/002199838501900607.
[11] H. Ono, A. Kariya, Micromechanical analysis for macroscopic elastic constants and thermal expansion coefficients of composite materials including double inhomogeneous inclusions (1st report, derivation of solutions for spheroidal shapes), Transactions of the JSME 88 (913) (2023), https://doi.org/10.1299/transjsme.22-00184 (in Japanese).
[12] H. Ono, A. Kariya, Micromechanical analysis for macroscopic elastic constants and thermal expansion coefficients of composite materials including double inhomogeneous inclusions (2nd report, numerical calculation of macroscopic elastic constants), Transactions of the JSME 88 (913) (2023), https://doi.org/10.1299/transjsme.22-00185 (in Japanese).
[13] Z. Hashin, On elastic behavior of fiber reinforced materials of arbitrary transverse phase geometry, J. Mech. Phys. Solids 13 (1965) 119–134, https://doi.org/10.1016/0022-5096(65)90015-3.
[14] Z. Hashin, Analysis of properties of fiber composites with anisotropic constituents, J. Appl. Mech. 46 (1979) 543–550, https://doi.org/10.1115/1.3424603.
[15] Z. Hashin, S. Shtrikman, A variational approach to the theory of the elastic behavior of multiphase materials, J. Mech. Phys. Solids 11 (1963) 127–140, https://doi.org/10.1016/0022-5096(63)90060-7.
[16] Y.P. Qiu, G.J. Weng, Elastic moduli of thickly coated particle and fiber-reinforced composites, J. Appl. Mech. 58 (1991) 388–398, https://doi.org/10.1115/1.2897198.
[17] H. Ono, Micromechanical analysis for macroscopic dielectric constants of composite materials including double inhomogeneous inclusions, Transactions of the JSME 89 (917) (2013), https://doi.org/10.1299/transjsme.22-00256 (in Japanese).
[18] G.P. Tandon, G.J. Weng, Average stress in the matrix and effective moduli of randomly oriented composites, Compos. Sci. Technol. 27 (1986) 111–132, https://doi.org/10.1016/0266-3538(86)90067-9.
[19] S. Li, G. Wang, Introduction to Micromechanics and Nanomechanics, World Scientific Publishing Co., 2008.
[20] H. Ono, Micromechanical analysis for effective elastic moduli and thermal expansion coefficient of composite materials containing ellipsoidal fillers oriented randomly, Composite Part C (Submitting paper).
[21] H. Ono, Micromechanical analysis for effective thermal and electromagnetic properties of composite materials containing anisotropical and ellipsoidal fillers oriented randomly, Heliyon 9 (6) (2023), https://doi.org/10.1016/j.heliyon.2023.e17445.
[22] W. Xu, Y. Wu, M. Jia, Elastic dependence of particle-reinforced composites on anisotropic particle geometries and reinforced/weak interphase microstructures at nano- and micro-scales, Compos. Struct. 203 (2018) 124–131, https://doi.org/10.1016/j.compstruct.2018.07.009.
[23] W. Guo, F. Han, J. Jiang, W. Xu, A micromechanical framework for thermo-elastic properties of multiphase cementitious composites with different saturation, Int. J. Mech. Sci. 224 (2022) 107313, https://doi.org/10.1016/j.ijmecsci.2022.107313.
[24] R.M. Christensen, Mechanics of Composite Materials, Dover Publications, 2005.
[25] P. Lu, Y.W. Leong, P.K. Pallathadka, C.B. He, Effective moduli of nanoparticle reinforced composites considering interphase effect by extended double-inclusion model – theory and explicit expressions, Int. J. Eng. Sci. 73 (2013) 33–55, https://doi.org/10.1016/j.ijengsci.2013.08.003.
[26] W. Xu, F. Wu, Y. Jiao, M. Liu, A general micromechanical framework of effective moduli for the design of nonspherical nano- and micro-particle reinforced composites with interface properties, Mater. Des. 127 (2017) 162–172, https://doi.org/10.1016/j.matdes.2017.04.075.
[27] J. Jiang, F. Wang, W. Guo, W. Xu, Hydraulic transport properties of unsaturated cementitious composites with spheroidal aggregates, Int. J. Mech. Sci. 212 (2021) 106845, https://doi.org/10.1016/j.ijmecsci.2021.106845.
[28] S. Araki, H. Yamashita, H. Ono, Effect of change in shape of ellipsoidal reinforcement on macroscopic elastic moduli of a composite material, Trans. Jpn. Soc. Mech. Eng. 75 (760) (2009) 1702–1709, https://doi.org/10.1299/kikaia.75.1702.
[29] S. Araki, H. Yamashita, Micromechanical analysis of macroscopic elastic moduli and coefficients of thermal expansion for a composite material containing ellipsoidal reinforcements, Trans. Jpn. Soc. Mech. Eng. C 74 (745) (2008) 1227–1234, https://doi.org/10.1299/kikaia.74.1227.
[30] B. Budiansky, On the elastic moduli of some heterogeneous materials, J. Mech. Phys. Solids 13 (1965) 223–227, https://doi.org/10.1016/0022-5096(65)90011-6.
[31] S. Kanaun, V. Levin, Self-Consistent Methods for Composites Volume 1-Static Problems, Springer, 1986.
[32] R.A. Schapery, Thermal expansion coefficients of composite materials based on energy principles, J. Compos. Mater. 2 (1968) 380–404, https://doi.org/10.1177/002199836800200308.
[33] B.W. Rosen, Z. Hashin, Effective thermal expansion coefficients and specific heats of composite materials, Int. J. Eng. Sci. 8 (1970) 157–173, https://doi.org/10.1016/0020-7225(70)90066-2.
[34] H. Ono, A. Kariya, Analysis for macroscopic physical properties of composite materials containing ellipsoidal reinforcements oriented randomly, Transactions of the JSME 89 (924) (2024), https://doi.org/10.1299/transjsme.22-00329 (in Japanese).
[35] X. Shi, M. Kazem, H. Aghdam, R. Ansari, Effect of aluminum carbide interphase on the thermomechanical behavior of carbon nanotube/aluminum nanocomposites, proceedings of the institution of mechanical engineers, part l, J. Mater.: Design Appl. 233 (9) (2018) 1843–1853, https://doi.org/10.1177/1464420718794716.
[36] M. Ahmadi, R. Ansari, M.K. Hassanzadeh-Aghdam, Micromechanical analysis of elastic modulus of carbon nanotube-aluminum nanocomposites with random microstructures, J. Alloys Compd. 779 (30) (2019) 433–439, https://doi.org/10.1016/j.jallcom.2018.11.326.
[37] M.K. Hassanzadeh-Aghda, R. Ansari, M.J. Mahmoodi, Thermal expanding behavior of carbon nanotube-reinforced metal matrix nanocomposites - a micromechanical modeling, J. Alloys Compd. 744 (2018) 637–650, https://doi.org/10.1016/j.jallcom.2018.02.100.
[38] M. Haghgoo, R. Ansari, M.K. Hassanzadeh-Aghdam, Effective elastoplastic properties of carbon nanotube-reinforced aluminum nanocomposites considering the residual stresses, J. Alloys Compd. 752 (2018) 476–488, https://doi.org/10.1016/j.jallcom.2018.04.168.
[39] S. Araki, H. Yamashita, A. Minami, Study on equivalent expressions for composite materials containing incompressible constituent, Trans. Jpn. Soc. Mech. Eng. 71 (701) (2005) 157–164, https://doi.org/10.1299/kikaia.71.157.
[40] M. Toda, Classical Mechanics (an Introductory Course of Physics 1), Iwanami Shoten, 2002.